LINEAR AND NONLINEAR OPTICAL PROPERTIES OF NOBLE METAL NANOPARTICLES AND THEIR APPLICATIONS

LAKSHMINARAYANA POLAVARAPU

NATIONAL UNIVERSITY OF SINGAPORE
2011

NOBLE METAL NANOPARTICLES FOR NONLINEAR OPTICS AND PRINTABLE ELECTRONICS

LAKSHMINARAYANA POLAVARAPU
(M.SC, University of Hyderabad, India)

A THESIS SUBMITTED
FOR THE DEGREE OF DOCTOR OF PHILOSOPHY
DEPARTMENT OF CHEMISTRY
NATIONAL UNIVERSITY OF SINGAPORE
2011

ACKNOWLEDGEMENTS

It would not have been possible to write this doctoral thesis without the help and support of the kind people around me, to only some of whom it is possible to give particular mention here.

I would like to express my deep and sincere gratitude to my supervisor, Prof. Xu, Qing-Hua for his support, encouragement and guidance through out the course. His wide knowledge and his detailed and constructive comments have been of great value for me. His understanding, encouraging and personal guidance have provided a good basis for the present thesis. I have learnt a lot from his dedication and hard work. My association with him for the last five years has been a wonderful experience.

I wish to express my warm and sincere thanks to Prof. Ji Wei (Department of Physics, NUS), Prof. Loh Kian Ping (Department of Chemistry, NUS) and Prof. Thorsten Wohland (Department of Chemistry, NUS) for allowing me to use the instrumental facilities in their laboratories.

I wish to thank all the technical staff, especially Mdm. Adeline Chia Hwee Cheng, Mdm. Patricia Tan Beng Hong, Ms. Tang Chui Ngoh, Mr. Gopal Selvarajoo, Mr. Guan Kok Yew**,** Mr. Goh Ah Bah and Mdm.Loy Gek Luan. Their superb technical support and services are essential for the completion of this study.

I would like to acknowledge the financial, academic and technical support of the National University of Singapore, and its staff, particularly in the award of a Graduate Research Studentship that provided the necessary financial support for this research. I also thank the Department of Chemistry and its academic and administrative staff for the kind support and assistance since the start of my doctoral studies at NUS.

I wish to thanks all my past and present lab mates and friends in NUS, Dr. Cheng Daming, Dr. Manoj Parameswaran, Dr. YAN Yongli, Dr. Venkatram, Mr. Kiran Kumar, Mr. Santosh, Mr. Manoj Manna, Mr. Anupam, Mr. Kalesh, Mr. Janardhan, Mr. Venkatesh, Mr. Dhoni, Mr. Ravi, Ms. Praveena, Ms. Monica Gupta, Ms. Tian Ning, Ms. REN Xinsheng, Ms. LEE Yih Hong, Mr. YU, Kuai, Mr. SHEN, Xiaoqin, Ms ZHAO, TingTing, Mr. LIM, Guan Hui, Mr. GAN, Ching Ruey Raymond, Mr. GUAN, Zhenping, Ms. JIANG, Cuifeng, Ms. YUAN, Peiyan, Ms. YE, Chen, Mr. CHEN, Jianqiang, Mr. ZHUO, Lin, Mr. GAO, Nengyue, Ms. JIANG Xiaofang, Ms. ZHOU Na, Mr. PAN, Yanlin and other Singapore telugu friends for their help, continuous encouragement and support. I had a wonderful time in Singapore with my friends and colleagues.

Last but not the least, I wish to thank my parents and sister for their blessings. I dedicate this thesis to my parents.

TABLE OF CONTENTS

Chapter 2. Nonlinear optical properties of silver nanoprisms 42

Chapter 7. Alkylamine capped metal nanoparticle "Inks" for printable SERS substrates, electronics and broadband photo detectors 148

SUMMARY

Noble metal nanoparticles attract great interest because of their current and future applications in the field of plasmonics, sensors, catalysis, electronics, optoelectronics, and many more. They exhibit new optical properties which are observed neither in molecules nor in bulk metals. One of the most attractive properties of noble metal nanoparticles is their strong nonlinear optical (NLO) behavior. In this thesis, we report the NLO properties of gold and silver nanoparticles of various shapes such as silver nanoprisms, gold nanochains and alkylamine capped gold nanoparticles. Another part of study will concentrate on the preparation and applications of gold and silver nanoparticle inks for Surface enhanced Raman scattering, printable electronics and broad band photodetectors.

In Chapter 2, we reported exceptional optical limiting properties of pure Ag nanoprisms and Au@Ag core-shell nanoprisms in solution that were photochemically prepared. Fluence-dependent transmittance measurements using 7 ns laser pulses of 532 nm wavelength showed that the optical limiting properties of two kinds of silver nanoprisms in solution were slightly better than that of carbon nanotube suspensions, which is known as a benchmark optical limiter. Nonlinear scattering experiments suggested that nonlinear scattering should play an important role in the observed optical limiting effects.

Chapter 3 presents a simple method for large scale preparation of monodisperse gold nanoparticles by simple mixing of chloroauricacid ($HAuCl_4$) with oleylamine (OA) at room temperature. The as-prepared gold nanoparticles have high monodispersity with an average diameter of 13 nm and can self-organize into two-dimensional (2D) hexagonal

close-packed arrays. The size of the gold nanoparticles can be experimentally controlled. The electron relaxation dynamics of these gold nanoparticles in toluene was studied by femtosecond pump-probe measurements, in comparison with the citrate stabilized gold nanoparticles in water. The phonon-phonon relaxation time of gold nanoparticles in toluene is slower than that of citrate capped gold nanoparticles in water, due to a lower thermal conductivity of toluene than water. The electron-phonon relaxation of the gold nanoparticles in toluene was found to display weaker pump-energy dependence, compared to that of citrate capped gold nanoparticles in water. The different electron-phonon relaxation dynamics is ascribed to the extra vibrational states provided by gold-NH_2, which serves as extra nonradiative relaxation pathway for the e-ph relaxation in oleylamine capped gold nanoparticles in toluene.

In Chapter 4, we have reported strong broadband optical limiting properties of oleylamine capped gold nanoparticles in solution for both femtosecond and nanosecond laser pulses. The nanosecond optical limiting effects were characterized by using fluence-dependent transmittance measurements with 7-ns laser pulses at 532 nm and 1064 nm; and the femtosecond optical limiting effects were characterized with a z-scan technique using 300-fs laser pulses at 780 nm. The oleylamine capped gold nanoparticles were found to show strong broadband optical limiting effects for nanosecond laser pulses at 532 nm and 1064 nm and femtosecond laser pulses at 780 nm. Those oleylamine capped gold nanoparticles displayed exceptional optical limiting effects with thresholds lower than that of carbon nanotube suspension, a benchmark optical limiter. Input fluence and angle dependent scattering measurements suggested that nonlinear scattering played an important role in the observed optical limiting behavior at 532 nm and 1064 nm.

In Chapter 5, we have reported the one- and two-photon excitation emission properties of water soluble glutathione monolayer protected gold clusters. Strong two-photon emission was observed from the gold clusters. The two-photon absorption cross section of these gold clusters in water was deduced from the z-scan measurement to be 189 740 GM, which is much higher compared to organic fluorescent dyes and quantum dots. These gold clusters also showed high photo-stability. The MTT assay showed that these gold clusters have low toxicity even at high concentrations. We have successfully demonstrated their applications for both one and two-photon excitation live cell imaging.

In Chapter 6, Simple strategies to assemble the gold nanoparticles into 1D nanostructure by using amino acid or water soluble conjugated polymer has been demonstrated. In the first method, we have synthesized the self assembled gold nanoparticles in a single step by reducing aqueous chloroaurate ions ($AuCl^{-4}$) with sodiumborohydride in the presence of an amino acid (glutamic acid and histidine) as a stabilizer. The open aperture *z*-scan measurements on self assembled gold nanoparticles showed an optical switching behavior from saturable absorption to reverse saturable absorption as the pump intensity increase. In another method, gold nanochains were prepared by the assembly of citrate-stabilized gold nanospheres induced by cationic conjugated polymers. This assembly method was rapid, and the assembled product was very stable. A longitudinal plasmon resonance band was formed as a result of the plasmon coupling of gold nanoparticles and can be tuned from visible to near infrared by adjusting the polymer/Au molar ratio. The gold nanochains were used as a SERS substrate and gave a large enhancement, which was~400 times larger than that on the isolated gold nanosphere substrate.

In Chapter 7, a facile and general method for the preparation of alkylamine capped metal (Au & Ag) nanoparticle inks with high solubility has been reported. Using metal nanoparticle “inks”, we have demonstrated their applications for large scale fabrication of highly efficient surface enhanced Raman scattering substrates (SERS) by a facile solution processing method. These SERS substrates can detect analytes down to a few nM and flexible plastic substrates have also been demonstrated. Insulator-to-metal transition properties of the alkylamine capped metal nanoparticle films were investigated. The transition temperatures could be tailored to the plastic compatible temperatures by using proper alkylamine as the capping agent. The ultrafast electron relaxation studies of the nanoparticle films demonstrated that faster electron relaxation was observed at higher annealing temperatures due to stronger electronic coupling between the nanoparticles. The applications of these high concentrated alkylamine capped metal nanoparticle inks for the printable electronics were demonstrated by printing the oleylamine capped gold nanoparticles ink as source and drain for the graphene field effect transistor. Furthermore, the broadband photoresponse properties of the Au and Ag nanoparticle films have been studied by using visible and IR lasers.

In Chapter 8, we have reported a simple method for the preparation of aqueous silver nanoparticle ink that can be printable at very mild temperature. We have demonstrated that the silver ink can be used to fabricate highly conductive films on glass and plastic substrates by depositing the nanoparticle dispersion onto the substrate and evaporating the solvent. High conductivity was achieved at very mild temperature due to the self aggregation of nanoparticles by drying the nanoparticle film. No significant change in the conductivity was observed after deformating the plastic substrate. The

application of Ag nanoparticle ink for printable cathode material for P3HT-PCBM bulk heterojunction solar cells with an efficiency of 2.25% has been demonstrated.

LIST OF FIGURES

LIST OF PUBLICATIONS

1. **L.Polavarapu** and Qing-Hua Xu
   A single-step synthesis of gold nanochains using an amino acid as a capping agent and characterization of their optical properties,
   NANOTECHNOLOGY, 2008, 19, 075601.

2. **L. Polavarapu**, Q.-H. Xu, M. S. Dhoni and W. Ji
   Optical limiting properties of silver nanoprisms
   APPL. PHYS. LETT., 2008, 92, 263110

3. **L. Polavarapu** and Q.-H. Xu
   Water Soluble Conjugated Polymers Induced Self-Assembly of Gold Nanoparticles and it's Application to SERS
   LANGMUIR, 2008, 24, 10608.

4. **L. Polavarapu** and Q.-H. Xu
   A Simple Method for Large Scale Synthesis of Highly Monodisperse Gold Nanoparticles at Room Temperature and Their Electron Relaxation Properties
   NANOTECHNOLOGY, 2009, 20, 185606**.**

5. Y.H. Lee, Y.L. Yan, **L. Polavarapu,** Q.-H. Xu
   Nonlinear Optical Switching Behavior of Au Nanocubes and Nanooctahedra Investigated by Femtosecond Z-scan Measurements
   APPL. PHYS. LETT., 2009, 95, 023105.

6. **L. Polavarapu,** N. Venkatram, Wei Ji, and Qing-Hua Xu,
   Optical Limiting Properties of Oleylamine Capped Gold Nanoparticles for Both femtosecond and Nanosecond Laser Pulses
   ACS APPLIED MATERIALS & INTERFACES, 2009, 1, 2298.

7. N. Venkatram*, **L Polavarapu***, K K Manga, Qing-Hua Xu and Wei Ji
   Transient photoconductivity and femtosecond nonlinear optical properties of a conjugated polymer–graphene oxide composite
   NANOTECHNOLOGY, 2010, 21, 415203**(*Equal Contribution)**

8. **L. Polavarapu,** Manoj Manna, Qing-Hua Xu
   One and Two-photon Imaging of Cancer Cells Using Biocompatible Water Soluble Quantum Size Gold Clusters as Fluorescent labels
   NANOSCALE, 2010 **(In press)**

9. Venkatesh Mamidala*, **L. Polavarapu*,** Wei Ji, and Qing-Hua Xu
   Enhanced Nonlinear Optical response in Donor-Acceptor complexes via Photo induced Electron/Energy Transfer
   OPTICS EXPRESS, 2010, 18, 25928 **(*Equal Contribution)**

10. Yu Kuai, **L Polavarapu,** Qing-Hua Xu
    Excitation Wavelength and Intensity Dependent Femtosecond Transient Absorption Studies on Electron Dynamics of Gold Nanorods
    JOURNAL OF PHYSICAL CHEMISTRY A, 2011, 115, 3820

11. Zhenping Guan, **L. Polavarapu**, and Qing-Hua Xu
    Enhanced Two-photon Emission in Coupled Metal nanoparticles Induced by Conjugated Polymers
    LANGMUIR, 2010, 26, 18020

12. Y.H. Lee, **L. Polavarapu**, C.F. Jiang, P.Y. Yuan and Q.-H. Xu
    Recent advances in metal enhanced optical studies
    COMOS, 2010, 6 (2), 1-29

13. Qiaoliang Bao, Han Zhang, Zhenhua Ni, Yu Wang, **L. Polavarapu**, Kian Ping Loh, Zexiang Shen, Qing-Hua Xu, and Ding Yuan Tang
    Monolayer Graphene as Saturable Absorber in Modelocked Laser
    NANORESEARCH, 2011, 4, 297

14. Janardhan Balapanuru, Jia-Xiang Yang, Si Xiao, Qiaoliang Bao, Maryam Jahan, **L Polavarapu**, Qing- Hua Xu, Ji Wei, Kian Ping Loh
    Graphene Oxide-Organic Dye Ionic Complex with DNA Sensing and Optical Limiting Properties,
    ANGEWANDTE CHEMIE, 2010, 49, 1

15. M. D. Regulacio, C. Ye, S.H. Lim, M. Bosman, **L. Polavarapu**, Q.-H. Xu and M.-Y. Han,
    One-Pot Synthesis of Cu1.94S-CdS and Cu1.94S-ZnxCd1-xS Nanodisk Heterostructures,
    J. Am. Chem. Soc. 2011, 133, 2052

16. **L. Polavarapu**, Kiran Kumar Manga, Yu Kuai, Priscilla Kailian Ang, Cao Hanh Duyen, Janardhan Balapanuru, Kian Ping Loh, Qing-Hua Xu.
    Alkylamine Capped Metal Nanoparticle "Inks" for Printable SERS Substrates, Electronics and Broadband Photo Detectors, **Nanoscale**, 2011, 3, 2268

17. **L. Polavarapu**, , Cao Hanh Duyen, Kiran Kumar Manga, Kian Ping Loh, and Qing-Hua Xu.
    Preparation of Conductive Silver Films at Mild Temperatures for Printable Organic Electronics, **Chemistry of Materials,** 2011, In press

18. **L. Polavarapu**, Janardhan Balapanuru, Kian Ping Loh, Qing- Hua Xu
    Ultrafast dynamics of graphene-oxide and the effect of laser pulse irradiation on their Optical properties **(To be submitted)**

19. Ting Ting Chng, **L. Polavarapu,** Qing-Hua Xu, Wei Ji, and Hua Chun Zeng
Rapid Synthesis of Highly Monodisperse Au_xAg_{1-x} Alloy Nanoparticles *via* a Half-Seeding Approach, **Langmuir,** 2011, 27, 5633

20. **L. Polavarapu,** Venkatesh Mamidala, Zhenping Guan, Wei Ji, Qing-Hua Xu
Huge enhancement of optical nonlinearity in coupled metal nanoparticles induced by conjugated polymers **(To be submitted)**

21. Yu Kuai, **L Polavarapu**, Qing-Hua Xu.
Bimetallic Au/Ag Core-Shell Nanorods Studied by Ultrafast Transient Absorption Spectroscopy under Selective Excitation,
JOURNAL OF PHYSICAL CHEMISTRY C, 2011, In press

22**. L. Polavarapu**, N. Venkatram, Wei Ji, and Qing-Hua Xu
Optical nonlinearities of silver nanoprisms: Effect of Edge length and Thickness
(To be submitted)

23. Jiang Cuifeng, Guan Zhenping, **L. Polavarapu,** and Qing-Hua Xu
Two-Photon Ratiometric Sensing of Hg2+ by Using Cysteine Functionalized Ag Nanoparticles", **Nanoscale,** 2011, In press

CHAPTER 1

INTRODUCTION, BASIC THEORY AND EXPERIMENTAL TECHNIQUES

1.1 Noble metal nanoparticles

Noble metal nanoparticles have received great interest owing to their unique properties and potential wide applications. The applications of noble metal nanoparticles in the fields of catalysis, biosensing, electronics and optics have been under intensive study.[1, 2, 3, 4] Because of their structure, which is intermediate between that of molecules and of bulk material, they enable to bridge the gap between molecular chemistry and surface science (Fig.1). Metal Nanoparticles are known to display many unique optical and electronic properties.[5, 6] For example, gold colloidal nanoparticles are responsible for the brilliant red colour seen in stained glass windows.[7, 8] Spherical silver particle solutions are typically yellow in colour.[9] These properties have been of interest for centuries, and scientific research on metal nanoparticles dates back to Michael Faraday.[10] The linear optical properties like extinction and scattering of small spherical metal particles accounting for the surface plasmon resonance were explained theoretically by the groundbreaking work of Mie in 1908 .[11] The optical and electronic properties of metal nanoparticles mainly depend on the surface plasmon resonance (SPR) absorption. The SPR mainly depend on the size, shape and the refractive index of the medium that are dispersed in.[12] Among these, the shape of the nanoparticles has amongst the largest influence on the SPR band.[12]

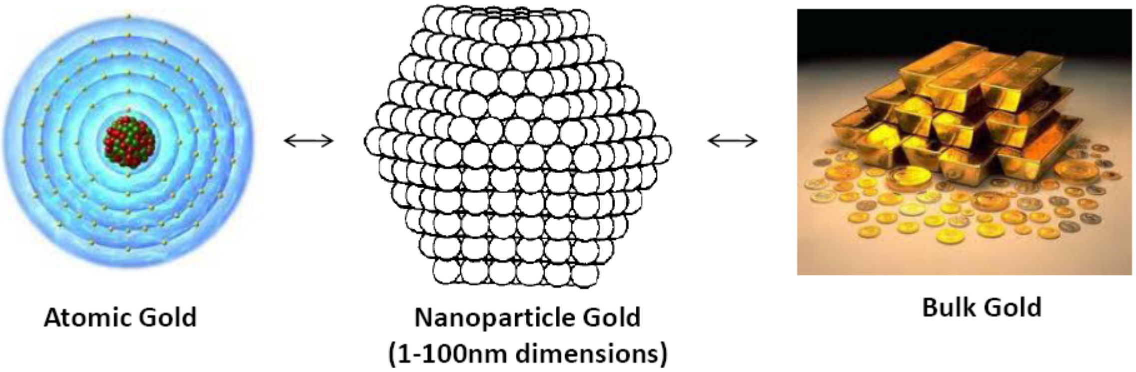

Fig. 1.1 Representation of atomic, nano and bulk gold, nanoparticle is a bridge between atom and bulk

1.2 Surface plasmon resonance

When a small spherical metallic nanoparticle is irradiated by light, the oscillating electric field causes the conduction electrons to oscillate coherently.[13, 14, 15] This is schematically pictured in Figure 1.2. When the electron cloud is displaced relative to the nuclei, a restoring force arises from Coulomb attraction between electrons and nuclei that results in oscillation of the electron cloud relative to the nuclear framework. The oscillation frequency is determined by four factors: the density of electrons, the effective electron mass, shape and size of the nanoparticle. The collective oscillation of the electrons is called the plasmon resonance of the particle and the surface plasmon dynamics nanoparticles of different sizes and shapes have been extensively studied. [5, 6, 12]

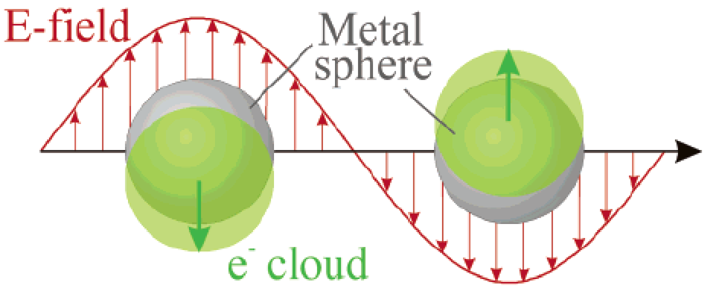

Fig. 1.2 Schematic of plasmon oscillation for a sphere, showing the displacement of the conduction electron charge cloud relative to the nuclei.

The transition from atom to bulk metal leads to splitting of the atomic energy levels to form a conduction band of closely spaced energy levels of free electrons. [13, 14, 15] The optical properties of metals involve both interactions of light with the free electrons and electron transitions from one band to another. As the size of the metal nanoparticle decreases, the mean free path of the free electrons in the cluster is also reduced, which results in the change in the optical properties of the metal clusters. Noble metal (Au, Ag) nanoparticles show plasma absorption band spanning from visible to infrared depending on the shape resulting from collective oscillations of the free electrons excited by light of a particular wavelength. This phenomenon in metal nanoparticles can be understood from the Mie equations for optical absorption of spheres[11] and the optical properties of free electrons. Modified Mie equation for the small particle size is[16]

$$\alpha = \frac{18\pi Q n^3 \varepsilon_2}{\lambda\left(\left(\varepsilon_1 + 2n^2\right)^2 + \varepsilon_2^2\right)} \tag{1.1}$$

where Q is the volume fraction of particles, α the absorption coefficient, χ is the wavelength of the light, n is the refractive index of the medium, ε_1 and ε_2 are the real and imaginary parts of the complex dielectric constant $\varepsilon^*=\varepsilon_1 - i\varepsilon_2$ of the particles,

As the radii of noble metal particles decrease below the mean free path of electrons in them, the plasma absorption band broadens. This reduction in mean free path causes a reduction in effective optical conductivity in the particle, which translates into an increase in the effective ε_2 of the particles, because ε_2 is inversely proportional to the conductivity in the classical Drude model for free electrons.[16] Therefore for smaller particles $(\varepsilon_1 + 2n^2)^2 << \varepsilon_2^2$

The final equation becomes

$$\alpha = \frac{18\pi Q n^3}{\lambda \varepsilon_2} \tag{1.2}$$

This equation represents that the surface plasmon absorption depends on particle size, shape and the refractive index of the matrix. For example spherical gold nanoparticles exhibit only one SPR band, but gold nanorods exhibit two SPR band due to longitudinal and transverse mode absorption.[12b] Figure 1.3 shows the typical TEM images of Au nanoparticles of different shapes and sizes and their extinction spectra are shown in figure 1.4. Au nanospheres and nanocubes have one surface plasmon peak. Au nanobranches, nanorods, and nanobipyramids exhibit two major surface plasmon peaks. One is associated with electron oscillation along the transverse direction, and the other is associated with electron oscillation along the longitudinal direction.[12b]

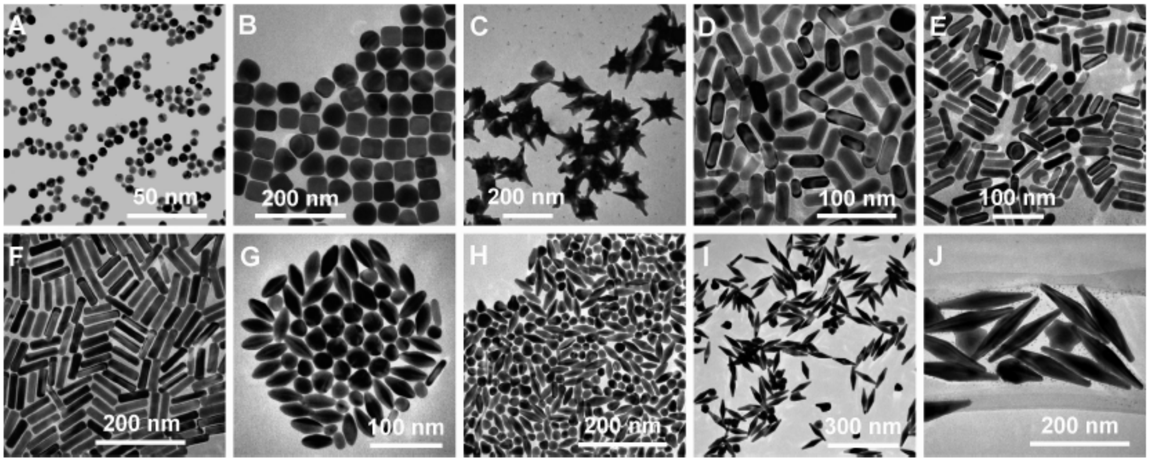

Fig. 1.3 TEM images of Au nanoparticles of different shapes and sizes.[12b] (A) Nanospheres. (B) Nanocubes. (C) Nanobranches. (D) Nanorods (aspect ratio = 2.4. (E) Nanorods (aspect ratio=3.4. (F) Nanorods (aspect ratio=4.6. (G) Nanobipyramids (aspect ratio =1.5. (H) Nanobipyramids (aspect ratio = 2.7. (I) Nanobipyramids (aspect ratio = 3.9. (J) Nanobipyramids (aspect ratio = 4.7) (Reproduced by permission of American Chemical Society [12b])

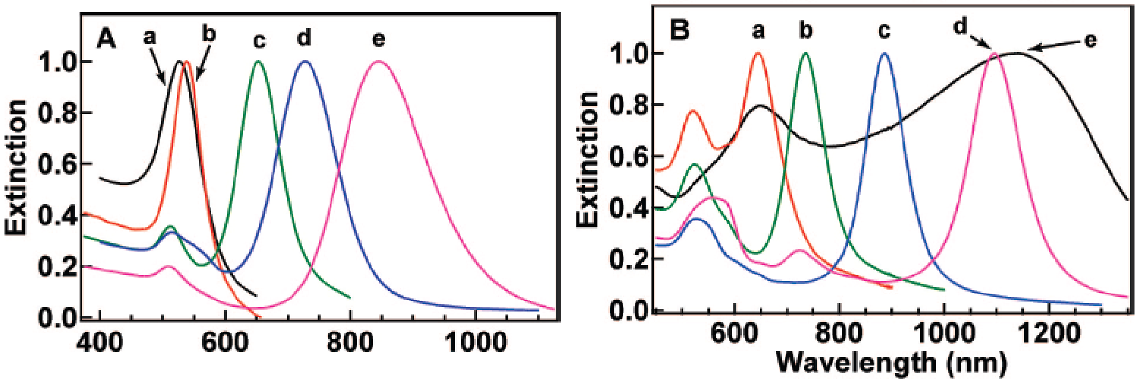

Fig. 1.4 Normalized extinction spectra of Au nanoparticles of different shapes and sizes.[12b] (A) Spectra a-e correspond to nanospheres, nanocubes, and nanorods with aspect ratios of 2.4, 3.4, and 4.6 respectively. (B) Spectra a-e correspond to nanobipyramids with aspect ratios of 1.5, 2.7, 3.9, and 4.7, and nanobranches, respectively. Reproduced by permission of American Chemical Society [12b])

1.3. Nonlinear optical properties

1.3.1. Two-photon and multi-photon Absorption (TPA and MPA)

Two-photon absorption (TPA) involves the transition from ground state (N_1) to a higher-lying state (N_2) by the simultaneous absorption of two photons via an intermediate virtual state, as schematically shown in Fig. 1.5.

In this case, the attenuation of the incident light can be described by

$$\frac{dI}{dz} = -\beta I^2 \tag{1.3}$$

Where β is the two-photon absorption coefficient and I is the intensity of the incident light

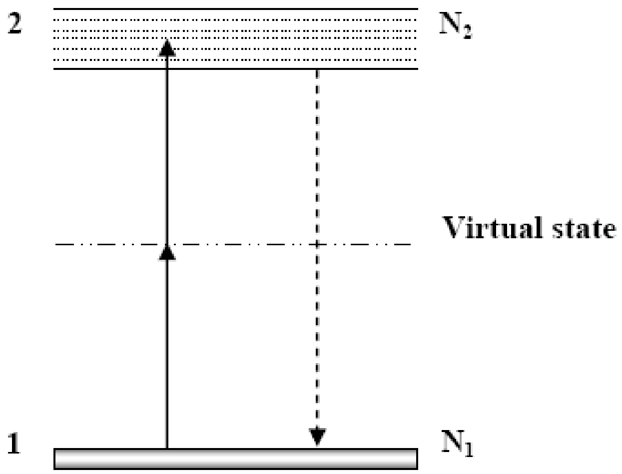

Fig.1.5 Energy level diagram for two-photon absorption (TPA) process.

Three-photon or multi photon absorption involves the transition from the ground state to a higher-lying state by the simultaneous absorption of three or more number photons via multiple numbers of virtual states. (Fig. 1.6)

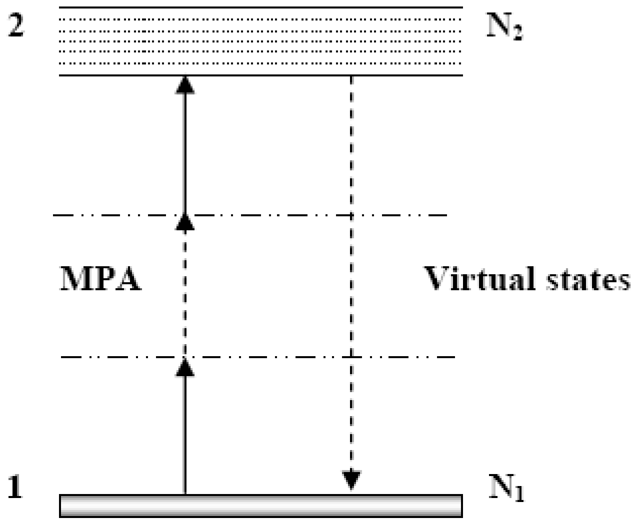

Fig.1.6 Energy level diagram for Multi-photon absorption (MPA) process.

In this case, the attenuation of the incident light can be described by

$$\frac{dI}{dz} = -\alpha_n I^n \tag{1.4}$$

Where α_n is the n-photon absorption coefficient.

The nonlinear transmittance with respect to the input intensity is derived by solving the above equation

$$\frac{dI(z)}{dz} = -\alpha_n I^n(z) \tag{1.5}$$

$$\int_{I_{in}}^{I_{out}} \frac{1}{I^n(z)} dI(z) = -\alpha_n \int_0^L dz \tag{1.6}$$

$$-\alpha_n L = \left[\frac{I^{-n+1}}{-n+1} \right]_{I_{in}}^{I_{out}} \tag{1.7}$$

$$\alpha_n L = \frac{1}{n-1} \left[\frac{1}{I_{in}^{n-1}} - \frac{1}{I_{out}^{n-1}} \right] \tag{1.8}$$

$$\alpha_n L = \frac{1}{(n-1) I_{in}^{n-1}} \left[1 - \frac{1}{T^{n-1}} \right] \tag{1.9}$$

$$where\ T = \frac{I_{out}}{I_{in}}$$

$$T^{n-1} = \frac{1}{1 + \alpha_n L (n-1) I_{in}^{n-1}}$$

$$T = \frac{1}{\left[1 + \alpha_n L (n-1) I_{in}^{n-1}\right]^{\frac{1}{n-1}}} \tag{1.10}$$

$$\frac{I_{in}}{\omega_0^2} = \frac{I_{00}}{\omega_Z^2}$$

$$I_{in} = \frac{I_{00}}{1 + \frac{Z^2}{Z_0^2}} \tag{1.11}$$

$$where\ \ \omega_Z^2 = \omega_0^2 \left(1 + \frac{Z^2}{Z_0^2} \right)$$

$$T = \frac{1}{\left[1 + (n-1)\alpha_n L \left(I_{00} / \left(1 + \left(Z / Z_0 \right)^2 \right) \right)^{n-1} \right]^{1/_{n-1}}}$$

$$\Rightarrow T_{OA(nPA)} = \frac{1}{\left[1 + (n-1)\alpha_n L \left(I_{00} / \left(1 + \left(Z / Z_0 \right)^2 \right) \right)^{n-1} \right]^{1/_{n-1}}} \tag{1.12}$$

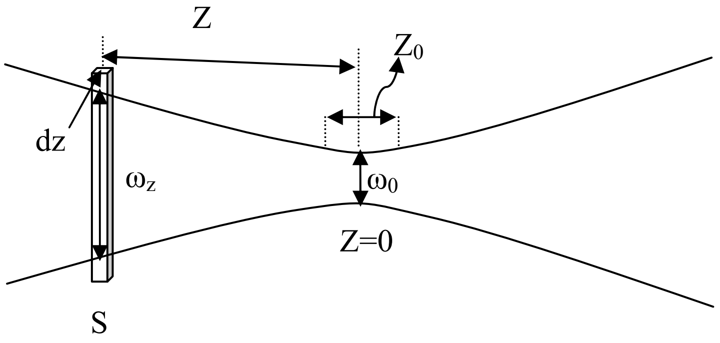

Fig.1.7 Schematic diagram of focused laser beam.

where I_{00} is the peak intensity (at Z=0), I_{in} is intensity at sample position (if Z- is the distance from focal point I_{in} (I_Z) is the intensity at that point), $Z_0 = \pi\omega_0^2/\lambda$ is Rayleigh range, ω_0 is the beam waist at the focal point (Z=0), dz is small slice of the sample, I_{in} is input intensity and I_{out} is output intensity of the sample and T is the transmittance.

1.3.2. Excited State Absorption (ESA)

The excited state absorption process usually takes place at higher intensities due to significant population of the excited states. The excited electrons can rapidly undergo a transition to higher excited states before it decays back to the ground state. The ESA mechanism for nonlinear absorption, is usually understood by a five-level model that refers to five distinct electronic states [17, 18] as shown in Fig. 1.8. The absorption of an incident photon promotes the molecules to the first excited singlet state, S_1, and then the molecules can relax back to the ground state by radiative or nonradiative transition with rate constant k_f or it can undergo spin flip transition to a triplet state T_1 (intersystem crossing) with rate constant, k_{isc}, or the material can absorb another photon, promoting the molecules to a higher-lying singlet state, S_2 from which they can relax back to the first excited singlet state. Molecules in the lowest triplet state can relax back to the ground state by another spin flip transition, leading to phosphorescence, with rate constant k_{ph} , or the material can absorb another photon, promoting the molecules to a higher-lying triplet state T_2, from which it can relax back to T_1.

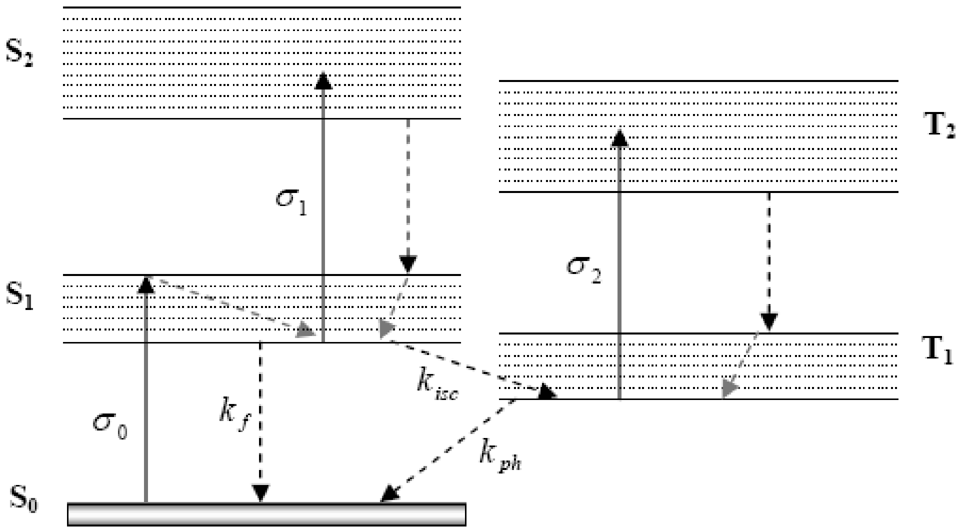

Fig.1.8 Energy level diagram for the excited state absorption (ESA) process.

1.3.3. Saturable Absorption (SA) and Reverse Saturable Absorption (RSA)

Saturable absorption is a property of materials where the absorption of light decreases with increasing light intensity. Most materials show some saturable absorption, but often only at very high optical intensities If the absorption cross-section of the excited state is smaller than that of the ground state, the transmission of the system at higher energies will be increased with the increase of the light excitation intensity. On the other hand, if the absorption cross-section of the excited state is larger than that of the ground state, the system will be less transmissive with the increase of the light excitation intensity; since this phenomenon is opposite to that of saturable absorption, it is called reverse saturable absorption (RSA). Free carrier absorption (FCA) has similar characteristics as RSA. Among these three nonlinear processes RSA and FCA contribute to optical limiting. Materials which exhibit RSA show enhanced nonlinear absorption as the input optical intensity/fluence is increased.[19] Reverse saturable absorbers are of special interest due to large nonlinear attenuation while maintaining high linear transmittance, making the limiting process more reliable and useful in fast optical systems.

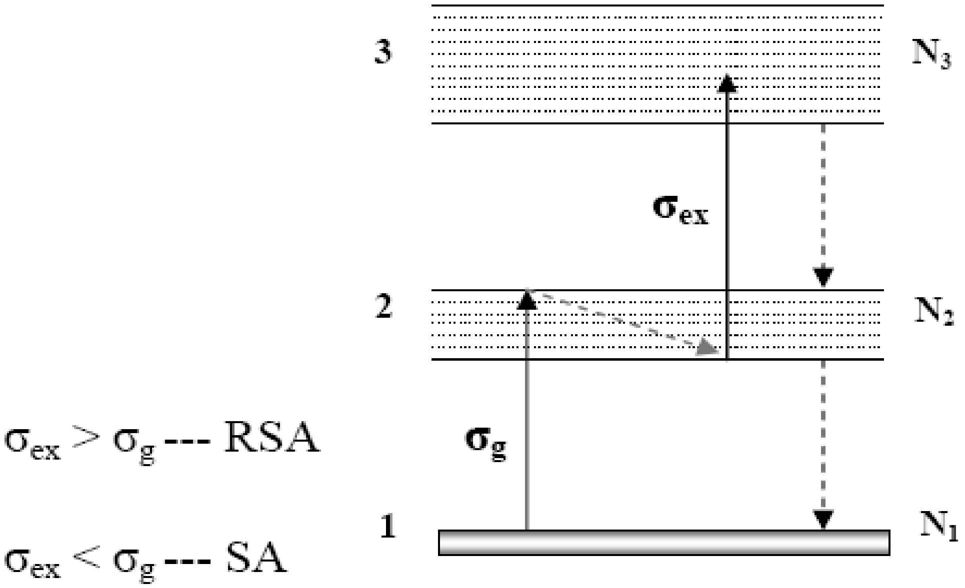

Fig.1.9 Energy level diagram for reverse saturable absorption (RSA) process.

A simple model of sequential one-photon absorption in a two-step process [17, 18] can be used to explain RSA as shown schematically in Fig. 1.9. the labels 1, 2 and 3 are the ground, first and higher-lying excited states respectively, with N_1, N_2 and N_3 as their respective populations. σ_g and σ_{ex} are the absorption cross-sections for the ground and excited states respectively. If the material has resonant linear absorption for the incident laser, excitation of a definite population to state 2 occurs, followed by further transition from state 2 to 3 via further photon absorption. Probability of the latter transition depends on N_2, σ_{ex} and the incident intensity, I; N_2 is determined by N_1, σ_g and I. With increase in the intensity, N_2 increases continuously and hence the sequential one-photon absorption from state 2 to 3 becomes significant provided $\sigma_{ex} >> \sigma_g$. Under steady state conditions,

$$\frac{dI}{dz} = -\sigma_g (N_1 - N_2) I - \sigma_{ex} N_2 I \tag{1.13}$$

In the simplest situation, it can be assumed that, $N_1 >> N_2$, $N_3 \approx 0$ and $N \approx N_1$ where N is the total population of the absorbing species. If $N_2 \approx b\sigma_g N$, where b is a proportionality constant, the attenuation of the light inside the medium,

$$\frac{dI}{dz} = -\sigma_g N I - b\sigma_g \sigma_{ex} N I^2 \tag{1.14}$$

$$\frac{dI}{dz} = -\alpha_0 I - \beta' I^2 \tag{1.15}$$

The linear and nonlinear absorption coefficient α_0 and β' are defined as

$$\alpha_0 = \sigma_g N$$

$$\beta' = b\sigma_g \sigma_{ex} N$$

The solution of Eq. 1.15 gives the intensity of the light at a distance, z inside the medium,

$$I(z) = \frac{I_0 e^{-\alpha_0 z}}{1 + (1 - e^{-\alpha_0 z}) \frac{\beta'}{\alpha_0} I_0} \tag{1.16}$$

where I_0 is the input intensity incident on the medium. If the linear absorption is small, then $e^{-\alpha_0 z} \approx 1 - \alpha_0 z$, and the transmittivity is given as,

$$T(I_0) = \frac{I}{I_0} = \frac{T_0}{1 + \beta' z I_0} \tag{1.17}$$

Here $T_0 = e^{-\alpha_0 z}$ is the linear transmittivity of the material for low input intensity. T(I_0) is the intensity dependent transmittivity of the same material at high input intensity. This simplified quantitative description of RSA shows how the transmittivity decreases with increasing input intensity.

1.3.4. Free Carrier Absorption (FCA)

Absorption of photons with energy greater than the band gap will promote electrons to the conduction band, where they become free carriers. With sufficiently high intensities, there is a high probability for them to absorb more photons eventhough they are still in the conduction band. This can lead to nonlinear absorption. Once free carriers are generated in semiconductors, they may experience phonon-assisted absorption to higher lying states in the conduction band.

1.4. Optical Limiting

The advances in the development of lasers have led to revolutionary changes and applications of lasers in various science and technological applications. Very high energy density can easily be obtained from the ultra short light pulses from nanosecond, picosecond and femtosecond laser sources. High-powered pulsed lasers have found many applications in academic research as well as in many industrial and military applications. Semiconductor and solid-state lasers are portable, compact and efficient, and hence of special interest in the realm of laser weaponry. With the advent of such high power laser sources operating over wide ranges of wavelengths and pulse durations, the necessity for protection of sensors, optical components and human eyes from laser inflicted damages has increased enormously over the last few years. In this context, Optical limiters which display a decreasing transmittance as a function of laser fluence or irradiance are important.[20] Fast response optical limiting materials with low thresholds can be used for protection of eyes and sensitive optical devices from laser-induced damage. A lot of efforts have been devoted to develop ideal broadband optical limiting materials. In an ideal optical limiter, the transmittance change abruptly at some critical input intensity or threshold and therefore exhibits an inverse dependence on the intensity; the output is thus clamped at a certain value (Fig. 1.10). If this value is below the minimum that can damage the particular equipment, the optical limiter becomes an efficient safety device. The limiting threshold ($I_{1/2}$) of the material is defined as the input intensity/fluence at which the transmittance reduces to 50% of the linear transmittance.[21] The effective optical limiting materials should possesses (i) low limiting threshold and high optical damage threshold and stability, leading to a large dynamic range, (ii) sensitive broadband response to long and short pulses, (iii) fast response time, and (iv) high linear transmittance, optical clarity, and robustness.[22]

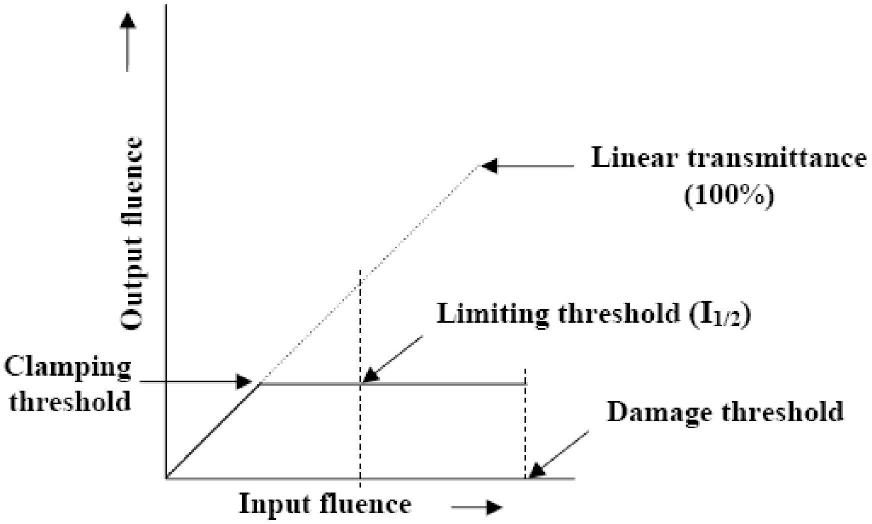

Fig.1.10 Schematic representation of the behavior of an ideal optical limiter.

1.4.1. The Processes that Lead to the Optical Limiting

Materials exhibit optical limiting based on several nonlinear optical mechanisms and the optical limiting processes such as nonlinear scattering, multi-photon absorption, excited state absorption (ESA), free carrier absorption (FCA) and reverse saturable absorption (RSA).[23, 24] Various type of processes that lead to the optical limiting are shown in fig.1.11. The optical limiting materials can be designed based on these mechanisms. Fig. 1.9 summarizes various mechanisms that can lead to optical limiting, which are mainly based on energy is spreading and energy absorbing mechanisms.

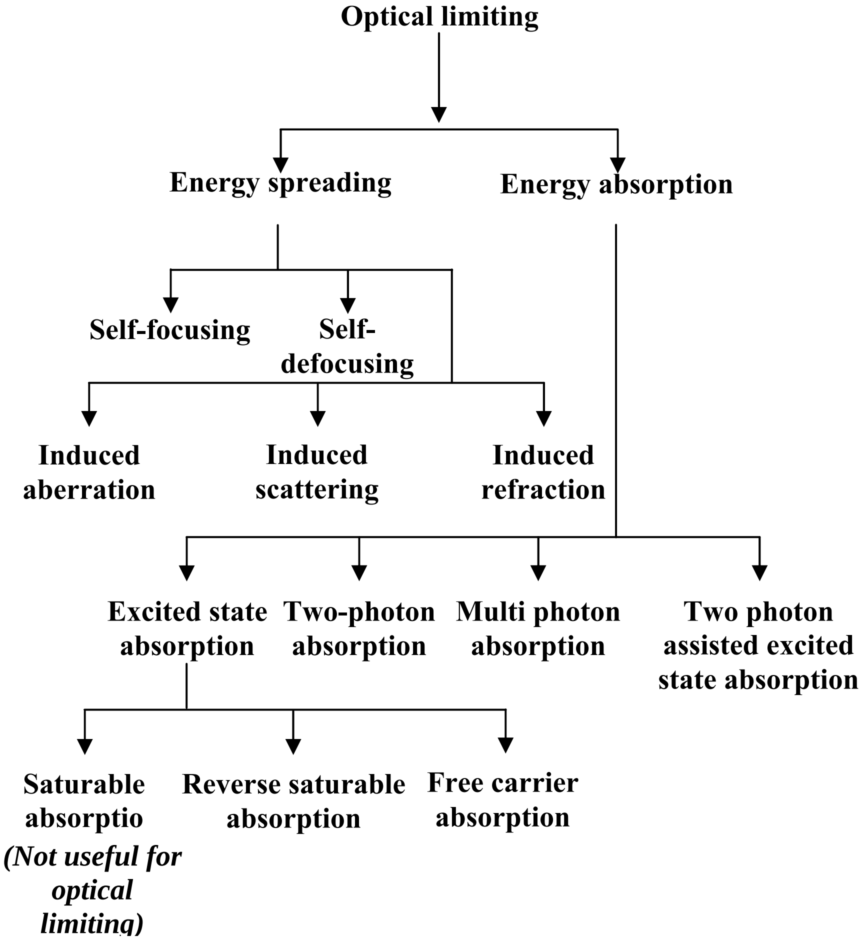

Fig. 1.11 Schematic representation of the various mechanisms responsible for optical limiting.

1.4.1.1. Optical Limiting Based Nonlinear Absorption

Nonlinear absorption plays an important role for optical limiting in various materials like quantum dots, conjugated polymers and many other organic chromophores.[25,26] In this case, the transmittance of nonlinear absorption media decreases with the increase of the input laser intensity. The materials absorb two or multi photons at sufficiently high intensities, which leads to enhanced optical limiting. The optical limiting devices based on this mechanism can also be called as energy-absorption type optical limiters. Various other type of energy absorption process that responsible for the optical limiting are shown in fig.1.11

1.4.1.2 Optical Limiting Based On Energy-Spreading Process

Another mechanism for the optical limiting is based on the energy spreading process. Nonlinear scattering is the major contribution in this process. Various type of energy spreading process such as self-focusing, self defocusing, induced aberration, induced scattering and induced refraction is shown in fig.1.12. Typical effects operating in energy- spreading type of optical limiting materials are schematically shown in Fig. 1.12. Although all these mechanisms lead to slow temporal response, the opto-thermal effect-induced refractive index change is considered to be important for optical limiting. Even though impurities or external particles cause only small residual linear absorption in transparent and non-resonantly absorptive medium, this small absorption is strong enough to create remarkable thermally induced refractive index changes at higher input laser intensity. The induced refractive index change will be significant for a resonant and linearly absorbing medium even at low input intensity. The nanoparticles studied in the current work exhibit optical limiting mainly based on nonlinear scattering. The nonlinear scattering usually arises from the formation of two types of scattering centers after photo-excitation of the nanoparticles. At higher pump fluence, the excitation energy absorbed by the nanoparticle creates a fast expansion of the metal nanoparticle, which acts as a scattering center. The absorbed energy is subsequently transferred to the surrounding solvent. Consequently the solvent is heated up and bubbles are formed, which act as secondary scattering centers.[271] The solvent in which nanoparticles are dispersed plays an important role in enhancing the optical limiting activity of the nanoparticles through micro bubble formation. The micro bubbles formation usually occurs at the interface of the solvent and nanoparticle. Solvents with good thermal conductivity can quickly transfer the thermal energy from the nanoparticle to solvent after photo-excitation to dissipate the energy. Solvents with low thermal conductivity can help to confine the energy at the interface and promote solvent vaporization and bubble formations. Nanoparticles dispersed in solvents with low thermal conductivity, low heat capacity and low boiling point are expected to show good performance for generating scattering centers and hence give rise to optical limiting effects. It has been recently reported by Wang et al.[28] that the optical limiting properties of CNTs are better in low boiling solvents such as DMF (*N*,*N*-dimethylformamide) compared to CNTs dispersed in NMP (*N*-methyl-2-pyrrolidone), DMA (*N*,*N*-dimethylacetamide).

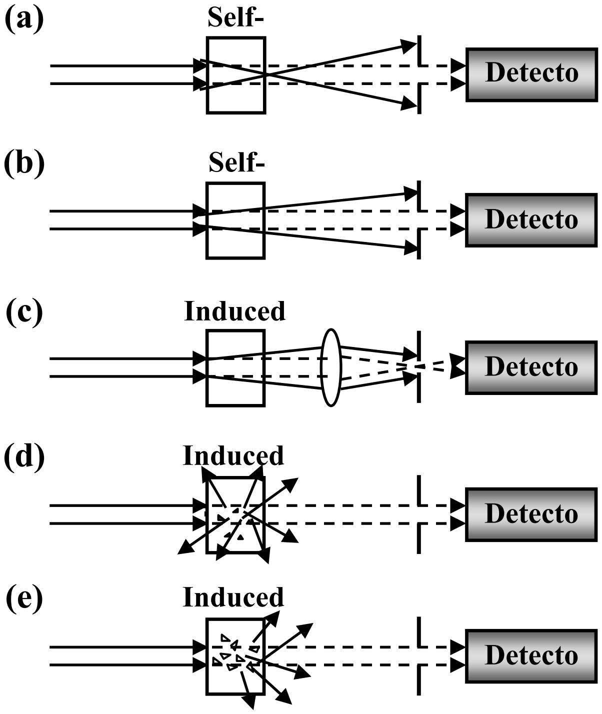

Fig.1.12 Schematic illustration of energy-spreading type optical limiters

1.4.2. Materials for Optical Limiting

A wide variety of materials have been studied for optical limiting applications based on different mechanisms. Development of optical limiting materials with negligible linear absorption with low limiting threshold is the prime consideration incorporation into sensitive optical components. Recently pulsed lasers have been using in eye surgery, so great attention has been focused on optical limiters for pulsed lasers in the visible and near infrared range, in view of their importance for eye protection.[29] Many colloidal suspensions exhibit optical limiting in the UV to near IR range, using nonlinear scattering mechanisms.[30] Previously many research groups have studied the nonlinear optical properties of various quantum dots. Size and shape dependent optical limiting properties have also investigated. The optical limiting behavior of quantum dots for femtosecond laser pulses mainly arises due to two-photon or multi-photon absorption processes. Venkatram et al[30f] reported the optical limiting properties of CdS nanoparticles for nanosecond laser pulses at 532nm, which arises due to nonlinear scattering. These reports show that the optical limiting activity of QDs is mainly due to the multiphoton absorption for femtosecond laser pulses and nonlinear scattering and nonlinear absorption for nanosecond laser pulses. Optical limiting properties of several dye molecules and semiconducting polymers and small molecules have also been investigated. The most extensively studied systems are phthalocyanines,[31] porphyrins,[32] fullerenes and their derivatives[33] in which long-lived triplet excited state can be produced conveniently. Liquid crystals are another class of materials studied in the visible to mid IR region and these materials exhibit optical limiting via refraction and TPA.[34] Other materials such as bacteriorhodopsin,[35] Photorefractive materials,[36] photonic band gap materials,[37] nonlinear absorbers doped in xerogels and sol-gel films,[38] glasses,[39] filters,[40] and layered systems[41] have been investigated and showed efficient optical limiting properties. Several inorganic nanomaterials such as CNTs, metal nanowires have also been investigated for broad band optical limiting applications. Among all the inorganic nanomaterials CNTs have been extensively studied and exhibit broad band optical behavior.[27] So CNTs are also known as benchmark optical limiting materials. Optical limiting properties of gold nanoparticles have also been studied and their size effect has been investigated.[42a] However most of the nonlinear optical studies on noble metal nanoparticles have been investigated for nanosecond laser pulses at 532nm.[42a-42d] The optical limiting properties of gold and silver nanoparticles of spherical and anisotropic nanoparticles have been investigated.[42] Broad band optical limiting properties of amine capped gold nanoparticles have been studied for both nanosecond and femtosecond laser pulses.

1.5. Surface enhanced Raman spectroscopy (SERS)

Surface-enhanced Raman scattering (SERS) spectroscopy is the most widely pursued and powerful spectroscopic technique for molecular sensing applications since it identifies molecules by their unique “fingerprints” (a set of vibrational modes that are characteristic of each type of molecule). As the name indicates, SERS is a branch of Raman spectroscopy. Conventional Raman scattering is inherently weak due to the low efficiency of inelastic photon scattering by molecules. The Raman cross section of molecules is typically 10^{-30} cm^2, which is not comparable with the typical absorption or fluorescence cross section (10^{-14}–10^{-15} cm^2). The extremely low efficiency of Raman scattering limits the practical applications of Raman spectroscopy. The invention of lasers in the 1960s, enabled the wide applicability of Raman spectroscopy. The major discovery in the 1970s that a silver electrode surface can greatly enhance the Raman signals by a factor of 10^5–10^6 ,which allows the monitoring of electrochemical processes at the electrode surface at the molecular level.[43] Van Duyne et. al[43a] have done lots of research and development in the field of SERS spectroscopy. In a systematic study by Van Duyne et.al found a fourth-power dependence of the observed Raman signals and further proposed an electric field enhancement apart from a resonance enhancement.[43a] Subsequently, Schatz et al.[44] provided a theoretical model to explain the large enhancement of Raman intensity. Due to these initial observations of large enhancement of SERS signal on rough metal surfaces, surface-enhanced Raman spectroscopy has revolutionized in the 1980s. Several studies were performed on gold and silver nanoparticles of different sizes and shapes, which precluded an in-depth study of the SERS enhancing mechanisms. Currently, two mechanisms are generally accepted for the observed large enhancement of SERS signals: surface electromagnetic (EM) field enhancement and chemical contribution. The chemical effect usually contributes a factor of 10^2, enhanced electromagnetic field contributes dominantly with an enhancement factor of up to $10^{7\sim}10^{12}$. Recent studies on gold nanoparticles aggregates suggested that enhancement factor of 10^{14} times could be achieved [45]. The large enhancement factor for the gold nanochains is comparable to the enhancement factor reported by Zhang et al. [46] In their SERS study (Zhang et al.[46]) of Na_2 S induced gold aggregates, a SERS enhancement of 10^7-10^9 was reported.

The intensity of the Raman scattered radiation is proportional to the square of the magnitude of any electromagnetic (em) fields incident on the analyte.

$I_R \propto E^2$, where I_R is the intensity of the Raman field, and E is the total em fields coupling with the analyte; and where

$E = E_a + E_p$

for which E_a is the em field on the analyte in the absence of any roughness features and E_p is the electromagnetic field emitted from the particulate metal roughness feature.

The enhancement factor (EF) is determined by comparing the concentration-normalized SERS signal of the Raman reporters with their bulk Raman intensity. The surface enhancement factor can be calculated from the equation,

$SEF = (I_{sig}/C_{sig})/(I_{ref}/C_{ref})$, where I_{sig} and I_{ref} represents the integrated intensities of the SERS signal and reference respectively, whereas C_{sig} and C_{ref} represent the concentration of the sample on the SERS substrate (for example: Nanoparticle film) and on reference (for example: quartz).

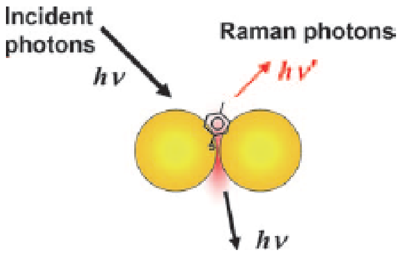

Fig.1.13 Schematic representation of Hot spots between two nanoparticles (Reproduced by permission of John Wiley and Sons[45])

It has been observed that the strong electromagnetic enhancement in the gap between the two nanospheres is due to particle coupling (See fig.1.13).[45] So, the molecules in this hot spot region sense the huge electric field and give rise to dramatically enhanced Raman signals, typically a few orders of magnitude greater than that achievable with single nanoparticles. The enhancement is quite sensitive to the gap between the nanospheres. Recently active research has been carried out to understand the SERS enhancement on coupled nanoparticles of different coupling strength. In this thesis I present our studies of the applications of gold nanochains (coupled nanoparticles) for SERS and observed 400 times stronger signal compared to individual spherical nanoparticles.

1.6. Ultrafast Dynamics of Metal Nanocrystals

The behavior of electron dynamics in metallic nanoparticles is different than these observed in the corresponding bulk metal. Femtosecond techniques have been extensively used to investigate the different elementary scattering mechanisms in bulk metal, and, recently metal nanoparticles.[47, 48] These are based on selective electron excitation on a time scale shorter than that of the electron-electron relaxation time. Fig. 1.14, shows the energy relaxation following the excitation of the nanoparticle with a femtosecond pulse. Different time scales are involved after the excitation of nanoparticles with ultra short laser pulse. Initially, the energy is transferred to the electrons by absorption of photons via interband and intraband transitions. The injected energy is subsequently redistributed among the electrons by electron-electron (e-e) scattering eventually leading to the establishment of an electron temperature, and transferred to the lattice by electron-phonon (e-ph) interactions, leading to thermalization of the metal electron gas and lattice (Figure 1.14). These two processes usually take place on similar time scales (for instance, about 0.5 and 1 ps, respectively, in gold) and mutually influence each other on a subpicosecond time scale. Finally the energy is transferred to the solvent via phonon-phonon relaxation.[49, 50] These processes can be selectively monitored by measuring the transient optical properties of metal nanocrystals using pump-probe spectroscopy. The ultrafast dynamics of noble metal nanocrystals of various sizes and shapes have been studied in the past.[50]

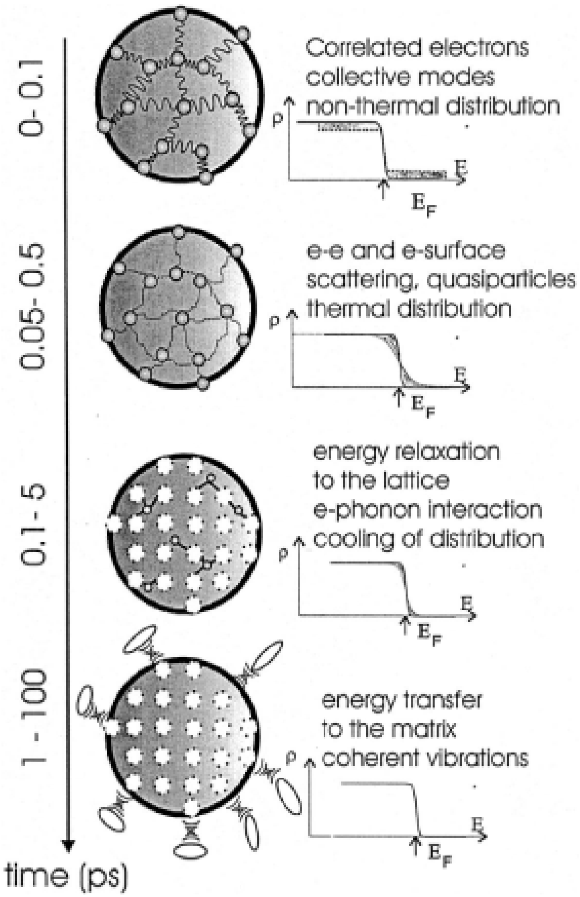

Fig. 1.14 Sketch of the relaxation processes in a metallic nanoparticle (Reproduced by permission of Elsevier[50])

1.7. Noble metal nanoparticle inks for printable electronics

Printed electronics represent an emerging area of research that promises large markets due to the ability to bypass traditional expensive and inflexible silicon-based electronics to fabricate a variety of devices on flexible substrates using high-throughput printing approaches .Recent devolopments in printed electronics has opened the doors for the manufacturing of light weight, flexible, cost-efficient electronic devices that have advantages beyond those of conventional silicon-based devices.[51-55] A recent report has valued the market for printed and thin film electronics at \$1.92 billion in 2010 and this is predicted to grow to \$335 billion by 2030.[56] Currently printed electronic devices such as field effect transistors, photovoltaics, radio frequency identification tags, displays and sensors are driving the market. All these devices require electrical contacts and various materials such as graphene, carbon nanotubes, polymers and metals have been used as electrodes. Among all these conductive materials metal electrodes have been widely used for majority of the electronic devices due to their high conductivity. Different physical methods such as vacuum evaporation, photolithography, sputtering etc have been conventionally used to fabricate conductive metal electrodes for various electronic devices. The fabrication of conductive electrodes by a solution process offers several advantages such as flexibility, low temperature, role-to-roll processing and reduced cost over conventional deposition techniques. Several research groups are actively involved in developing metal nanoparticle inks (NP ink) and metal organic decomposition inks (MOD ink) for printable electronics Inkjet printing technology can be utilized to direct printing of metal contacts using the conductive metal nanoparticle inks, overcoming the disadvantages of physical deposition methods.[57] Among all the metals noble metals (Ag, and Au) are highly conductive. So the noble metal nanocrystals are good candidates for printing the electrical contacts.

1.7.1. Post-printing processes for metallic inks

The nanoparticle inks used for the printing of electrical contacts are either organic or aqueous dispersions of metal NPs protected by organic capping agents. These organic ligands usually prevent the electrons moving from one particle to another and acts as insulators. After printing the electrical contact using the nanoparticle ink, the resistivity of the resultant electrical contact is too high due to the presence of insulating organic capping agents on the nanoparticles. This problem can be overcome by sintering the electrical contact after printing it and the sintering can be achieved by annealing the substrate to higher temperatures, laser irradiation, microwave irradiation, or chemical treatment.[58] The particles diffuse into one another as schematically depicted in Fig.1.15 after the sintering process. However, only expensive high-performance polymers, like polytetrafluoroethylene, polyetheretherketone and polyimide can be used at high temperatures, which represent a drawback for implementation in large area production and are not favorable in terms of costs.

Both NP and MOD inks require an additional processing step to form a conductive pattern. In MOD inks, this additional step typically uses heat to precipitate the metal and burn off the organic component or, in the case of NP inks, the heat decomposes the organic stabilizer. Both types of ink require that the particles then sinter together to form a conductive feature. The reduced sintering temperatures offered by NP inks are due to the size of the nanoparticles.[59, 60] On the other hand, MOD inks generate the conductive films at lower temperatures.[61] For the metal NP inks, the curing temperature is defined as the temperature where particles lose their organic shell and start showing conductance by direct physical contact. But, the sintering takes place at a higher temperature when all the organic material has been burnt off and necks begin to form between particles. So it is very important that the sintering temperature and sintering time must as low for the plastic compatibility. Recently several research groups are actively involved in developing the nanoparticle inks that can be sintered at low temperature to make the conductive films.[62, 63, 64, 65]

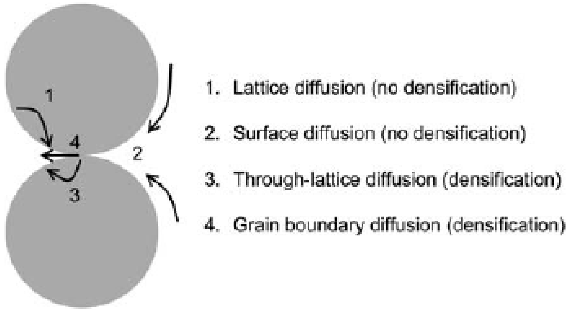

Fig.1.15 A schematic representation of various atomic diffusion paths between two contacting particles. Paths 1 and 2 do not produce any shrinkage while paths 3 and 4 enable the sphere centres to approach one another, resulting in densification (Reproduced by permission of Royal Society of Chemistry [65])

1.8. Experiment Techniques

1.8.1. Optical limiting technique

The optical limiting properties of metal nanoparticles at 532 nm and 1064 nm with pulse durations of 7 ns were measured by fluence-dependent transmittance measurements. The experimental set-up is shown in figure 1.16. The laser pulses were generated from a *Q*-switched Nd: YAG (yttrium aluminum garnet) laser (Spectra Physics

DCR3). The primary laser output had a center wavelength of 1064 nm, with pulse duration of 7 ns and a repetition rate of 10 Hz. The 1064 nm output was frequency-doubled to obtain 532 nm laser pulses. The laser beam was focused onto the nanoparticle solution contained in a 1-cm-pathlength quartz cuvette. The transmittance of the laser pulses were measured at different excitation intensities. The nonlinear scattering measurements were performed by placing the detector at different angles from the direction of the transmitted laser beam. The experimental set-up used in our laboratory is shown in figure 1.17

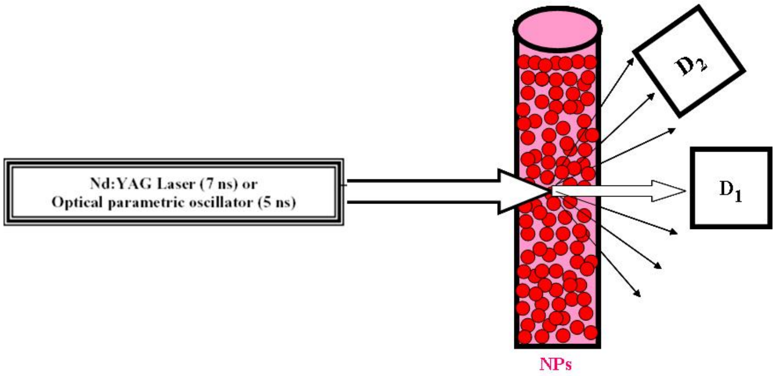

Fig. 1. 16 Experimental setup for optical limiting measurements. D_1, D_2 are detectors

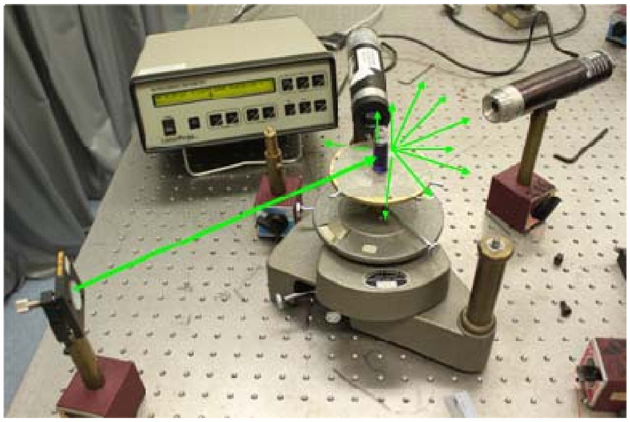

Fig. 1.17 Photograph of the experimental set-up used for the Optical limiting measurements

1.8.2. Pump-Probe technique

The transient absorption measurements were carried out with a standard pump-probe setup by using a femtosecond Ti: sapphire laser system (Spectra Physics), which is shown in Fig. 1.18. The laser pulses were generated from a mode-locked Ti:sapphire oscillator seeded regenerative amplifier with a pulse width and energy of 100fs and 2mJ at 800 nm and a repetition rate of 1 kHz. The 800 nm laser beam was split into two portions. The larger portion of the beam was passed through a BBO crystal to generate the 400 nm pump beam by frequency-doubling. A small portion of the 800 nm pulses was used to generate white light continuum in a 1 mm sapphire plate. The white-light continuum was split into two beams, a probe and a reference beam. The signal and reference beams were detected by photodiodes that are connected to lock-in amplifiers and the computer. The intensity of the pump beam was attenuated with a neutral density filter. The pump beam is focused onto the sample with a beam size of 300 μm and overlaps with the smaller-diameter (100 μm) probe beam. The delay between the pump and probe pulses was varied by a computer-controlled translation stage. The pump beam was modulated by an optical chopper at a frequency of 500 Hz. In a pump-probe scan the value of the normalized pump-induced absorption change (ln (T/T_0)) was determined as a function of the delay τ between the pump and probe pulses. The transient absorption spectra at different delay times was measured by passing the probe beam through a monochromator before detected by a photodiode that is connected to the lock-in amplifier.

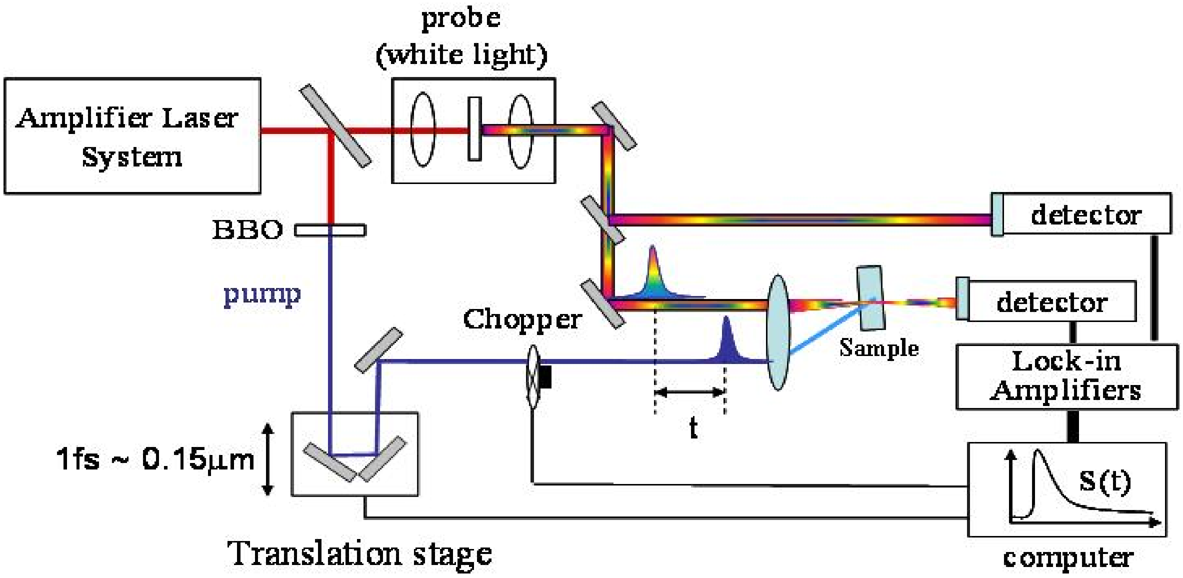

Fig. 1.18 Pump- Probe experimental set up used in our study

1.8.3. Z-scan technique

The measurements of nonlinear optical properties with femtosecond laser pulses were conducted using Z-scan technique. The experimental set-up is shown in figure 1.19. This technique is based on the variation of light intensity by altering geometrical parameters of light-matter interaction. This is achieved by scanning or moving a sample along the axis of propagation (z) of a focused laser beam through its focal plane and measuring the transmission (T) of the sample for each z position. As the sample experiences different electric field strengths at different z positions, the recording of the transmission as a function of the z coordinate provides accurate information about the nonlinear effects present in the sample.

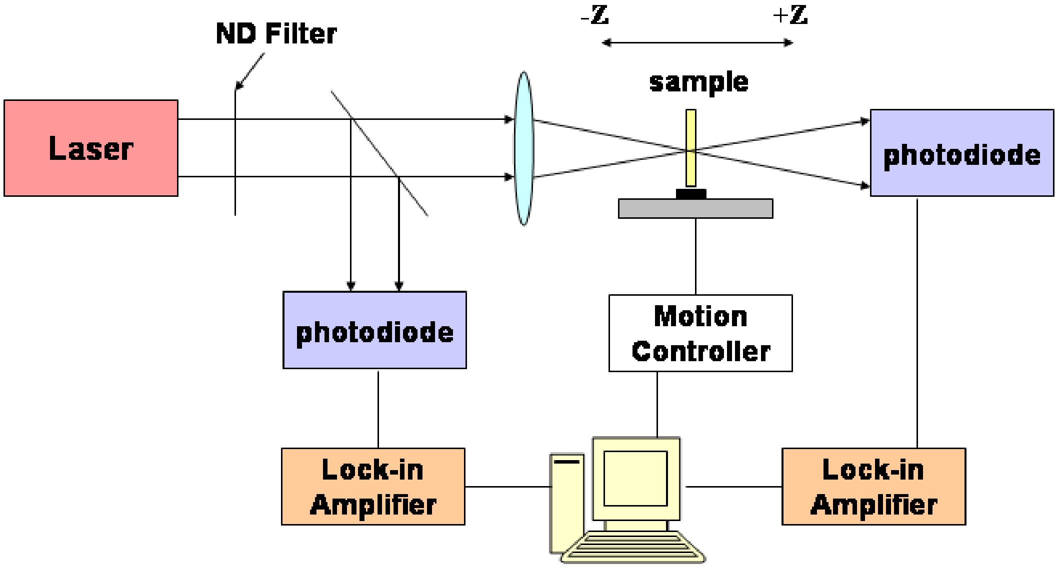

Fig. 1.19 Z-scan experimental set-up used in our study

1.8.4. Two-Photon Induced Fluorescence

The two-photon induced fluorescence of gold nanoparticles was measured by exciting with 800nm femtosecond laser pulses (pulse width of 30fs) . The experimental setup for the TPIF technique is illustrated in Figure 1.20. The laser beam was first focused on our sample with a convex lens. The intensity of the beam at the sample was then high enough for two-photon absorption to take place. The emission from the sample was collected at a 90^0 angle by a pair of high numerical aperture lens and optical fibers and directed to the spectrometer, which is a monochromator coupled CCD system.

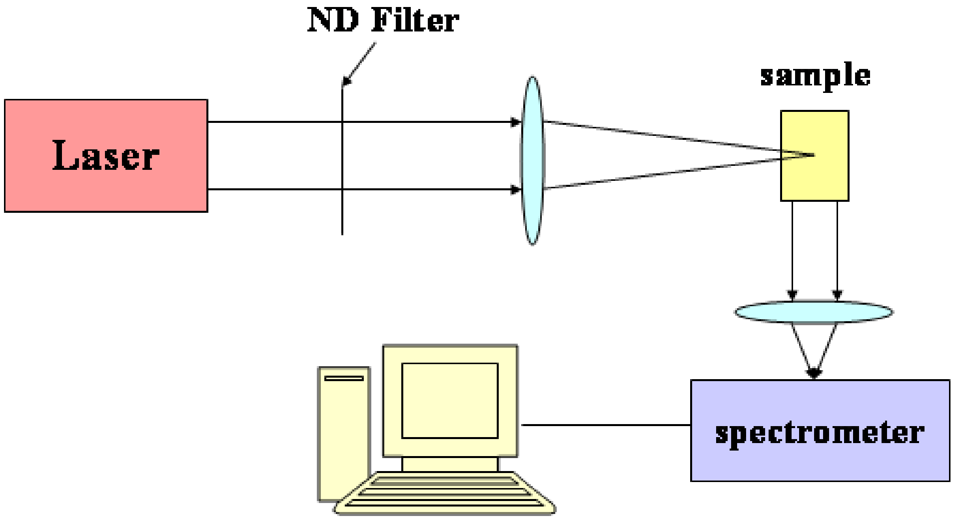

Fig. 1.20 Schematic diagram for the two-photon induced fluorescence (TPIF)

1.9. Objective and scope of thesis

This thesis investigates the nonlinear optical properties of gold and silver metal nanoparticles of various shapes and sizes using nanosecond and femtosecond laser pulses. In the current study we also focus on the development of simple methods for the preparation of organic and aqueous dispersions of gold and silver nanoparticle inks with low preparation cost. The sintering temperature was tuned by changing the protecting agent.

In Chapter 2, we explored the nonlinear optical properties of pure Ag nanoprisms and Au@Ag core-shell nanoprisms in solution that were photochemically prepared. The results showed that the optical limiting properties of two kinds of silver nanoprisms in solution were slightly better than that of carbon nanotube suspensions, which is a known benchmark optical limiter. Nonlinear scattering experiments suggested that nonlinear scattering should play an important role in the observed optical limiting effects.

In Chapter 3, we explored a simple method for the large scale preparation of monodisperse gold nanoparticles by a simple method at room temperature. The as-prepared gold nanoparticles have high monodispersity with an average diameter of 13 nm and can self-organize into two-dimensional (2D) hexagonal close-packed arrays. The electron relaxation dynamics of these gold nanoparticles shows that the phonon-phonon relaxation time of gold nanoparticles in toluene is slower than that of citrate capped gold nanoparticles in water, due to a lower thermal conductivity of toluene than water. The electron-phonon relaxation of the gold nanoparticles in toluene was found to display weaker pump-energy dependence, compared to that of citrate capped gold nanoparticles in water.

In Chapter 4, we have explored the broadband optical limiting properties of oleylamine capped gold nanoparticles in solution using both femtosecond and nanosecond laser pulses. The oleylamine capped gold nanoparticles were found to show strong broadband optical limiting effects with threshold lower than that of carbon nanotubes for nanosecond laser pulses at 532 nm and 1064 nm and femtosecond laser pulses at 780 nm. Input fluence and angle dependent scattering measurements suggested that nonlinear scattering played an important role in the observed optical limiting behavior at 532 nm and 1064 nm.

In Chapter 5, we explored the one- and two-photon excitation emission properties of water soluble biocompatible glutathione monolayer protected gold clusters. Strong two-photon emission was observed from the gold clusters. The two-photon absorption cross section of these gold clusters in water was deduced from the z-scan measurement to be 189 740 GM, which is much higher compared to organic fluorescent dyes and quantum dots. These gold clusters also showed high photo-stability. We have successfully demonstrated their applications for both one and two-photon excitation live cell imaging.

In Chapter 6, we presented simple strategies to assemble the gold nanoparticles into a 1D nanostructure by using amino acid or water soluble conjugated polymer. In the first method, the self assembled gold nanoparticles were prepared in a single step by reducing aqueous chloroaurate ions ($AuCl^{-4}$) with sodiumborohydride in the presence of an amino acid (glutamic acid and histidine) as a stabilizer. The nonlinear optical properties of self assembled gold nanoparticles showed an optical switching behavior from saturable absorption to reverse saturable absorption as the pump intensity increase. In another method, gold nanochains were prepared by the assembly of citrate-stabilized gold nanospheres induced by cationic conjugated polymers. A longitudinal plasmon resonance band was formed as a result of the plasmon coupling of gold nanoparticles and can be tuned from visible to near infrared by adjusting the polymer/Au molar ratio. The gold nanochains were used as a SERS substrate and gave a large enhancement, which was~400 times larger than that of an isolated gold nanosphere substrate.

In Chapter 7, we have demonstrated a facile and general method for the preparation of alkylamine capped metal (Au & Ag) nanoparticle inks with high solubility. Using metal nanoparticle “inks”, we have demonstrated their applications for the large scale fabrication of highly efficient surface enhanced Raman scattering substrates (SERS) by a facile solution processing method. Insulator-to-metal transition properties of the alkylamine capped metal nanoparticle films were explored and the transition temperatures could be tailored to plastic compatible temperatures by using proper alkylamine as the capping agent. The applications of these high concentrated alkylamine capped metal nanoparticle inks for the printable electronics were demonstrated by printing the oleylamine capped gold nanoparticles ink as source and drain for a graphene field-effect transistor. Furthermore, the broadband photoresponse properties of the Au and Ag nanoparticle films have been studied by using visible and IR lasers.

In Chapter 8, we have developed a simple method for the preparation of aqueous silver nanoparticle ink that can be printable at room temperature. We have demonstrated that the silver ink can be used to fabricate highly conductive films on glass and flexible plastic substrates by depositing the nanoparticle dispersion onto the substrate and evaporating the solvent. The application of Ag nanoparticle ink for printable cathode material for P3HT-PCBM bulk heterojunctions solar cells with an efficiency of 2.25% has been demonstrated**.**

1.10. References

1. Nam, J. M.; Thaxton, C. S.; Mirkin, C. A. *Science,* 2003, **301**, 1884–1886.
2. Seker, F.; Malenfant, P. R. L.; Larsen, M.; Alizadeh, A.; Conway, K.; Kulkarni, A. M.; Goddard, G.; Garaas, R. *Ad*V. *Mater.,* 2005, **17,** 1941–1945.
3. Reece, P. J. *Nat. Photonics,* 2008, **2**, 333–334.
4. Ramakrishna, G.; Varnavski, O.; Kim, J.; Lee, D.; Goodson, T. *J. Am. Chem. Soc.,* 2008, **130,** 5032
5. Kamat PV, *J.Phys.Chem.B,* 2002, **106,** 7729

6. Xia YN, Halas NJ, *MRS BULLETIN,* 2005, **30,** 338

7. D. J. Barber and I. C. Freestone, Archaeometry, 1990, **32**, 33.

8. G. L. Hornyak, C. J. Patrissi, E. B. Oberhauser, C. R. Martin, J.C. Valmalette, L. Lemaire, J. Dutta and H. Hofmann, *Nanostruct. Mater*., 1997, **9**, 571.

9. Sun YG, Xia YN, *Science,* 2002, **298**, 5601

10. Faraday, M. *Philos. Trans.* 1857, **147**, 145.

11. G. Mie, Ann. Phys. (Leipzig), 1908, **25**, 377.

12. (a) U. Kreibig and M. Vollmer, *Optical Properties of Metal Clusters, Springer, Berlin,* 1995; (b) Huanjun Chen, Xiaoshan Kou, Zhi Yang, Weihai Ni, and Jianfang Wang, *Langmuir*, 2008, **24**, 5233-5237

13. Stephan Link and Mostafa A. El-Sayed, *Annu. Rev. Phys. Chem*., 2003, **54,** 331

14. Bohren C.F, Huffman D.R. *Absorption and Scattering of Light by Small Particles,* Wiley, New York ,1983.

15. Papavassiliou G.C.. *Prog. Solid State Chem.*1979, **12**, 185.

16. Mott, N.F., Jones, H. *The Theory and Properties of Metals and Alloys,* Oxford Press, Oxford, 1936, 105.

17. He, G .S., Liu S. H., *Physics of Nonlinear Optics,* World Scientific Publishing Co. Pvt. Ltd., Singapore (1999).

18. Sutherland R. L., *Handbook of Nonlinear Optics*, Marcel Dekker Inc., New York (1996).

19. (a) Kim S., McLaughlin D., Potasek M., *Phys. Rev. A*, 2000, **61**, 025801; (b) Lepkowicz R., Koyakov A., Hagan D. J., Strylabd E.W.V., *J. Opt. Soc. Am. B*, 2002, **19**, 94.

20. L. W. Tutt and A. Kost, Nature (London), 1992, **356**, 225.

21. Hagan D. J., Van Stryland E. W., Wu Y. Y., Wei T. H., Sheik-Bahae M., Said A., Mansour K., Young J., Soileau M.J., *Materials for Optical Switches, Isolators, and Limiters*; Proceedings of SPIE, SPIE: Bellingham, WA, 1981, **1105**, 103.

22. Van Stryland E. W., Soileau M. J., Ross S., Hagan D., *J. Nonlinear Optics*, 1999, **21**, 29 .

23. Tutt, L. W.; Boggess, T. F. *Prog. Quant. Elcetron.,* 1993, **17**, 299.

24. Kukaswadia, A. K.; Feng, Z. C.; Tang, S. H. *J. Appl. Phys.,* 1994, **75**, 3340.

25. W. Vanstryland, Y. Y. Wu, D. J. Hagan, M. J. Soileau, and K. Mansour, J. Opt. Soc. Am. B, 1988, **5**, 1980.

26. R. G. Ispasoiu, L. Balogh, O. P. Varnavski, D. A. Tomalia, and T. Goodson, J. Am. Chem. Soc., 2000, **122**, 11005.

27. P. Chen, X. Wu, X. Sun, J. Lin, W. Ji, and K. L. Tan, Phys. Rev. Lett., 1999, **82**, 2548.

28. Jun Wang and Werner J. Blau, *J. Phys. Chem. C,* 2008, **112,** 2298.

29. Wood, G. L.; Mott, A. G.; Sharp, E. J. *Proc. SPIE*, 1992, **2**, 1692.; (b) Hollins, R. C. *Nonlinear Optics*, 2001, **27**, 1.

30. (a) Lawson, C. M.; Euliss, G. W.; Michael, R. R. *Appl. Phys. Lett.,* 1991, **58**, 2195 ; (b) Micheal, R. R.; Lawson, C. M. *Opt. Lett.,* 1992, **17**, 1055; (c) Durand, O.; Grolier-Mazza, V.; Frey, R. *Opt. Lett.,* 1998, **23**, 1471; (d) Fougeanet, F.; Riehl, D. *Nonlin. Opt.,* 1999, **21**, 435; (e) Hernandez, F. E.; Shensky, W.; Cohanoschi, I.; Hagan, D. J.; Strylabd, E. W. V. *Appl. Opt*., 2002, **41**, 1103. (f) N. Venkatram, D.Narayana rao, M.A. Akundi, *Optics express,* 2005, 13, 867.

31. (a) Messier, J.; Kajzar, F.; Prasad, P. *Organic molecules for Nonlinear Optics and Phtotonics*, Series E, applied Science, Kluwer Academic Publishers: New York, **194** (1991); (b) Shirk, J. S.; Pong, R. G. S.; Bartoli, F. J.; Snow, A. W. *Appl. Phys. Lett.*, 1993, **63**, 1880.

32. Kiran, P. P.; Srinivas, N. K. M. N.; Reddy, D. R.; Maiya, B. G.; Sandhu, A. S.; Dharmadhikari, A.; Kumar, G .R.; Rao, D. N. *Opt. Commun*., 2002, **202**, 347.

33. a) Taheri, B.; Liu, H.; Jassemnejad, B.; Appling, D.; Powell, R. C.; Song, J. J. *Appl. Phys. Lett*., 1996, **68**, 1317.; (b) Sun, Y-P.; Riggs, J. E.; Liu, B. *Chem. Mater*., 1997, **9**, 268 ; (c) Ma, B.; Riggs, J. E.; Sun, Y.-P. *J. Phys. Chem. B*, 1998, **102**, 5999.

34. (a) Khoo, I. C.; Wood, M. V.; Lee, M.; Guenther, B. D. *Opt. Lett.*, 1996, **21**, 1625 ; (b) Ono, H.; Kawatsuki, N. *Opt. Commun*., 1997, **139**, 60.

35. Rao, D. N.; Yelleswarapu, C. S.; Kothapalli, S. R.; Rao, D. V. G. L. N. *Optics Express*, 2003, **11**, 2848.

36. Rao, D. N.; Kiran, P. P. *Nonlinear Optics*, 2001, **27**, 347.

37. Scalora, M.; Dowling, J. P.; Bowden, C. M.; Blemer, M. J. *Phys. Rev. Lett*., 1994, **73**, 1368

38. (a) Bentivegna, F.; Canve, M.; Georges, P.; Brun, A.; Chaput, F.; Malier, L.; Boilot, J. C. *Appl. Phys. Lett*., 1993, **62**, 1721; (b) Schell, J.; Brinkmann, D.; Ohlmann, D.; Honerlage, B.; Levy, R.; Joucia, M.; Rehspringer, J. L.; Serughetti, J.; Bovier, C. *J. Chem. Phys*., 1998, **108**, 8599.

39. Bindra, K. S.; Oak, S. M.; Rustagi, K. C. *Opt. Commun*., 1996, **124**, 452.

40. Fischer, G. L.; Boyd, R. W.; Moore, T. R.; Sipe, J. E. *Opt. Lett*., 1996, **21**, 1643.

41. (a) Herbert, C. J.; Cpinski, W. S.; Malcuit, M. S. *Opt. Lett.*, 1992, **17**, 1037; (b) Kahn, L. M. *Phys. Rev. B*, 1996, **53,** 1429.

42. (a) Francois, L.; Mostafavi, M.; Belloni, J.; Delaire, J. A. *Phys. Chem. Chem. Phys.* 2001, **3**, 4965; (b) S. Porel, S. Singh, S. S. Harsha, D. N. Rao, and T. P. Radhakrishnan, Chem. Mater., 2005, **17**, 9; (c) M. Anija, J. Thomas, N. Singh, A. S. Nair, R. T. Tom, T. Pradeep, and R. Philip, Chem. Phys. Lett., 2003, **380**, 223; (d) H. I. Elim, J. Yang, J. Y. Lee, J. Mi, and W. Ji, Appl. Phys. Lett., 2006, **88**, 083107.

43. (a) D. L. Jeanmaire, R. P. Van Duyne, J. Electroanal. Chem., 1977, **84**, 1; (b) M. G. Albrecht, J. A. Creighton, J. Am. Chem. Soc., 1977, **99**, 5215; (c) M. Fleischmann, P. J. Hendra, A. J. McQuillan, Chem. Phys. Lett., 1974, **26**, 163.

44. F. W. King, R. P. Van Duyne, G. C. Schatz, J. Chem. Phys., 1978, **69**, 4472

45. a) S. Nie, S. R. Emory, Science 1997, **275**, 1102; b) K. Kneipp, Y. Wang, H. Kneipp, L. T. Perelman, I. Itzkan, R. R. Dasari, M. S. Feld, Phys. Rev. Lett., 1997, **78**, 1667.

46. Schwartzberg, A. M.; Grant, C. D.; Wolcott, A.; Talley, C. E.; Huser, T. R.; Bogomolni, R.; Zhang, J. Z. *J. Phys. Chem. B,* **2004**, *108*, 19191–19197.

47. W.S. Fann, R. Storz, H.W.K. Tom, J. Bokor, Phys. Rev. Lett., 1992, **68**, 2834.

48. W.S. Fann, R. Storz, H.W.K. Tom, J. Bokor, Phys. Rev. B, 1992, **46**, 13592.

49. Link, S.; El-Sayed, M. A., *Int. Rev. Phys. Chem.* 2000, **19** 409

50. J. -Y. Bigot, V. Halté, J. -C. Merle and A. Daunois, Chem. Phys., 2000, **251**, 181

51. R. A. J. Jansen and M. Gr€atzel, J. Mater. Chem., 2009, **19**, 5261.

52. V. Shrotriya, Nat. Photonics, 2009, **3**, 447.

53. M. Hilder, B. Winther-Jensen and N. B. Clark, *J. Power Sources*, 2009, **194**, 1135.

54. S.-C. Chang, J. Liu, J. Bharathan, Y. Yang, J. Onohara and J. Kido, Adv. Mater., 1999, **11**, 734.

55. T. Sekitani, H. Nakajima, H. Maeda, T. Fukushima, T. Aida, K. Hata and T. Someya, Nat. Mater., 2009, **8**, 494.

56. http://www.lope-c.com, accessed 20th January 2010.

57. J. Perelaer, A. W. M. de Laat, C. E. Hendriks and U. S. Schubert, J. Mater. Chem., 2008, **18**, 3209.

58. P. J. Smith, D.-Y. Shin, J. E. Stringer, N. Reis and B. Derby, *J. Mater. Sci.*, 2006, **41**, 4153.

59. D. Huang, F. Liao, S. Molesa, D. Redinger and V. Subramanian, *J. Electrochem. Soc.*, 2003, **150**, 412.

60. C.-A. Lu, P. Lin, H.-C. Lin and S.-F. Wang, Jpn. J. Appl. Phys., 2007, **46**, 251.

61. J. J. P. Valeton, K. Hermans, C. W. M. Bastiaansen, D. J. Broer, J. Perelaer, U. S. Schubert, G. P. Crawford and P. J. Smith, *J. Mater. Chem.*, 2010, **20**, 543.

62. P. Kr€ober, J. T. Delaney, J. Perelaer and U. S. Schubert, *J. Mater. Chem.*, 2009, **19**, 5234.

63. D. P. Li, D. Sutton, A. Burgess, D. Graham and P. D. Calvert, *J. Mater. Chem*., 2009, **19,** 3719.

64. S. M. Bidoki, D. M. Lewis, M. Clark, A. Vakorov, P. A. Millner and D. McGorman, *J. Micromech. Microeng.*, 2007, **17**, 967.

65. Jolke Perelaer, Patrick J. Smith, Dario Mager, Daniel Soltman, Steven K. Volkman, Vivek Subramanian, Jan G. Korvinkd and Ulrich S. Schubert, *J. Mater. Chem*., 2010, **20**, 8446

CHAPTER 2

NONLINEAR OPTICAL PROPERTIES OF SILVER NANOPRISMS

2.1 Introduction

The fine control over the synthesis of metal nanostructures of different sizes and shapes opened up new possibilities to design ideal building blocks for future optical devices. Optical limiters display a decreasing transmittance as a function of laser intensity, fluence, or irradiance.[1] Fast response optical limiting materials can be used for eyes and sensors protection from laser induced damage. Strong optical power limiting properties have been observed in various materials such as carbon nanotubes (CNTs),[2] C_{60},[3] carbon-black suspension,[4] metallophtalocyanines,[5] quantum dots,[6] and dendrimer molecules.[7] Metal nanoparticles, such as silver and gold, have attracted a lot of attention due to their potential applications in biological, optoelectronic, and photonic technologies.[8–11] Metal nanoparticles are easy to prepare, have good chemical and thermal stability, and display many interesting linear and nonlinear optical properties.[12,13] The linear and nonlinear optical properties of gold and silver nanoparticles are strongly dependent on their sizes, shapes, and the dielectric environment of the nanoparticles.[12,13] Recently, gold and silver nanoparticles have also been found to exhibit strong optical limiting properties.[14–21] The development of optical limiting materials using metal nanoparticles is attractive because gold and silver nanoparticles are easy to prepare and are highly soluble and stable in aqueous solution.

Here we present exceptional optical limiting properties of two kinds of Ag nanoprisms that were photochemically prepared. One is pure Ag nanoprisms with an 8 nm thickness and another is Au@Ag core-shell nanoprisms with a 16 nm thickness. The optical limiting properties of the two kinds of silver nanoprisms in solution are slightly better than that of carbon nanotube suspensions, which is known as a benchmark optical limiter.[1, 2] Furthermore, the silver nanoprisms reported here are highly soluble and stable in solution and are easy to prepare films on the quartz substrate for various device applications.

2.2 Experimental Section

2.2.1 Synthesis of Ag & Au@Ag core-shell nanoprisms by photochemical method:

The silver nanoprisms were prepared by using a previously reported photochemical method[22] and the Au@Ag core-shell nanoprisms were prepared by using a slightly modified method. The pure nanoprisms were prepared by photo conversion of Ag nanospheres. Briefly, 1.0 mL of 5.0 mM AgNO3 solution and 0.5 mL of 30.0 mM trisodiumcitrate were sequentially added into 47.5 mL of de-ionized water, followed by quickly introducing 0.5 mL of freshly prepared 50.0 mM NaBH4 solution under vigorous stirring. 0.5 mL of 5.0 mg mL^{-1} polyvinylpyrrolidone was then quickly added into the reaction mixture. The mixture was kept stirring for another 30 min until the solution turned to a deep yellow color. 20.0 mL of the prepared silver sphere seeds were then illuminated with a 40 W Philips bulb for 48 h. The yellowish seed solution gradually changed into a dark blue color solution, indicating formation of silver nanoprisms. Au@Ag core-shell nanoparticles were prepared by adding 1.0 ml of 13 nm gold nanoparticles to a 4 nm silver seed solution. These gold nanoparticles were prepared by using a previously reported method.[23] Proper amount of gold nanoparticles were added to the silver seeds so that the ratio of optical densities of silver and gold were 10:1. The mixture of silver and gold nanoparticles was kept under a 40 W Philips bulb for 48 h. The as-prepared Au@Ag core-shell nanoparticles were centrifuged at 1500 rpm for 60 min to separate from the residue gold nanospheres. The nanoprisms were characterized by using UV-visible spectroscopy (Shimadzu UV 2450 spectrometer) and transmission electron microscopy (Philips CM10 electron microscope at an accelerating voltage of 100 Kv). The composition of Au@Ag core-shell nanoprisms was confirmed by energy-dispersive x-ray spectrum (EDS) analysis.

2.2.2 Optical limiting measurements

The optical limiting properties of nanoprism solutions in 1 cm quartz cuvette were characterized by fluence-dependent transmittance measurements using 532 nm and 7 ns pulses generated from a frequency-doubled *Q*-switched Nd:YAG (yttrium aluminum garnet) laser (Spectra Physics DCR3). The laser pulses at 10 Hz repetition rate were focused into the quartz cuvette of 1 cm path length with a spot size of 165 μm. During the experiments, the nanoparticle solutions were stirred to refresh the samples at the laser illumination spot to avoid potential thermal or photoinduced shape transformation. To investigate the mechanism of observed optical limiting behavior, the nonlinear scattering experiments on the solution samples were performed. In the nonlinear scattering experiment, the same 532 nm laser was used as the excitation source. The detector was placed at different planar angles from the propagation axis of the transmitted laser beam and the scattered laser light was collected with a solid angle of 0.00256 sr.

2.3 Results and discussion

Figure 2.1 shows the transmission electron microscopy (TEM) images of two kinds of nanoprisms as well as their corresponding UV-visible extinction spectra in solution. The in-plane sizes are ~100 nm on average for both nanoprisms. The thickness of Au@Ag core-shell nanoprisms (~16 nm) is larger than that of pure silver nanoprisms (~8 nm). The spectral features of the Au@Ag core-shell nanoprisms are quite similar to those of the pure Ag nanoprisms. The in plane plasmon resonance band of the Au@Ag core-shell nanoprisms is well-pronounced and peaked at 800 nm. This in-plane plasmon band is broader in the pure Ag nanoprisms compared to that in Au@Ag core shell nanoprisms due to a larger size distribution, which is consistent with the TEM results shown in Figs. 2.1(a) and 2.1 (b). The peak at 490 nm in the Au@Ag core-shell nanoprisms is due to the gold core. Initially the dipole plasmon resonance bands of the gold and silver nanoparticles are located at 520 and 395 nm, respectively. After 48 h of light irradiation, the 395 nm peak diminished and the gold peak blue shifted from 520 to 490 nm, resulting from formation of Au@Ag core-shell nanoprisms. The similar blue shift of the Au Plasmon band due to coating of an Ag shell has also been previously observed.[24] The EDS analysis showed the gold peak in the Au@Ag core-shell nanoprisms, which is shown in fig.2.2

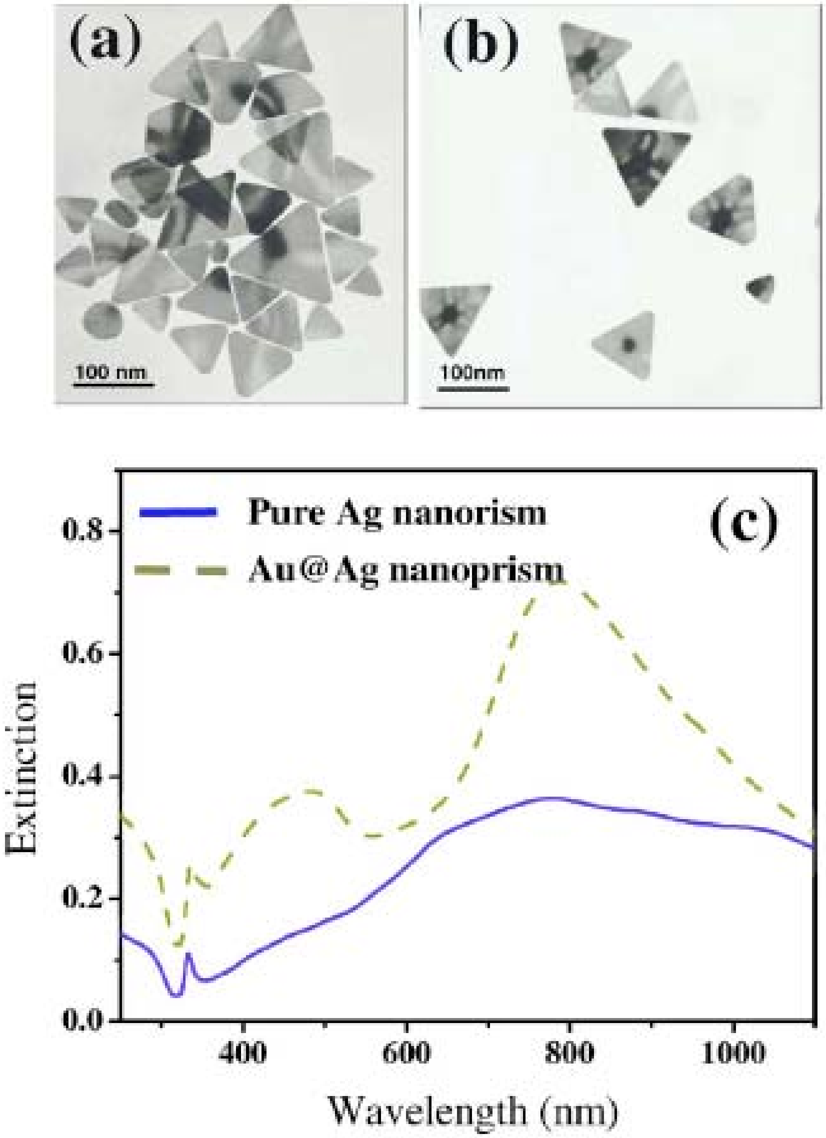

Fig. 2.1 (a) TEM image of pure Ag nanoprisms. (b) TEM image of Au@Ag core-shell nanoprisms. (c) UV-visible spectra of pure Ag nanoprisms and Au@Ag core-shell nanoprisms.

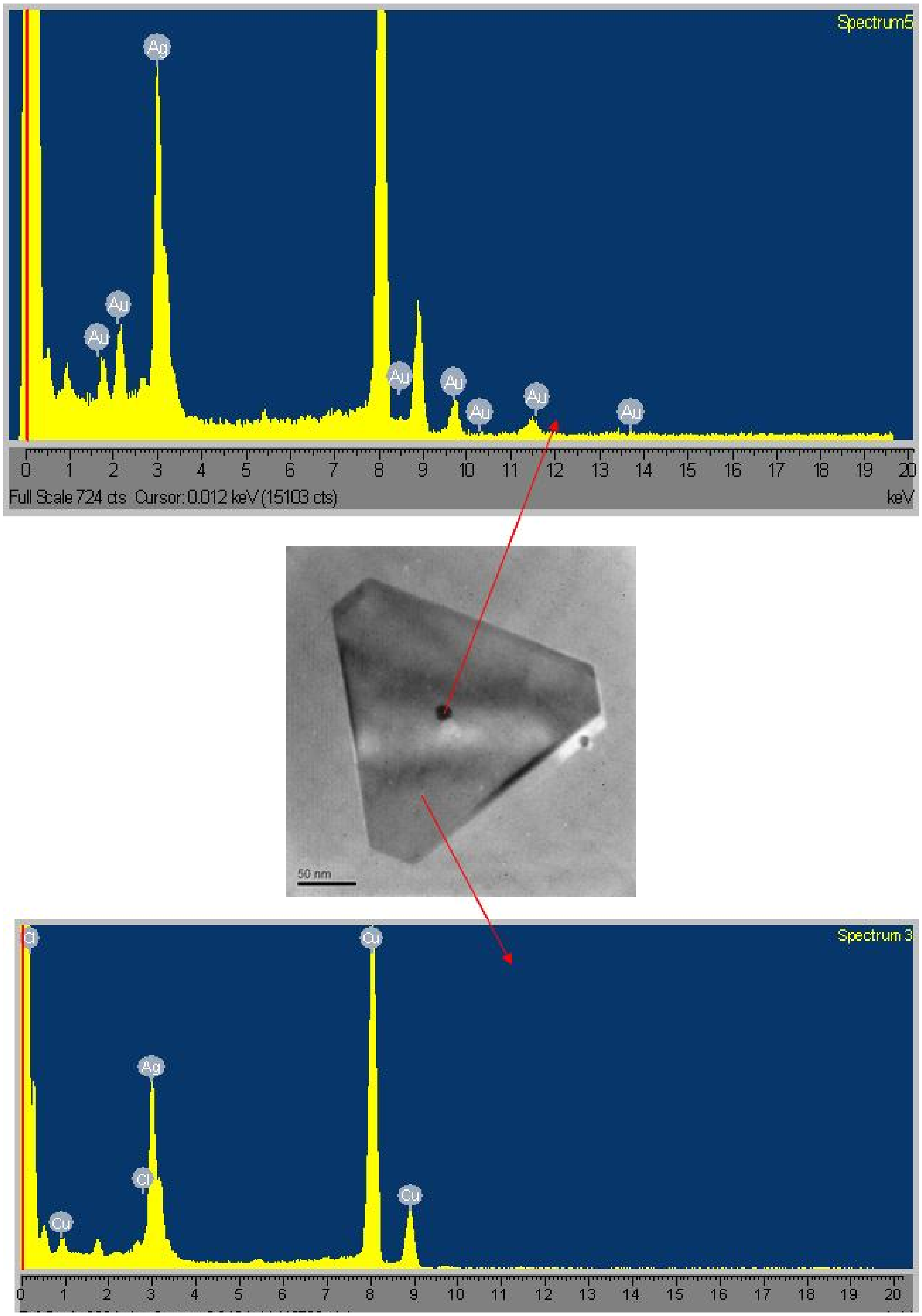

Fig. 2.2 Energy-dispersive x-ray spectrum (EDS) taken on the core and shell of Au@Ag core-shell nanoprism.

2.3.1 Nonlinear optical measurements

The optical limiting properties of the nanoprisms in solution were investigated with fluence-dependent transmittance measurements at 532 nm and the data is shown in Fig. 2.3. The measurements on CNTs suspended in water were also performed under identical experimental conditions for direct comparison. The linear transmittances of all the solutions were adjusted to 70%. The results of CNT suspension are similar to the results previously reported.[2] The transmittance of the CNT suspension was almost constant at low input fluences and the transmittance started to decrease as the irradiance fluence exceeded 0.12 J /cm^2. The fluence dependent transmittance behaviors of two nanoprism samples were quite similar to that of CNT suspension sample and an only subtle difference was observed. For both nanoprisms samples, there was a slight increase in the transmittance at low irradiance fluences, as evidenced by a small hump observed in Fig. 2.3. The observation of small increase in transmittance at low fluences is typical for metal nanoparticle systems, which has been ascribed to plasma saturation.[16, 17] The transmittance also started to decrease when the input fluence exceeded 0.12 J /cm^2, displaying optical limiting activity. The optical limiting properties of two kinds of silver nanoprisms are quite similar to each other and are slightly better than that of the CNT suspension. The limiting threshold is defined as the incident fluence at which the transmittance falls to 50% of the normalized linear transmittance.[2] The limiting threshold was measured to be 1.6, 1.2, and 1.3 J /cm^2 for the CNTs suspension, pure Ag nanoprisms, and Au@Ag core-shell nanoprisms solutions, respectively. Despite the fact the two kinds of nanoprisms are of different thicknesses, their optical limiting properties are very similar to each other. In a previous study on the optical limiting properties of

CNT, it has also been found that the optical limiting properties of CNT with different diameters were similar.[2] Ag and Au nanoparticles have been known to enhance the performance of optical limiter in nanocomposites containing these noble metals, [20, 25] but optical limiting properties of individual three dimensionally confined pure Ag or Au nanoparticles have not been reported so far. Previously optical limiting activity of gold nanoparticle aggregates[18] (threshold of 1.8 J /cm^2) and silver nanowires[19] (threshold of 1.7 J /cm^2) have been reported. The aggregated gold nanoparticles tend to precipitate in shorter times and are not suitable for practical applications. Ag nanowires have a similar long term stability problem and are difficult to prepare. Our silver nanoprisms in solutions have good optical limiting properties, are easy to prepare and can stay stable for a few months. These silver nanoprisms are thus more promising for practical applications.

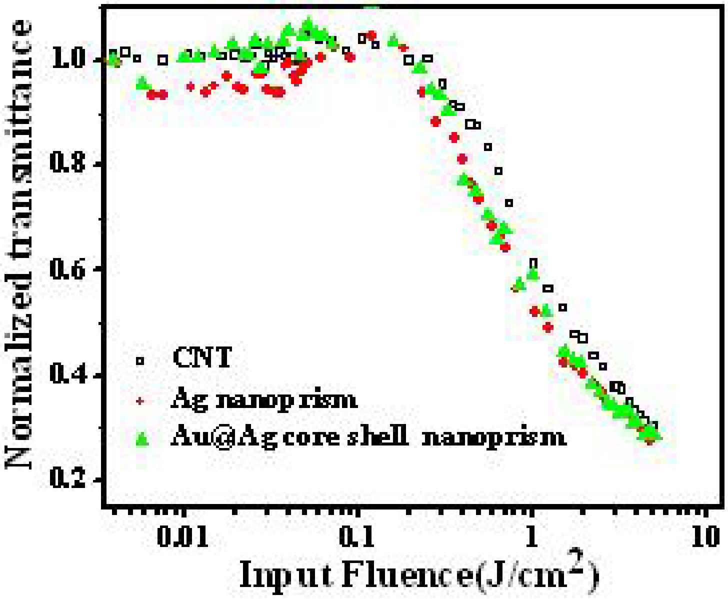

Fig. 2.3 The optical limiting response of the CNT suspension, pure Ag nanoprisms, and Au@Ag core-shell nanoprisms solutions measured using 7 ns laser pulses at 532 nm.

2.3.2 Nonlinear scattering Measurements

Several mechanisms, such as two-photon absorption, reverse saturable absorption, free carrier absorption, and nonlinear scattering, [2,6,19] have been previously proposed to explain the optical limiting effect. The optical limiting activity of semiconductor quantum dots was usually ascribed to two-photon or three-photon absorption.[6] However, the optical limiting activity of metallic nanostructures is more likely induced by nonlinear scattering.[19] To confirm the mechanism of the observed optical limiting activities, we have conducted the scattering measurements for all the samples. The scattering signals were collected at different angles from the propagation axis of the transmitted laser beam. Figure 2.4 shows input laser fluence dependent scattering signal collected at an angle of 20° to the propagation axis of the laser beam for three different samples. For all the three samples, the scattering signals were dominated by linear scattering at low input laser intensities, and became deviated from linear behavior as the input fluence exceeded some threshold value (~1.0 J /cm^2). The contribution from nonlinear scattering became larger with increasing input laser fluences and became the dominant contribution at high pump fluences. The results suggest that nonlinear scattering plays an important role in the optical limiting activity of the silver nanoprisms and CNT samples. These results are consistent with the previous studies on carbon black suspension and multiwalled CNT suspension, [2] in which the nonlinear scattering is the major contributions for optical limiting activity of these materials. The mechanism of nonlinear scattering is likely due to the photoinduced excitation, ionization, and heating of the metal atoms present in nanoprisms, giving rise to the expansion of nanoprisms and making them the scattering centers.[26] Furthermore, energy transfer to the solvent will result in a formation of microplasmas,[2, 26] which can act as secondary scattering centers and lead to further reduction in the transmittance with increasing input laser fluence.

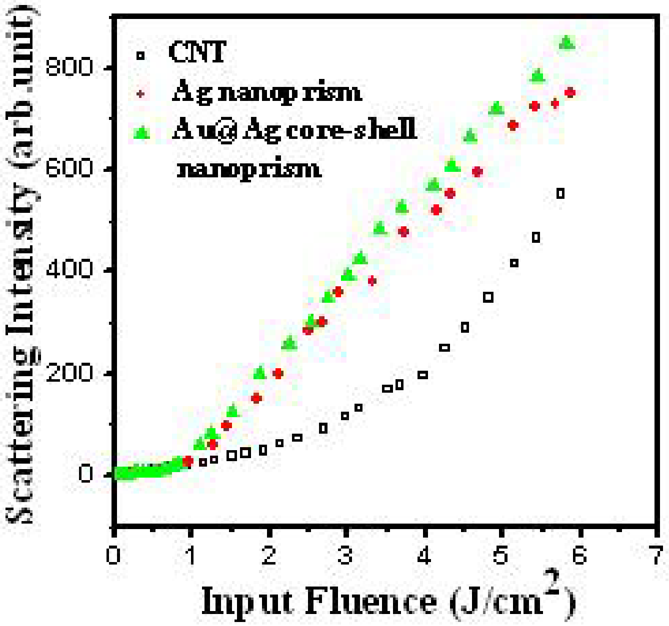

Fig. 2.4 Nonlinear scattering results for the CNT suspension, pure Ag nanoprisms, and Au@Ag core-shell nanoprisms solutions using a 532 nm and 7 ns laser pulses at a forward planar angle of 20° with a solid angle of 0.00256 sr.

2.4 Conclusion

Exceptional optical limiting properties have been observed in two kinds of Ag nanoprisms (pure Ag nanoprisms and Au@Ag core shell nanoprisms). Their optical limiting properties are even slightly better than that of CNT suspension, which was known as a benchmark optical limiter. Compared to CNT, these nanoprisms are attractive as optical limiting materials because they are easy to prepare, highly soluble and stable in an aqueous medium. The optical limiting properties of two kinds of nanoprisms are quite similar to each other, even though the thicknesses of two nanoprisms are different and their compositions are also slightly different. Nonlinear scattering experiments suggest that nonlinear scattering should play an important role in the observed optical limiting effects.

2.5 References

1. L. W. Tutt and A. Kost, Nature (London), 1992, **356**, 225.
2. P. Chen, X. Wu, X. Sun, J. Lin, W. Ji, and K. L. Tan, Phys. Rev. Lett., 1999, **82**, 2548.
3. M. P. Joshi, S. R. Mishra, H. S. Rawat, S. C. Mehendale, and K. C. Rustagi, Appl. Phys. Lett., 1993, **62**, 1763.
4. K. Mansour, M. J. Soileau, and E. W. Vanstryland, J. Opt. Soc. Am. B, 1992, **9**, 1100.
5. P. W. Zhu, P. Wang, W. F. Qiu, Y. Q. Liu, C. Ye, G. Y. Fang, and Y. L.Song, Appl. Phys. Lett., 2001, **78**, 1319.
6. W. Vanstryland, Y. Y. Wu, D. J. Hagan, M. J. Soileau, and K. Mansour, J. Opt. Soc. Am. B, 1988, **5**, 1980.
7. R. G. Ispasoiu, L. Balogh, O. P. Varnavski, D. A. Tomalia, and T. Goodson, J. Am. Chem. Soc., 2000, **122**, 11005.
8. V. Morandi, F. Marabelli, V. Amendola, M. Meneghetti, and D. Comoretto, Adv. Funct. Mater., 2007, **17**, 2779.
9. Y. Chen, C. G. Wang, Z. F. Ma, and Z. M. Su, Nanotechnology, 2007, **18**, 325602.
10. T. M. Whitney, J. S. Jiang, P. C. Searson, and C. L. Chien, Science, 1993, **261**, 1316.
11. K. Awazu, M. Fujimaki, C. Rockstuhl, J. Tominaga, H. Murakami, Y. Ohki, N. Yoshida, and T. Watanabe, J. Am. Chem. Soc., 2008, **130**, 1676.

12. R. C. Jin, Y. W. Cao, C. A. Mirkin, K. L. Kelly, G. C. Schatz, and J. G. Zheng, Science, 2001, **294**, 1901.

13. C. J. Orendorff, T. K. Sau, and C. J. Murphy, Small, 2006, **2**, 636.

14. S. Porel, S. Singh, S. S. Harsha, D. N. Rao, and T. P. Radhakrishnan, Chem. Mater., 2005, **17**, 9.

15. L. Francois, M. Mostafavi, J. Belloni, J. F. Delouis, J. Delaire, and P. Feneyrou, J. Phys. Chem. B, 2000, **104**, 6133.

16. M. Anija, J. Thomas, N. Singh, A. S. Nair, R. T. Tom, T. Pradeep, and R. Philip, Chem. Phys. Lett., 2003, **380**, 223.

17. H. I. Elim, J. Yang, J. Y. Lee, J. Mi, and W. Ji, Appl. Phys. Lett., 2006, **88**, 083107.

18. G. Wang and W. F. Sun, J. Phys. Chem. B, 2006, **110**, 20901.

19. H. Pan, W. Z. Chen, Y. P. Feng, W. Ji, and J. Y. Lin, Appl. Phys. Lett., 2006, **88**, 223106.

20. S. L. Qu, C. M. Du, Y. L. Song, Y. X. Wang, Y. C. Gao, S. T. Liu, Y. L. Li, and D. B. Zhu, Chem. Phys. Lett., 2002, **356**, 403.

21. Y. P. Sun, J. E. Riggs, H. W. Rollins, and R. Guduru, J. Phys. Chem. B, 1999, **103**, 77.

22. Y. A. Sun and Y. N. Xia, Adv. Mater., 2003, **15**, 695.

23. K. C. Grabar, R. G. Freeman, M. B. Hommer, and M. J. Natan, Anal. Chem., 1995, **67**, 735.

24. X. Can, J. E. Millstone, S. Li, and C. A. Mirkin, Angew. Chem., Int. Ed., 2007, **46**, 8436.

25. Y. C. Gaoa, Y. X. Wanga, Y. L. Song, Y. L. Lib, S. L. Qua, H. B. Liub, B., Dongc, and J. F. Zu, Opt. Commun., 2003, **223**, 103.

26. L. Francois, M. Mostafavi, J. Belloni, and J. A. Delaire, Phys. Chem. Chem. Phys., 2001, **3**, 4965.

CHAPTER 3

SIMPLE METHOD FOR LARGE SCALE SYNTHESIS OF HIGHLY MONODISPERSE GOLD NANOPARTICLES AT ROOM TEMPERATURE AND THEIR ELECTRON RELAXATION PROPERTIES

3.1. Introduction

Gold and silver nanoparticles have been the subject of intensive research due to their unique optical properties and various applications in many areas such as nanoscale optoelectronic devices,[1] two-photon imaging,[2] surface-enhanced Raman scattering (SERS),[3] optical limiting,[4] biosensing,[5] photonics,[6] and nonlinear optics.[7] The development of novel synthetic strategies for monodisperse metal nanostructures and assembly of these nanoparticles into one- and two-dimensional structures is very important for these applications.[8,9] Au nanoparticles were generally synthesized by using the Turkevich method,[10] in which sodium citrate acted as a reducing agent as well as a stabilizing agent. Brust et al.[11] synthesized gold nanoparticles with narrowly distributed sizes by reducing $HAuCl_4$ with $NaBH_4$ in the presence of alkanethiols. Hiramatsu et al.[12] reported the large scale synthesis of gold nanoparticles by using oleylamine as a reducing agent as well as a capping agent at relatively higher temperatures in the presence of toluene as a solvent. Very recently gold nanowires[13] and gold nanorods[14] have also been prepared by reducing $HAuCl_4$ with oleylamine at room temperature. Here we report a very simple method to prepare large scale, highly monodisperse gold nanoparticles at room temperature without using any external solvents that are dispersed in.

Understanding the ultrafast responses of metal nanoparticles to optical excitation is important for photothermal reshaping of nanoparticles and many potential applications such as optical switching, electronic device and photothermal therapy of cancer.[15-20] The ultrafast relaxation dynamics of gold nanoparticles have been extensively studied in the last decade.[18, 21-26] In these studies, a short laser pulse promotes the electrons to energy levels above the Fermi level. The subsequent electron-electron (e-e) scattering occurs on a time scale of a few hundred femtoseconds, leading to a hot electron distribution. The energy is subsequently transferred to the lattice via electron-phonon coupling on a time scale of a few picoseconds. The energy is eventually transferred to the surrounding medium via phonon-phonon (ph-ph) coupling on a time scale of hundreds of ps. Both electron-phonon coupling and phonon-phonon coupling have been found to be dependent on the surrounding matrix or solvent, though the detail mechanism is not well understood.[27,28] Mohamed et al.[27] have previously observed that the e-ph and ph-ph relaxation dynamics of gold nanoparticles in aqueous gels are faster than in organic gels. Hu et al.[28] observed similar e-ph relaxation time scales for Au/SiO_2 core-shell nanoparticles in water and ethanol, but faster ph-ph relaxation dynamics of Au/SiO_2 core-shell nanoparticles in water compared to that in ethanol. All these studies were performed on composite nanoparticles such as Au/SiO_2 or in Au/gels. It is instructive to study the electron relaxation dynamics of gold nanoparticles in direct contact with organic and aqueous solutions to investigate the solvent effects on their relaxation dynamics.

In this work, we report a very simple method for large scale preparation of highly monodisperse gold nanospheres, simply by mixing aqueous $HAuCl_4$ with oleylamine at room temperature. Here oleylamine acts as a reducing agent as well as a stabilizing agent. This method is superior to the previously reported methods in which the gold nanoparticles were prepared at higher temperatures in either organic or aqueous solvents and extensive further purification was needed.[8,12,29] Our method can be used to prepare large scale highly monodisperse gold nanoparticles at room temperature. The prepared nanoparticles settle down themselves at the bottom of the container upon the particle formation, so it is very easy to purify. In addition, the size of the nanoparticles can be experimentally controlled. We have also studied the electron dynamics properties of these monodisperse gold nanoparticles in toluene by using femtosecond pump-probe measurements, in comparison with 13 nm citrate stabilized gold nanoparticles in water. It was found that the energy exchange between the nanoparticles and the surrounding medium, i.e. ph-ph coupling, for oleylamine capped gold nanoparticles in toluene was slower than that of citrate capped gold nanoparticles in water due to lower thermal conductivity of toluene than water. The monodisperse gold nanoparticles in toluene displayed a weak pump-intensity dependence on the electron-phonon (e-ph) relaxation compared to citrate capped gold nanoparticles in water, due to the extra vibrational states provided by the NH_2 group of oleylamine.

3.2. Experimental Section

3.2.1 Chemicals

Chloroauricacid acid ($HAuCl_4$), oleylamine, toluene, acetone were purchased from Sigma-Aldrich. All the chemicals were used as received without further purification.

3.2.2 Synthesis of 13 nm and 11 nm oleylamine capped gold nanoparticles

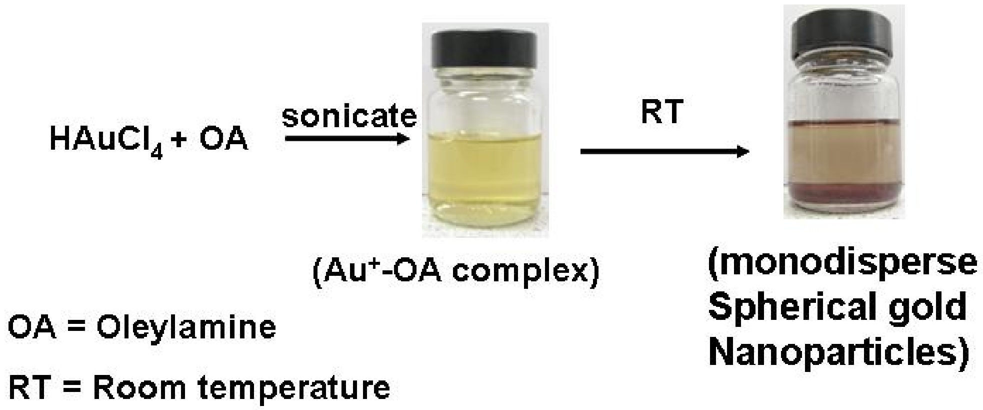

Fig. 3.1 synthetic procedure for the preparation of monodisperse gold nanoparticles

In a typical synthesis of 13 nm OA capped gold nanoparticles, 0.1 g of solid $HAuCl_4$ was first dissolved in 10 μL of water. Upon addition of 20 ml of oleylamine, the $HAuCl_4$ immediately precipitate at the bottom of the bottle. The precipitate was subsequently dissolved by sonication and the solution colour changes to light yellow and the solution then was kept at room temperature to complete the reaction. A white colour solid appeared in 24 hours due to formation of a complex between oleylamine and gold chloride. The white colour solid was dispersed into the solution by hand shaking. A pink colour precipitate appeared slowly in 3 days due to formation of monodisperse spherical gold nanoparticles (see fig.3.1). The pink colour solid was separated from the colorless supernant and then washed three times with 2 ml mixture of 1:3 toluene and ethanol to remove the excess oleylamine. For the preparation of 11 nm oleylamine capped gold nanoparticles, 0.2 g of $HAuCl_4$ was used. The remaining procedures are the same as that for preparation of 13 nm gold nanoparticles.

3.2.3 Synthesis of 13 nm citrate capped spherical gold nanoparticles in water

In a typical experiment, 10 mL of 38.8 mM sodium citrate was quickly injected into 100 mL of 1 mM boiling $HAuCl_4$ solution in a 250 mL round-bottom flask under vigorous stirring. The solution quickly changed the color from pale yellow to burgundy. The heating was continued for 10 min. Then the solution was kept stirring for another 15 min without heating. The obtained gold nanoparticles have the absorption maximum at 520 nm and TEM images showed an average particle size of 13 nm (see fig.3.2).

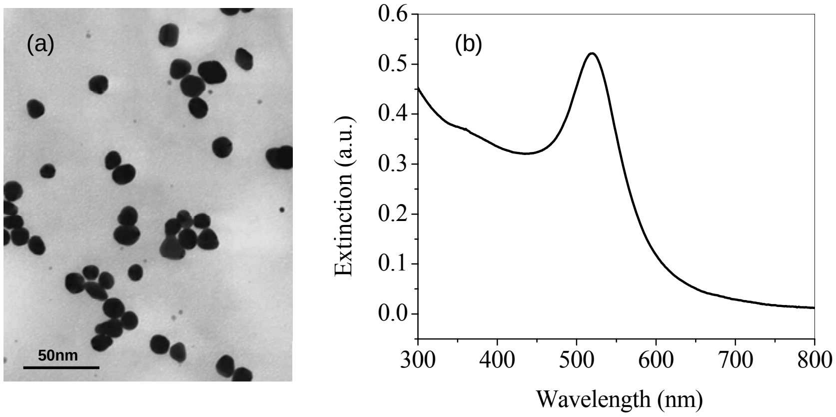

Fig. 3.2 TEM image (a) and the corresponding UV-visible extinction spectrum (b) of the 13 nm citrate capped gold nanoparticles.

3.2.4 Characterization of nanoparticles

The nanoparticles were characterized by UV–visible spectroscopy, Fourier transform infrared spectroscopy (FTIR), and transmission electron microscopy (TEM). UV–visible spectra of the nanoparticles were measured using a Shimadzu UV 2450 spectrometer. FTIR spectra of oleylamine capped gold nanoparticles were recorded using a Bio-rad Excalibur FTIR spectrometer. The oleylamine capped gold nanoparticles was dispersed in chloroform to prepare film sample for FTIR analysis. TEM images were taken using JEOL JEM3010 field high resolution emission transmission electron microscope. The nanoparticle samples were coated on carbon-coated grids (150 meshes) and dried before loading into the TEM machine.

3.2.5 Ultrafast relaxation measurements

The ultrafast relaxation dynamics of the gold nanoparticles in water and toluene were measured by using pump-probe experiments, which were performed by using a femtosecond Ti:sapphire laser system (Spectra Physics). The laser pulses were generated from a mode-locked Ti:sapphire oscillator seeded regenerative amplifier with a pulse energy of 2mJ at 800 nm and a repetition rate of 1 kHz. The 800 nm laser beam was split into two portions. The larger portion of the beam was passed through a BBO crystal to generate the 400 nm pump beam by frequency-doubling. A small portion of the 800 nm pulses was used to generate white light continuum in a 1 mm sapphire plate. The white light continuum was split into two beams, a probe and a reference beam. The signal and reference beams were detected by photodiodes that are connected to lock-in amplifiers and the computer. The intensity of the pump beam was attenuated with a neutral density filter. The pump beam is focused onto the sample with a beam size of 300 μm and overlapped with the smaller-diameter (100 μm) probe beam. The delay between the pump and probe pulses was varied by a computer-controlled translation stage. The pump beam was modulated by an optical chopper at a frequency of 500 Hz. The transient absorption spectra at different delay times was measured by passing the probe beam through a monochromator before detected by a photodiode that is connected to the lock-in amplifier.

3.3. Results and Discussion

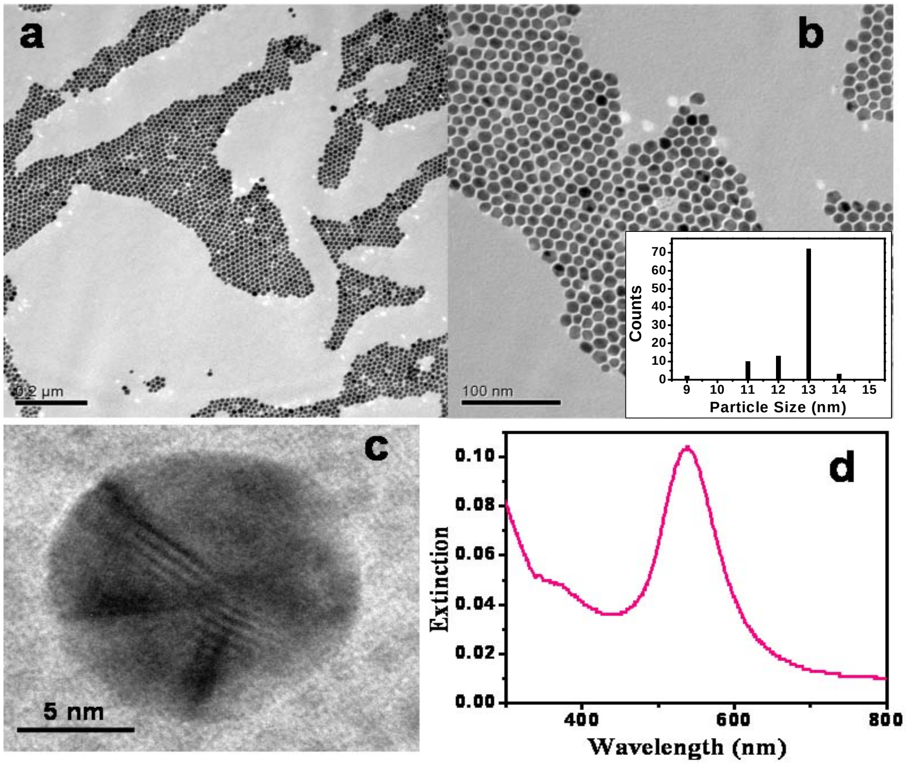

Fig. 3.3 Transmission electron microscope (TEM) images (a, b), HRTEM image of 13 nm gold nanoparticles (c) at different magnifications and the corresponding UV-visible extinction spectrum (d).

Monodisperse gold nanoparticles were prepared by simply mixing $HAuCl_4$ with oleylamine and kept at room temperature for formation of nanoparticles as detailed in the experimental section. $HAuCl_4$ was dissolved in oleylamine by sonication. During the sonication process, the solution underwent a series of color changes, from brownish yellow to light yellow and then light brown, and finally a red color after one hour of sonication (see fig.3.1). The final red color solution contains small gold nanoparticles with diameter of 1.5-2.5 nm. The color change from brownish yellow to red color during the sonication process is an indicator of the step-wise reduction reaction of $HAuCl_4$ (Au^{3+}- Au^{1+}- Au^{0}).[30] The intermediate with light yellow color was used as a precursor for further reactions to prepare monodisperse gold nanospheres with size of 13 nm (see the experimental section for the detailed procedure). In this reaction, oleylamine acts as both a reducing agent as well as stabilizing agent. The surfaces of the nanoparticles are covered by oleylamine, so the particles are hydrophobic and can be dissolved in nonpolar solvents such as hexane, toluene, or chloroform. In our studies, the particles were re-dispersed in toluene for further characterization.

Figure 3.3 shows the TEM images of highly monodisperse 13 nm spherical gold nanoparticles at different magnifications and their corresponding UV-Visible extinction spectrum. The particles were found to be self-organized to form hexagonal close-packed arrays on the carbon coated TEM grid (Figure 3.3a and 3.3b) after the solvent evaporation. It has been previously reported that particles with less than 2-3% polydispersities could form this kind of hexagonal close-packed arrays.[31] The HR-TEM image (Figure 3.3c) showed a multiply-twinned structure, which is typical for noble metals with a face-centered cubic structure at small sizes.[29] The UV-visible extinction spectrum of the monodisperse spherical gold nanoparticles is shown in Figure 3.3d. The plasmon resonance is characterized by a narrow band with a peak wavelength at 532 nm. The narrow Plasmon band suggests a uniform size distribution of the gold nanoparticles.

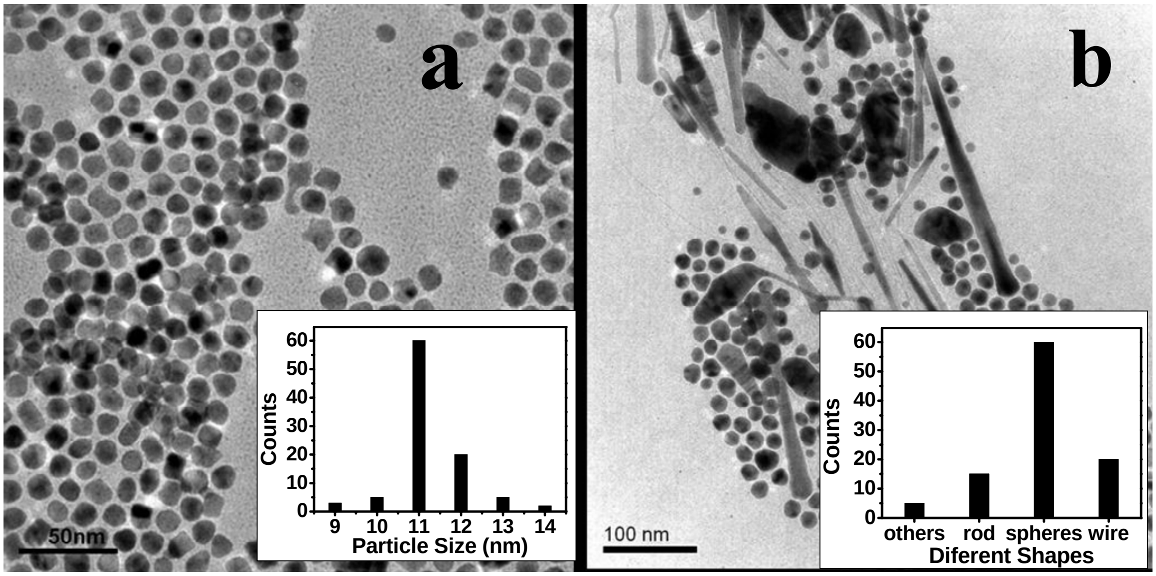

Fig.3.4 TEM images of 11 nm gold nanoparticles prepared by mixing 0.2 g of $HAuCl_4$ to 20 ml of oleylamine at room temperature (a) and by reaction of 0.1 g of $HAuCl_4$ and 20 ml of oleylamine at 120°C for 12hrs (b).

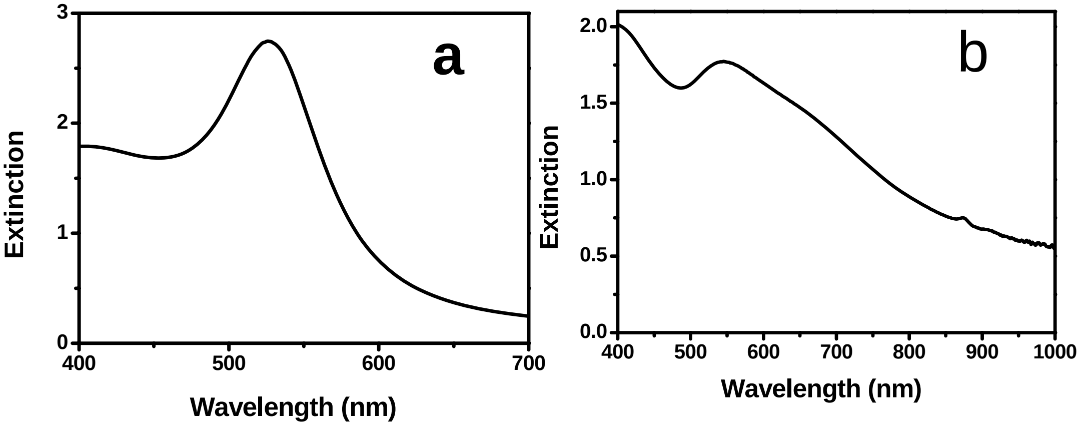

Fig. 3.5 (a) UV-visible spectrum of 11 nm gold nanoparticles ($\chi_{\text{max}\sim}$ 527) prepared by mixing 0.2 g of HAuCl4 to 20 ml of oleylamine at room temperature. (b) UV visible spectrum of mixture o particles ($\chi_{\text{max}\sim}$ 538) obtained by reaction of 0.1 g of HAuCl4 and 20 ml of oleylamine at 120oC for 12hrs (b).

The experimental conditions have significant effects on the size and morphology of the nanoparticles. When a different molar ratio of $HAuCl_4$ and oleylamine, for example, when 0.2 g of $HAuCl_4$ and 20 ml of oleylamine were used, the formed nanoparticles were nearly monodisperse with a size of ~11 nm (Figure 3.4a) (see fig.3.5 for extinction spectra). We have also investigated the temperature effects on the morphology of the gold nanoparticles. When the reactions were performed at a higher temperature by boiling aqueous $HAuCl_4$ with oleylamine at 120^o for 12 hrs, a mixture of wires, rods and spherical nanoparticles were obtained instead, as shown in Figure 3.4b (see the fig.3.5 for extinction spectra).

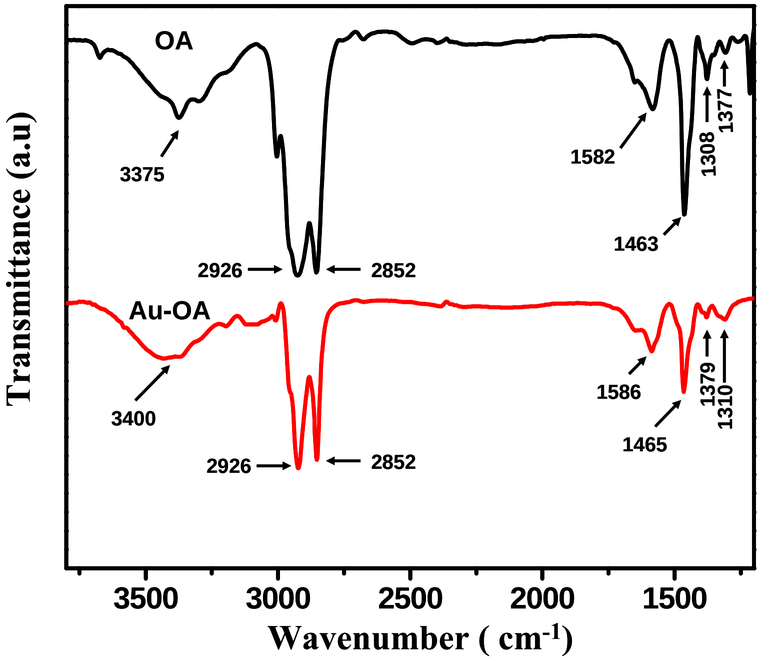

Fig. 3.6 FTIR spectra of pure oleylamine (OA) and oleylamine capped gold nanoparticles (Au-OA).

Figure 3.6 shows the Fourier-transform infrared (FTIR) spectra of pure oleylamine and oleylamine capped gold nanoparticles. The FTIR spectra of pure oleylamine and oleylamine capped gold nanoparticles are quite similar, except some peaks were slightly shifted due to the interactions of oleylamine with the gold nanoparticles. The band at 3375 cm^{-1} in IR spectrum of oleylamine is due to N-H stretching mode, which is red shifted to 3400 cm^{-1} in oleylamine capped gold nanoparticles due to absorption of N-H group onto the gold nanoparticle surface. There is a very small change in the C-H stretching mode (2850-2920 cm^{-1}) upon the binding of oleylamine to the gold nanoparticle. The N-H bending band at 1582 cm^{-1} in oleylamine is shifted to 1586 cm^{-1} in the oleylamine capped gold nanoparticles.

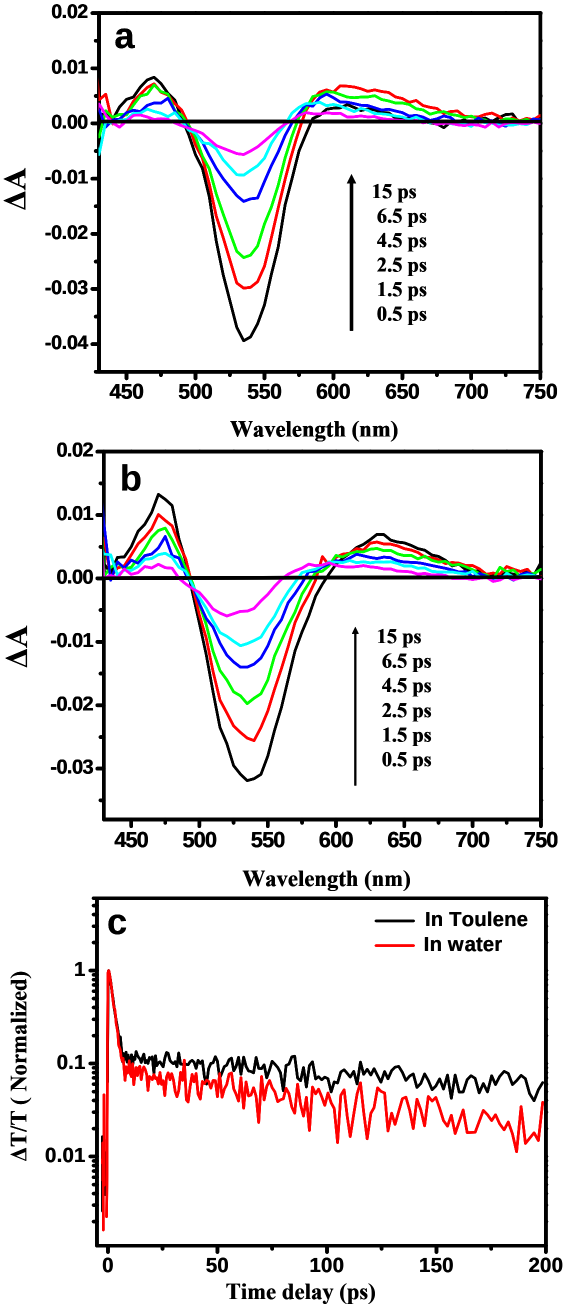

Fig. 3.7 a) Femtosecond transient absorption spectra of oleylamine capped gold nanoparticles in toluene and (b) citrate capped gold nanoparticles in water after excitation with 400 nm laser pulses at different delay times; (c) Electron dynamics of 13 nm oleylamine capped gold nanoparticles in toluene and citrate capped gold nanoparticles in water probed at 530 nm under an excitation intensity of 21 nJ/pulse.

The ultrafast electron dynamics of monodisperse 13 nm oleylamine capped spherical gold nanoparticles in toluene were studied by femtosecond pump-probe spectroscopy. The pump-probe measurements on 13 nm citrate capped gold nanoparticles in water were also performed under the same experimental conditions for direct comparison. The preparation of 13 nm citrate capped gold nanoparticles in water and its UV-visible extinction spectrum are presented in the experimental section (see fig.3.1). The UV-visible extinction spectra of the citrate capped gold nanoparticles in water is slightly broader than that of oleylamine capped gold nanoparticles in toluene due to a relatively broader size distribution of the citrate capped gold nanoparticles.

Figure 3.7a and b shows the femtosecond transient absorption spectra of oleylamine capped gold nanoparticles in toluene citrate capped gold nanoparticles in water after excitation at 400 nm at different delay times. The overall features of transient spectra of the two samples are quite similar. The transient absorption spectra show a strong bleaching signal near the surface plasmon band maximum at 530 nm and transient absorption signal in the wings of the band, which is similar to previous reports on gold nanoparticles in aqueous solution.[23, 34] The results are also consistent with the previously reported theoretical simulation results[35] and can be explained as a result of broadening of the Plasmon band due to the increase of the electronic temperature upon photo-excitation. The bleaching band of citrate capped gold nanoparticles in water is slightly broader, consistent with their steady state UV-Visible extinction spectra.

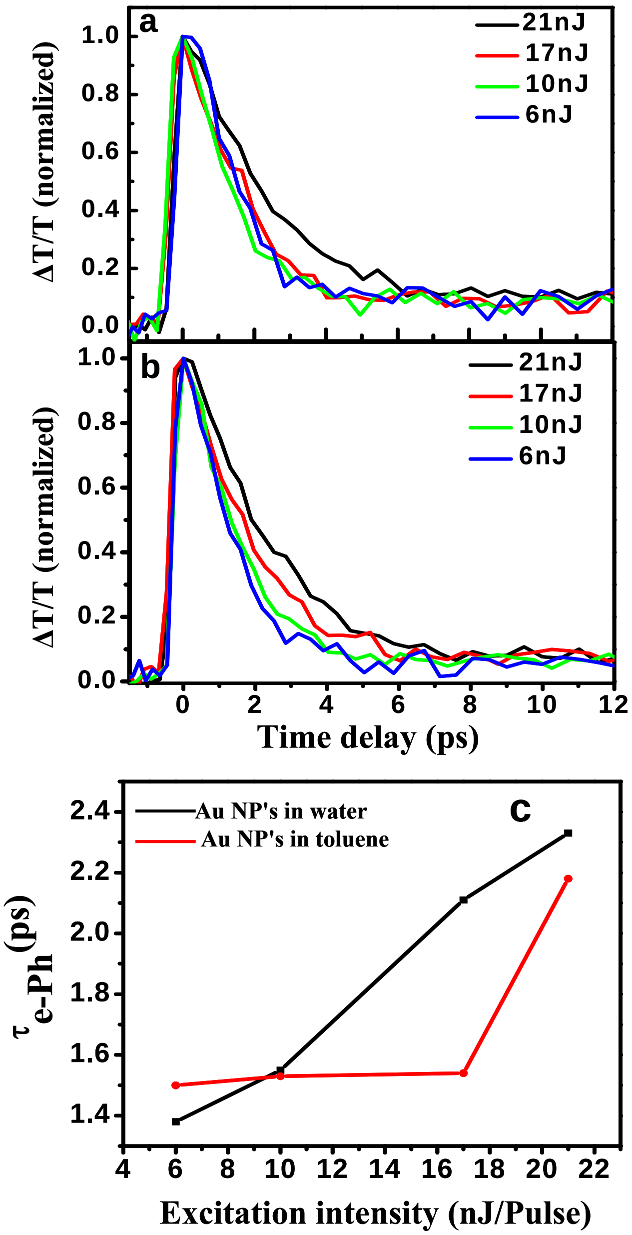

Fig. 3.8 Excitation intensity dependent electron-phonon (e-ph) dynamics probed at 530 nm for (a) oleylamine capped gold nanoparticles in toluene and (b) citrate capped gold nanoparticles in water under excitation intensities of 6~21 nJ/pulse. (c) Excitation intensity dependent electron-phonon relaxation times of oleylamine capped gold nanoparticles in toluene and citrate capped gold nanoparticles in water.

Figure 3.7c shows the surface plasmon dynamics of gold nanoparticles in toluene and water at a probe wavelength of 530 nm. The data are displayed in a semilog plot to highlight the long time dynamics. The decay profiles display a fast picosecond component followed by a slow component on the time scale of a few hundred picoseconds. The fast component is due to the thermal equilibration process between the hot electrons and the nanoparticle lattice by e-ph coupling, while the subsequent slower decay is due to the energy transfer processes between the nanoparticle lattice and the surrounding environment by ph-ph coupling.[23] The major difference between the two samples is that the ph-ph coupling of Au nanoparticles in water is faster (~130 ps) than that in toluene (~320 ps). Since the slow component is due to the heat dissipation from the nanoparticle lattice to the solvent, this difference can be ascribed to lower thermal conductivity of toluene compared to water. The results are consistent with the previous report that the ph-ph relaxation times of the gold nanoparticles were dependent on the environment of the nanoparticle system.[24, 27, 28, 36, 37]

We have also studied the pump intensity dependent electron relaxation dynamics of gold nanoparticles near the surface plasmon resonance (530 nm) in toluene and in water as shown in Figure 3.8. For both samples, the slow dynamics (ph-ph coupling) shows little dependence on the excitation density. However, the fast e-ph dynamics shows interesting and different dependence on the excitation intensity for two samples. The fitting results of the e-ph relaxation time scales at different excitation intensities are summarized in Figure 3.8c. For the oleylamine capped gold nanoparticles, the e-ph relaxation time is insensitive to the excitation intensity at low excitation intensities (6-17 nJ/pulse). The e-ph relaxation dynamics becomes slower when the excitation intensity increases to 21 nJ/pulse. In contrast, the e-ph relaxation gradually increases with increasing excitation intensity from 6 to 21 nJ/pulse for citrate capped gold nanoparticles in water. The relaxation time scale shows a linear dependence with the excitation intensity. The fast e-ph dynamics is known to be dependent on the excitation intensity. At higher excitation intensities, more energy will be pumped into the systems which results in initial temperatures of the electron gas will be resulted. It thus takes a longer time for the thermalization processes between the electron gas and the particle lattice.[27] In addition, the heat capacity of the electron gas is temperature dependent.[34, 38] It has been previously suggested that the interactions between surface phonon and the surrounding molecules affect the e-ph relaxation processes.[39] The weak dependence of e-ph relaxation time in oleylamine capped gold nanoparticles in toluene is likely due to the vibrational states provided by the amine group (NH_2), which serves as an extra relaxation pathway for the e-ph relaxation. This observation is similar to the previous reports on PAMAM (polyamidoamine) dendrimer capped gold nanoparticles,[24] in which weak dependence of the e-ph relaxation time of the gold nanoparticles on the excitation intensity was observed. The weak excitation intensity dependence was ascribed to the additional energy relaxation pathways provided by the PAMAM cage.[24]

3.4. Conclusion

In conclusion, we have prepared highly monodisperse spherical gold nanoparticles by simple mixing aqueous $HAuCl_4$ and oleylamine followed by sonication at room temperature. The obtained gold nanoparticles have an average size of 13 nm and can form a hexagonal close-packed array on the TEM grid after the solvent evaporation. The size of the nanoparticle can be controlled by varying the relative molar ratio of $HAuCl_4$ and oleylamine mixtures. The capping agent, oleylamine, can be easily replaced with other capping agents such as thiol groups for further functionalization. The electron relaxation properties of the gold nanoparticles dispersed in toluene were investigated by ultrafast pump-probe experiments in comparison with gold nanoparticles dispersed in water. The ph-ph coupling of monodisperse gold nanoparticles in toluene is slower than that of the citrate capped gold nanoparticles in water, due to the lower thermal conductivity of toluene compared to water. A weaker excitation intensity dependence of e-ph coupling dynamics was observed for the oleylamine capped gold nanoparticles in toluene compared to that for gold nanoparticles in water, which is likely due to the extra relaxation pathway for the electron-phonon relaxation provide by the vibrational states of the $-NH_2$ group in oleylamine.

3.5 References

1. Seker, F., Malenfant, P. R. L., Larsen, M., Alizadeh, A., Conway, K., Kulkarni, A. M., Goddard, G., Garaas, R., *Adv. Mater.,* 2005, **17,** 1941
2. Ramakrishna, G., Varnavski, O., Kim, J., Lee, D., Goodson, T., *J. Am. Chem. Soc.*, 2008, **130,** 5032
3. Schwartzberg, A. M., Grant, C. D., Wolcott, A., Talley, C. E., Huser, T. R., Bogomolni, R., Zhang, J. Z., *J. Phys. Chem. B,* 2004, **108,** 19191
4. Polavarapu, L., Xu, Q. H., Dhoni, M. S., Ji, W. 2008 *Appl. Phys. Lett.* **92** 263110
5. Hill, H. D., Vega, R. A., Mirkin, C. A., *Anal. Chem.* 2007, **79,** 9218
6. Morandi, V., Marabelli, F., Amendola, V., Meneghetti, M., Comoretto, D., *Adv. Funct. Mater.,* 2007, **17,** 2779

7. West, R., Wang, Y., Goodson, T., *J. Phys. Chem. B,* 2003, **107,** 3419

8. Pyrpassopoulos, S., Niarchos, D., Nounesis, G., Boukos, N., Zafiropoulou, I., Tzitzios, V., *Nanotechnology,* 2007 **18,** 485604

9. Ming, T., Kou, X. S., Chen, H. J., Wang, T., Tam, H.-L., Cheah, K.-W., Chen, J.-Y., Wang, J. F., *Angew. Chem. Int. Ed.,* 2008, **47,** 9685

10. John Turkevicphe, T. c. S. J. H., *Discuss. Faraday Soc.,* 1951, **11**, 55

11. Mathias Brust, M. W., Donald Bethell, David J. Schiffrin and Robin Whyman., *J. CHEM. SOC., CHEM. COMMUN.,* 1994, 801

12. Hiramatsu, H., Osterloh, F. E., *Chem. Mater.,* 2004, **16,** 2509

13. Huo, Z. Y., Tsung, C. K., Huang, W. Y., Zhang, X. F., Yang, P. D., *Nano Lett.,* 2008 **8,** 2041

14. Li, Z., Tao, J., Lu, X., Zhu, Y., Xia, Y., *Nano Lett.,* 2008, **8,** 3052

15. Oldenburg, S. J., Averitt, R. D., Westcott, S. L., Halas, N. J., *Chem. Phys. Lett.,* 1998, **288,** 243

16. Baba, K., Okuno, T., Miyagi, M., *J. Opt. Soc. Am. B,* 1995, **12,** 2372

17. El-Sayed, I. H., Huang, X. H., El-Sayed, M. A., *Nano Lett.,* 2005, **5,** 829

18. Link, S., El-Sayed, M. A., *Int. Rev. Phys. Chem.,* 2000, **19,** 409

19. Huang, X. H., Jain, P. K., El-Sayed, I. H., El-Sayed, M. A., *Laser Med. Sci.,* 2008, **23,** 217

20. Huang, Y. F., Sefah, K., Bamrungsap, S., Chang, H. T., Tan, W., *Langmuir,* 2008, **24,** 1860

21. Grant, C. D., Schwartzberg, A. M., Norman, T. J., Zhang, J. Z., *J. Am. Chem. Soc.*, 2003, **125** 549

22. Hartland, G. V., *Phys. Chem. Chem. Phys.,* 2004, **6,** 5263

23. Link, S., Ei-Sayed, M. A., *Ann. Rev. Phys. Chem.,* 2003, **54,** 331

24. Melinger, J. S., Kleiman, V. A., McMorrow, D., Grohn, F., Bauer, B. J., Amis, E., *J. Phys. Chem. A,* 2003, **107,** 3424

25. Ramakrishna, G., Dai, Q., Zou, J. H., Huo, Q., Goodson, T., *J. Am. Chem. Soc.,* 2007, **129,** 1848

26. Zhang, J. Z., *Acc. Chem. Res.,* 1997, **30,** 423

27. Mohamed, M. B., Ahmadi, T. S., Link, S., Braun, M., El-Sayed, M. A., *Chem. Phys. Lett.,* 2001, **343,** 55

28. Hu, M., Wang, X., Hartland, G. V., Salgueirino-Maceira, V., Liz-Marzan, L. M., *Chem. Phys. Lett.,* 2003**, 372,** 767

29. Lu, X. M., Tnan, H. Y., Korgel, B. A., Xia, Y. N., *Chem. Euro. J.,* 2008, **14,** 1584

30. Pazos-Perez, N., Baranov, D., Irsen, S., Hilgendorff, M., Liz-Marzan, L. A., Giersig, M., *Langmui,* 2008, **24,** 9855

31. B. L. V. Prasad, C. M. S., Kenneth J. Klabunde., *Chem. Soc. Rev,* 2008, **37**, 1871

32. Caruso, R. A., Ashokkumar, M., Grieser, F., *Langmuir*, 2002, **18,** 7831

33. Radziuk, D., Shchukin, D., Mohwald, H., *J. Phys. Chem. C*, 2008, **112**, 2462

34. Hodak, J. H., Martini, I., Hartland, G. V., *J. Phys. Chem. B,* 1998, **102,** 6958

35. Hartland, G. V., *Ann. Rev. Phys. Chem.*, 2006, **57,** 403

36. Link, S., Furube, A., Mohamed, M. B., Asahi, T., Masuhara, H., El-Sayed, M. A., *J. Phys. Chem. B,* 2002, **106,** 945

37. Link, S., Hathcock, D. J., Nikoobakht, B., El-Sayed, M. A., **Adv**. *Mater.,* 2003**, 15***,* 393

38. Cao, J., Gao, Y., Elsayed-Ali, H. E., Miller, R. J. D., Mantell, D. A., *Phys. Rev. B,* 1998, 58, 10948

39. Bigot, J. Y., Halte, V., Merle, J. C., Daunois, A., *Chem. Phys.,* 2000, **251,** 181

CHAPTER 4

OPTICAL LIMITING PROPERTIES OF OLEYLAMINE CAPPED GOLD NANOPARTICLES FOR BOTH FEMTOSECOND AND NANOSECOND LASER PULSES

4.1 Introduction

Optical limiters display a decreasing transmittance as a function of laser fluence or irradiance. Fast response optical limiting materials with low thresholds can be used for protection of eyes and sensitive optical devices from laser-induced damage. A lot of efforts have been devoted to develop ideal broadband optical limiting materials based on mechanisms such as nonlinear scattering,[2] multi-photon absorption,[3] and reverse saturable absorption.[4, 5] Strong optical limiting properties have been observed in various materials such as carbon nanotubes[2, 6, 7] carbon-black suspension,[8] metallophtalocyanines,[9] and porphyrins.[10] Inorganic nanomaterials provide an attractive alternative to organic materials for various photonic applications due to their stability and simple synthetic methods. Metal nanoparticles, such as gold and silver nanoparticles, have recently been found to exhibit strong optical limiting properties.[1, 4, 5, 11-18] The development of optical limiting materials using metal nanoparticles is attractive because gold and silver nanoparticles are easy to prepare, highly soluble and stable in both aqueous and organic solvents.

So far there are only a few reports on the optical limiting properties of gold and silver nanocomposites. Goodson et al[11] reported strong optical limiting performance in metal-dendrimer nanocomposites using nanosecond laser pulses. Philip et al.[13] reported optical limiting effects in monolayer protected gold nanoparticles using picoseconds laser pulses. The optical limiting properties of metal nanoparticles depend on the size of nanoparticles and their surrounding matrix[14] or solvent in which the nanoparticles are dissolved.[7] Francüois et al.[19] studied the effect of particle size on the optical limiting behavior of gold nanoparticles at 530 nm using picosecond laser pulses. They have observed that the threshold of the optical limiting effect decreased with the increasing particle size due to nonlinear scattering. Wang et al.[17] investigated the optical limiting properties of citrate stabilized gold nanoparticles and their aggregates. They found that aggregated gold nanoparticles showed strong optical limiting properties even though individual gold nanoparticles exhibited no optical limiting behavior. Very recently we have reported strong optical limiting effects of silver nanotriangles with a threshold comparable to carbon nanotubes.[5] The applications of carbon nanotubes (CNTs) are limited due to its poor solubility in aqueous and organic solvents, which tend to aggregate in a shorter amount of time.[20] Noble metal nanoparticles are very good alternative to CNTs, as noble metals are stable and can be well dispersed in solvents. Most of the above mentioned studies on optical limiting properties of metal nanoparticles were performed using nanosecond laser pulses with a central wavelength of 532 nm. There are very few reports on the ultrafast optical limiting using metal nanoparticles.[4, 21] Previously Scalora et al.[22] reported optical limiting and switching of ultrashort pulses in photonic band gap materials. Nanomaterials with optical limiting properties in near-Infrared usingr femtosecond laser pulses have been less stduied.[4, 5, 23, 24]

In this work, we have prepared oleylamine capped gold nanoparticles in toluene and studied their optical limiting response to laser pulses. The optical limiting properties of those gold nanoparticles were characterized by fluence-dependent transmittance measurements using 532 nm and 1064 nm laser pulses with pulse durations of ~7 ns. Their femtosecond optical limiting properties were studied by performing a z-scan experiment with 780 nm femtosecond laser pulses with pulse duration of 300 fs. The oleylamine capped gold nanoparticles were found to show strong broadband optical limiting effects for nanosecond laser pulses at 532 nm and 1064 nm and femtosecond laser pulses at 780 nm.

4.2 Experimental Section

4.2.1 Materials: Gold chloride trihydrate ($HAuCl4 \cdot 3H_2O$), oleylamine, oleic acid, and ascorbic acid were purchased from Sigma-Aldrich. Toluene was purchased from Merck. All the materials were used as received without further purification.

4.2.2 Synthesis of oleylamine capped gold nanoparticles

In a typical synthesis of gold nanoparticles, 100 μL of water was added to 30 mg of solid chloroauric acid. The solution was then mixed with 50 ml toluene containing 400 μL of oleylamine and 200 μL of oleic acid. The obtained yellow-colored solution was refluxed at 100 °C. The solution turned to colourless within 15 min. The heating of the solution was stopped upon the color change and the solution was aged for 12 hr until the solution eventually changed the color into pink. 40mg of ascorbic acid (in 25mL of toluene) was then added into the pinkish color solution. After ageing for 24 hr, the solution changed into a dark red color. The solution was centrifuged with a speed of 10000 rpm for 1 hr and the precipitate was dispersed in toluene. The transmission electron microscope (TEM) images of the obtained gold nanoparticles were taken from a Philips CM10 electron microscope at an accelerating voltage of 100 kV.

4.2.3 Synthesis of 13 nm citrate capped spherical gold nanoparticles in water

In a typical experiment, 10 mL of 38.8 mM sodium citrate was quickly injected into 100 mL of 1 mM boiling HAuCl4 solution in a 250 mL round-bottom flask under vigorous stirring. The solution quickly changed the color from pale yellow to burgundy. The mixture was heated to boil for 10 min and was then kept stirring for another 15 min without heating. The obtained gold nanoparticles have an absorption maximum at 520 nm. The TEM images showed an average particle size of 13 nm. The UV-visible spectrum and TEM image is shown in Fig.1.1

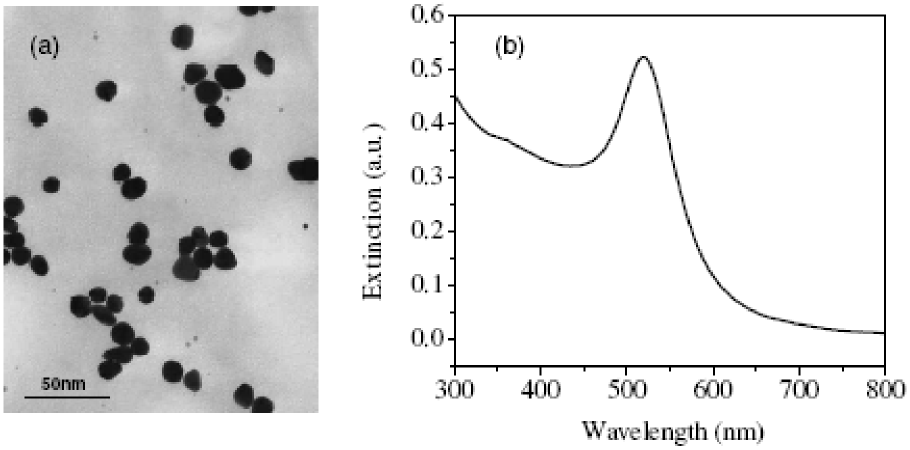

Fig. 4.1 TEM image (a) and the corresponding UV-visible extinction spectrum (b) of the 13 nm citrate capped gold nanoparticles.

4.2.4 FTIR measurement of the oleylamine capped god nanoparticles

The IR spectra were measured using a Bio-rad Excalibur FTIR spectrometer. The oleylamine capped gold nanoparticles were centrifuged for 4 times to fully remove the uncapped oleylamine molecules. The precipitate was dissolved in chloroform and a drop of solution was casted onto the NaCl substrate for FTIR measurements.

4.2.5 Optical limiting measurements

The optical limiting properties of the gold nanoparticles at 532 nm and 1064 nm were characterized by fluence-dependent transmittance measurements with 532 nm and 1064 nm laser pulses with pulse durations of 7 ns. The laser pulses were generated from a *Q*-switched Nd: YAG (yttrium aluminum garnet) laser (Spectra Physics DCR3). The primary laser output had a center wavelength of 1064 nm, with pulse duration of 7 ns and a repetition rate of 10 Hz. The 1064 nm output was frequency-doubled to obtain 532 nm laser pulses. The laser beam was focused onto the gold nanoparticle solution contained in a 1-cm-pathlength quartz cuvette with a spot size of 165 μm. The nanoparticle solution was stirred to refresh the samples at the laser illumination spot to minimize potential thermal- or photo-induced shape transformation. To understand the mechanisms of the optical limiting effects, the scattered light signal around the sample were collected at different angles from the laser focus.

The optical limiting properties at 780 nm were measured by using a femtosecond z-scan technique. The femtosecond laser pulses were generated by a mode-locked Ti: Sapphire laser (Quantronix, IMRA), which seeded a Ti:sapphire regenerative amplifier (Quantronix, Titan) with the pulse duration of 300 fs. The laser pulses were focused onto the gold nanoparticle solution in a 1-mm-pathlength quartz cuvette, with a beam waist of ~ 30 μm. The solution had a linear transmittance of 80%. The incident and transmitted laser powers were monitored as the cuvette moved along the z-direction, towards and away from the focus position.

4.3 Results and Discussion

4.3.1 Extinction spectrum of oleylamine capped gold nanoparticles

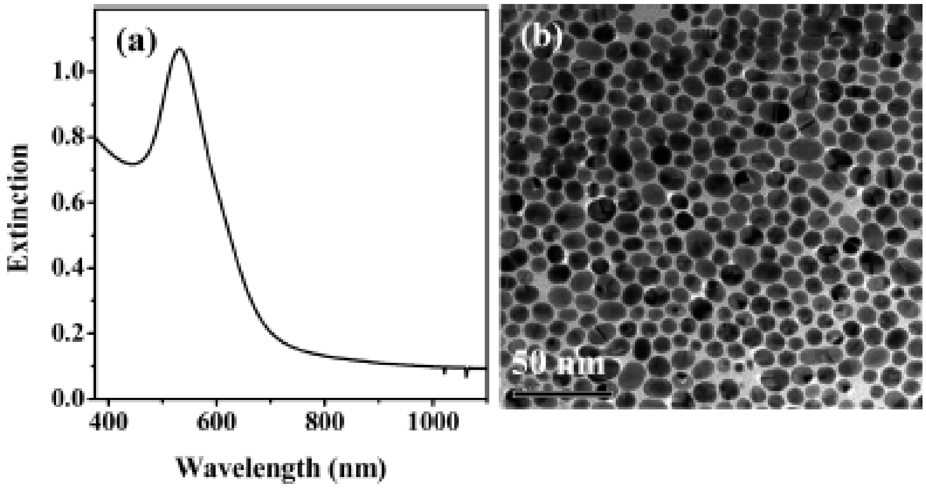

Fig. 4.2 **UV**-visible spectrum (a) the oleylamine capped gold nanoparticle solution and the corresponding TEM image (b). The scale bar is 50 nm.

In a typical synthesis, oleylamine capped gold nanoparticles were prepared using a procedure modified from the one reported by Halder et.al,[25] in which oleylamine and oleic acid were used as a capping agent to prepare thin nanowires. In our experiments, we found that the concentration of the $HAuCl_4$ played a very important role in the morphology of the obtained gold nanostructures. By using a low concentration of $HAuCl_4$ in the reaction, spherical gold nanoparticles instead of gold nanowires were obtained. Figure 4.2 shows the UV-visible extinction spectrum of the gold nanoparticles in toluene and the corresponding TEM image. The UV-visible spectrum of the gold nanoparticles in toluene has an extinction maximum at 535 nm with a tail stretching into longer wavelength regions up to near Infrared. The size of the obtained gold nanoparticles was in the range of 7-10 nm with an overall spherical shape, together with some larger particles with various non-spherical shapes.

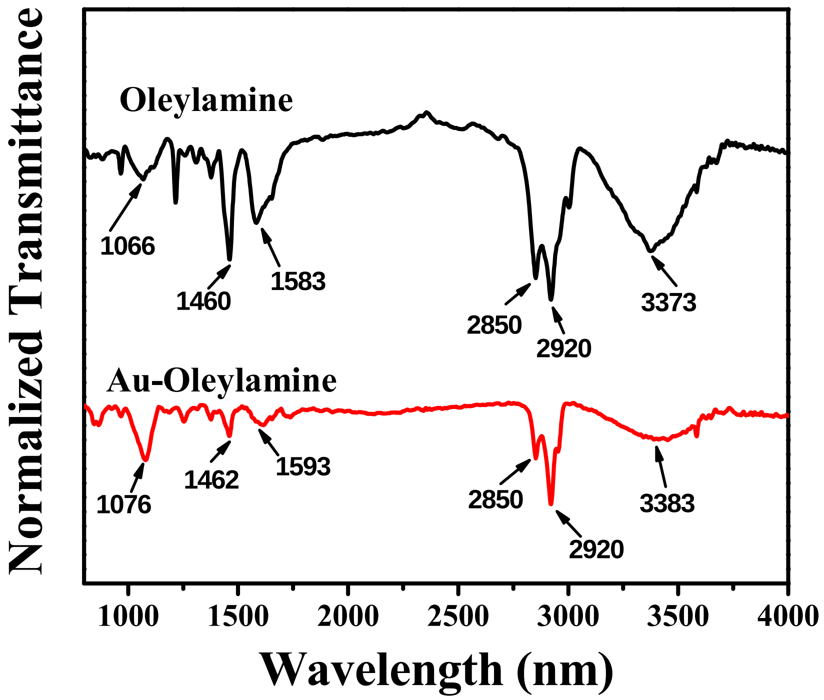

Fig. 4.3 The FTIR spectra of oleylamine and oleylamine-capped gold nanoparticles.

4.3.2 FTIR spectrum of oleylamine capped gold nanoparticles

Figure 4.3 shows the FTIR spectrum of pure oleylamine and oleylamine capped gold nanoparticles. The IR spectrum of oleylamine is similar to that previously reported.[26] The oleylamine capped gold nanoparticles have similar spectral signatures to those of pure oleylamine. Several bands are slightly shifted due to the surface effect of gold nanoparticles when oleylamine is capped onto the gold nanoparticles. For example, the band at 3373 cm^{-1} in the IR spectrum of oleylamine is due to the N-H stretching mode, which is red shifted to 3383 cm^{-1} for oleylamine capped gold nanoparticles. There is no shift for the C-H stretching band around 2850-2920 cm^{-1} after oleylamine is bound to the nanoparticle. The bands at 1066 cm^{-1} and 1460 cm^{-1} are attributed to the =C-H and –C-H bending modes in oleylamine, respectively, which were shifted to 1076 cm^{-1} and 1462 cm^{-1} in oleylamine capped gold nanoparticles. The band at 1583 cm^{-1} in the oleylamine is due to the N-H bending mode, which is shifted to 1593 cm^{-1} in the oleylamine capped gold nanoparticles.

4.3.3 Optical limiting properties for nanosecond laser pulses

Figure 4.4 displays the nonlinear transmittance of the oleylamine capped gold nanoparticles in toluene with 7-ns pulses at 532 nm (Figure 4.4a) and 1064 nm (Figure 4.4b). The insets are the corresponding plots of output energy density (J/cm^{-2}) as a function of input energy density. The linear transmittance of the nanoparticles at 532 nm and 1064 nm were adjusted to 70% and 77% respectively. Carbon nanotubes (CNTs) has been known as a benchmark optical limiting material[2] and its optical limiting property was also characterized under the same experimental conditions and with the same linear transmittance as oleylamine capped gold nanoparticles for direct comparison. It has been previously reported that toluene showed slight optical limiting activity at 532 nm.[13] The optical limiting property of pure toluene was also measured at the same conditions to clarify the solvent contribution.

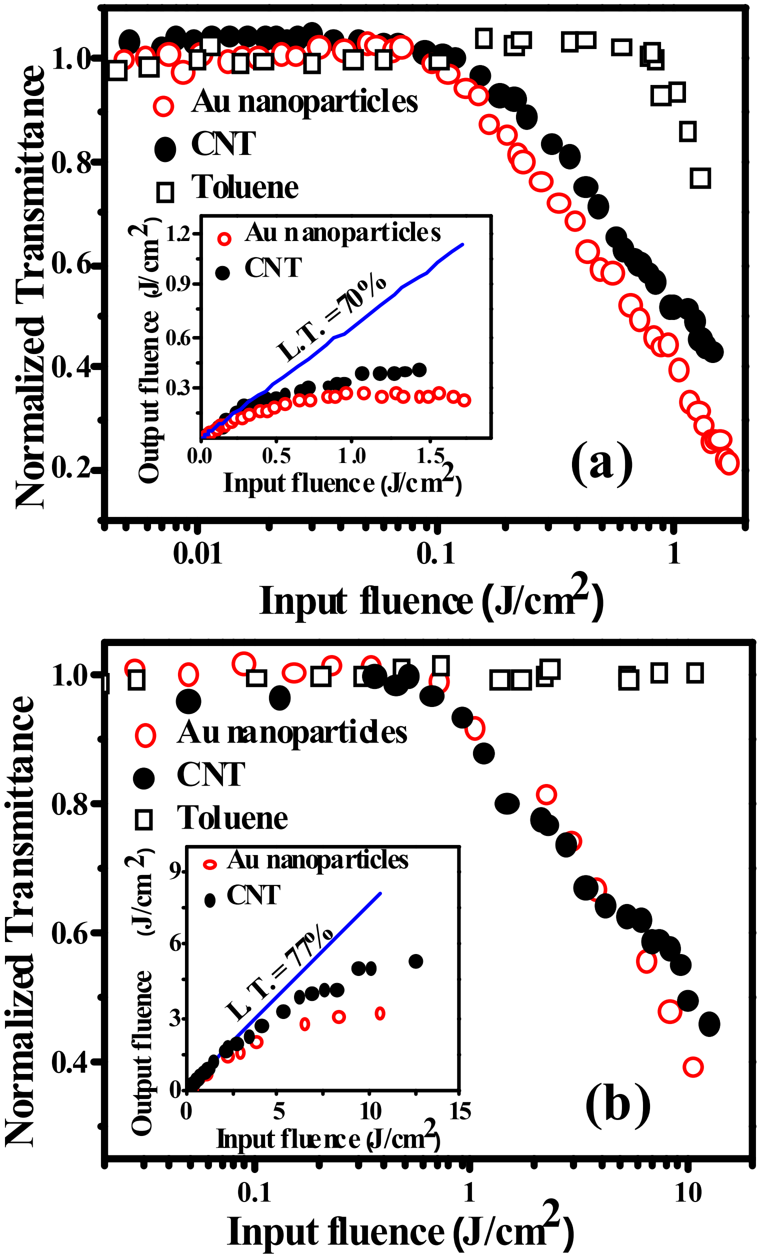

Fig. 4.4 The optical limiting response of the oleylamine capped gold nanoparticle solution, CNT suspension and toluene measured using 7ns laser pulses at 532 nm (a), and 1064 nm (b). The insets show the corresponding output energy (J/cm^2) as a function of input energy density (J/cm^2).

As shown in Figure 4.4a, the transmittance of the oleylamine capped gold nanoparticle solution slightly increases as the input energy density increases up to 0.07 J/cm^2, which was believed due to saturable absorption of the nanoparticles.[5] Saturable absorption of nanoparticles arises due to the ground-state plasmon bleaching at moderate intensities, which result in reduction of light absorptivity of materials with increasing light intensity. When input fluence further increases, the transmittance starts to decreases, displaying optical limiting activity. The optical limiting performance of these oleylamine capped gold nanoparticles is even better than that of carbon nanotubes (CNTs), a benchmark optical limiting material. The limiting threshold is defined as the incident fluence at which the transmittance falls to 50% of the normalized linear transmittance.[2] The limiting thresholds at 532 nm are 0.6 J/cm^2 and 1.0 J/cm^2 for the oleylamine capped gold nanoparticles and CNTs, respectively. In the pure toluene, we also observed optical limiting effects at 532 nm with a threshold much higher than that of oleylamine capped gold nanoparticles in toluene. These results suggest that the major contribution arises from the gold nanoparticles. The limiting threshold for these oleylamine capped gold nanoparticles is significantly better than those previously reported monolayer protected gold nanoparticles,[13] dendrimer capped gold nanoparticles[11] and covalently bonded gold nanoparticles.[15] In these previous studies, the threshold of these materials have been reported to be ~2 J/cm^2.

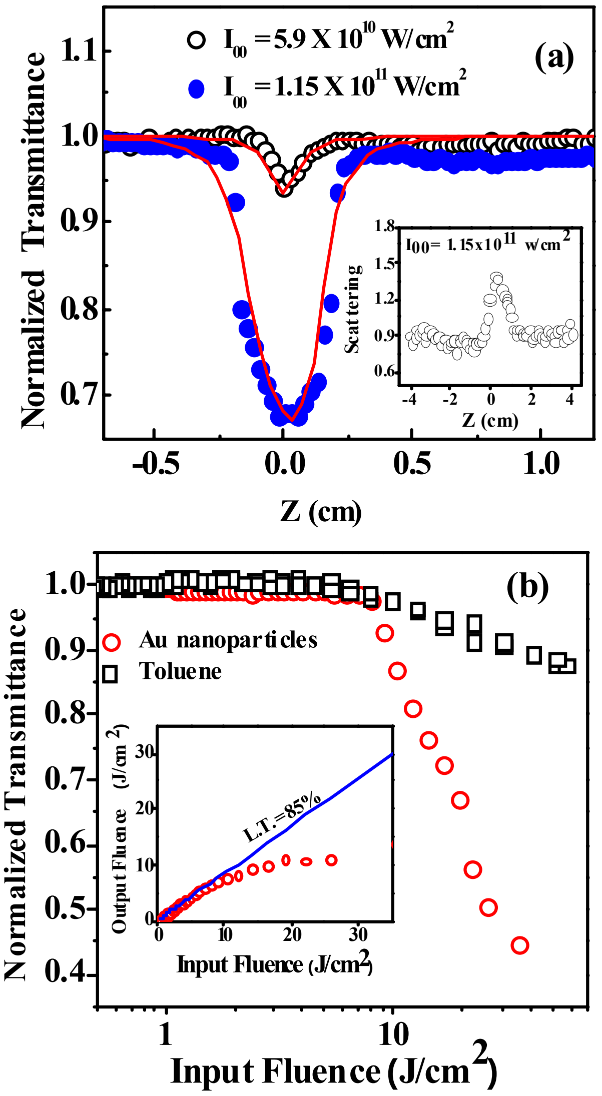

Fig. 4.5 (a) A typical open aperture *z*-scan measurement for oleylamine capped gold nanoparticle solution at 780 nm with a pulse width of 300 fs at two different input intensities. The inset is the results of scattering experiments by placing a detector at an angle of 45 degree to the laser beam direction during the z-scan experiments. (b) Optical limiting behavior of oleylamine capped gold nanoparticle solution and pure toluene at 780 nm. The data were extracted from the Z-scan measurement. The inset of Figure 4.5b shows the output fluence (J/cm^2) as a function of input fluence (J/cm^2) for oleylamine capped gold nanoparticle solution.

Figure 4.4b shows the optical limiting properties of oleylamine capped gold nanoparticle solution, CNT suspension and toluene at 1064 nm. The optical limiting performance of the gold nanoparticles at 1064 nm was found to be slightly better than that of CNTs, while no optical limiting effect was observed in the toluene solvent at 1064 nm. The limiting thresholds for the gold nanoparticles and CNTs at 1064 nm are 7.5 J/cm^2 and 10.0 J/cm^2 respectively.

4.3.4 Optical limiting properties for femtosecond laser pulses

The femtosecond optical limiting properties of the oleylamine capped gold nanoparticles in toluene were characterized using a femtosecond z-scan technique employing 300 fs laser pulses at 780 nm. Figure 4.5a shows the open-aperture z-scan measurement at two input intensities. In a z-scan experiment, the pump density increases as the sample moves into the beam focus. The z-scan measurements on the gold metal nanoparticle solution at both input intensities show a reverse saturable absorption behavior: the transmission of the sample decreases as the sample moves into the beam focus. The observed reverse saturable absorption is an indicator of optical limiting effect. The optical limiting effect can be manifested by plotting the output energy density versus input energy density as shown in Figure 4.5b (The data were extracted from the open aperture z-scan measurements). The sample exhibits high linear transmittance (85%) at lower input fluence and the transmittance decreases as the input fluence exceeds 8 J/cm^2, displaying optical limiting activity with a threshold of 26.0 J/cm^2.We have also measured the nonlinear transmission of the pure toluene under the same experimental conditions (See Fig. 4.6). Pure toluene was found to show much lower nonlinearity compared to that of oleylamine capped gold nanoparticles, suggesting that the major contribution arises from the gold nanoparticles (see Fig. 4.5b).

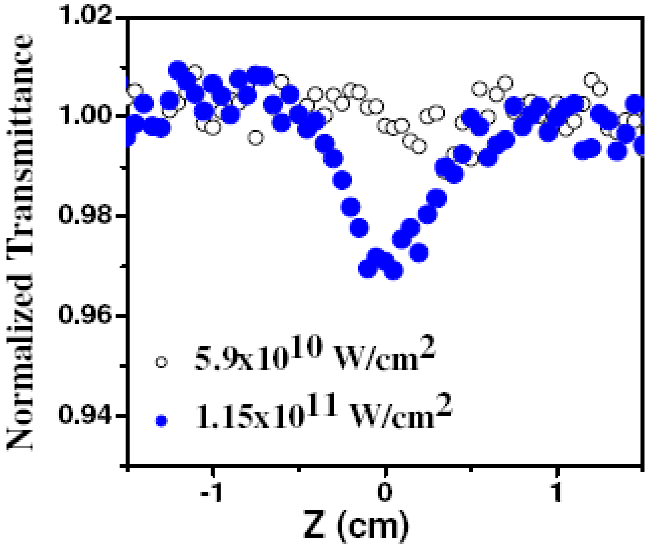

Fig. 4.6 A typical open aperture *z*-scan measurement for pure toluene solution at 780 nm with a pulse duration of 300 fs at two different input intensities.

4.3.5 Nonlinear scattering Measurements

Several mechanisms, such as multi-photon absorption[27] and nonlinear scattering,[2, 5] could be responsible for the optical limiting activity of materials. We have recently demonstrated that the optical limiting property of metal nanoparticles at 532 nm was mainly due to nonlinear scattering.[5, 12] To understand the mechanisms responsible for the strong optical limiting activity of these oleylamine capped gold nanoparticles at 532 nm and 1064 nm, we have also performed input fluence dependent scattering experiments on the oleylamine capped gold nanoparticle solution and CNT suspension using 532 nm and 1064 nm laser pulses (Figure 4.7). The scattering signals were monitored at different angles to the propagation axis of the transmitted laser beam. Figures 4.7a&4.7b show the input laser fluence dependent scattering signal collected at an angle of 40 degree to the propagation axis of the transmitted laser beam at 532 nm and 1064 nm. For both oleylamine capped gold nanoparticle solution and CNT suspension samples, the scattering signals were dominated by linear scattering at low input fluences, and became deviated from linear behavior as the input fluence increased above some threshold. The contribution from nonlinear scattering became the dominant contribution at high pump fluences. Figures 4.7c&4.7d show the scattering signals at different angles (every 5 degrees from 10 to 180 degree) with respect to the transmitted laser beam for both the oleylamine capped gold nanoparticle solution and CNT suspension with incident intensity of 1.5 J/cm^2 for 532 nm laser pulses and 5 J/cm^2 for 1064 nm laser pulses. For both gold nanoparticles and CNTs, the scattering signals in the forward directions were significantly larger than those in the backward directions. The light scattering signals of the gold nanoparticles were significantly larger than those of CNTs in both forward and backward directions at both 532 nm and 1064 nm. For the 532 nm laser pulses, the larger difference between the scattering signals of gold nanoparticles and CNTs occurred at smaller angles (<20 degrees). In the case of 1064 nm laser pulses, the larger difference in the scattering signals of gold nanoparticles and CNTs occurred at ~40 degrees. These results suggest that the nonlinear scattering played an important role in the observed optical limiting activity. The magnitude of the scattered signal for the oleylamine capped gold nanoparticles is higher than the scattering signal from CNTs at both 532 nm and 1064 nm, consistent with the better optical limiting performance of oleylamine capped gold nanoparticles compared to CNTs.

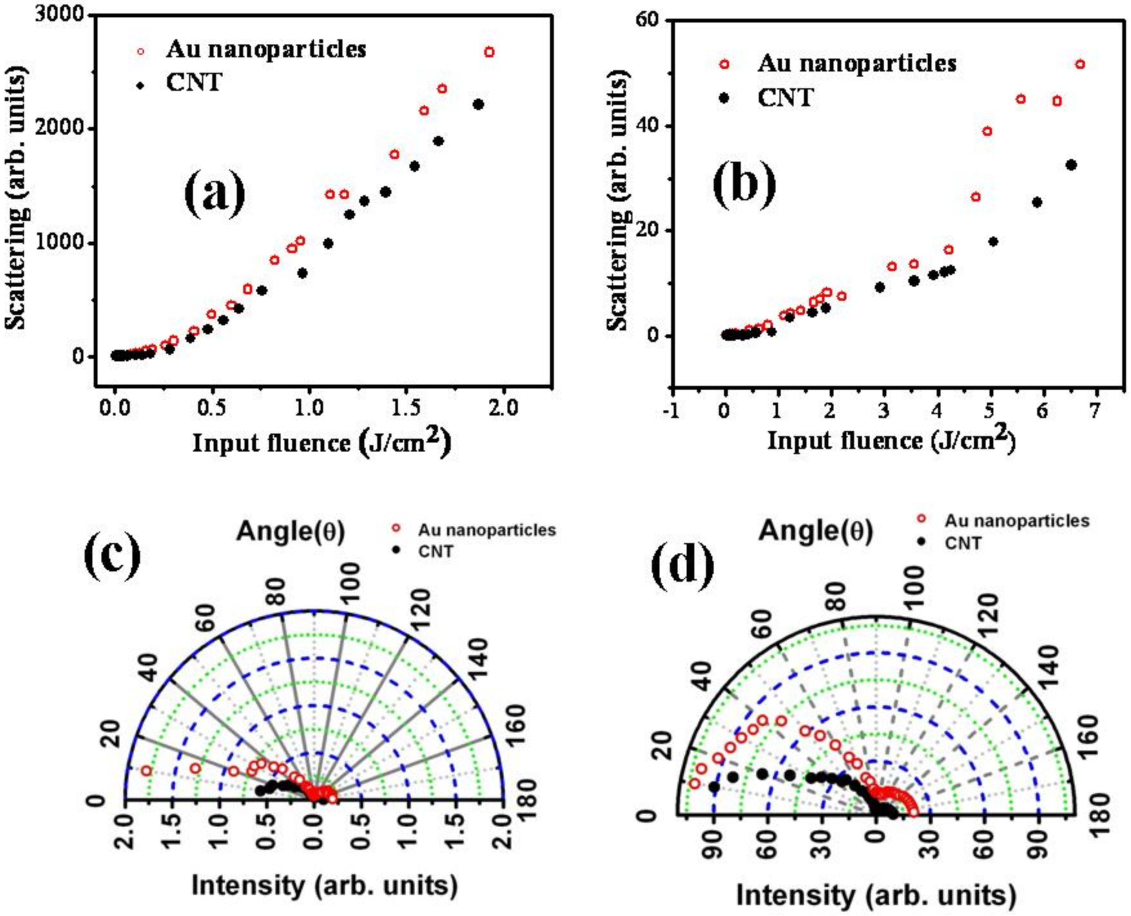

Fig. 4.7 Nonlinear scattering results for the oleylamine capped gold nanoparticle solution and CNT suspension using 532 nm (7 ns) (a and c) and 1064 nm (7 ns) (b and d) laser pulses. (a) and (b) are nonlinear scattering signals at an angle of 40^0 to the propagation axis of the transmitted laser beam. (c) and (d) are the polar plot of the scattering signal as a function of the angular position of the detector for oleylamine capped gold nanoparticles (c) and CNTs (d).

The nonlinear scattering usually arises from the formation of two types of scattering centers after photo-excitation of the nanoparticles. At higher pump fluence, the excitation energy absorbed by the nanoparticle creates a fast expansion of the metal nanoparticle, which acts as a scattering center. The absorbed energy is subsequently transferred to the surrounding solvent. Consequently the solvent is heated up and bubbles are formed, which act as secondary scattering centers.[1] The solvent in which nanoparticles are dispersed plays an important role in enhancing the optical limiting activity of the nanoparticles through microbubble formation. The microbubbles formation usually occurs at the interface of the solvent and nanoparticle. Solvents with good thermal conductivity can quickly transfer the thermal energy from the nanoparticle to solvent after photo-excitation to dissipate the energy. Solvents with low thermal conductivity can help to confine the energy at the interface and promote solvent vaporization and bubble formation. Nanoparticles dispersed in solvents with low thermal conductivity, low heat capacity and low boiling point are expected to show good performance in generating scattering centers and hence give rise to optical limiting effects. It has been recently reported by Wang et al. that the optical limiting properties of CNTs are better in low boiling solvents.[7]

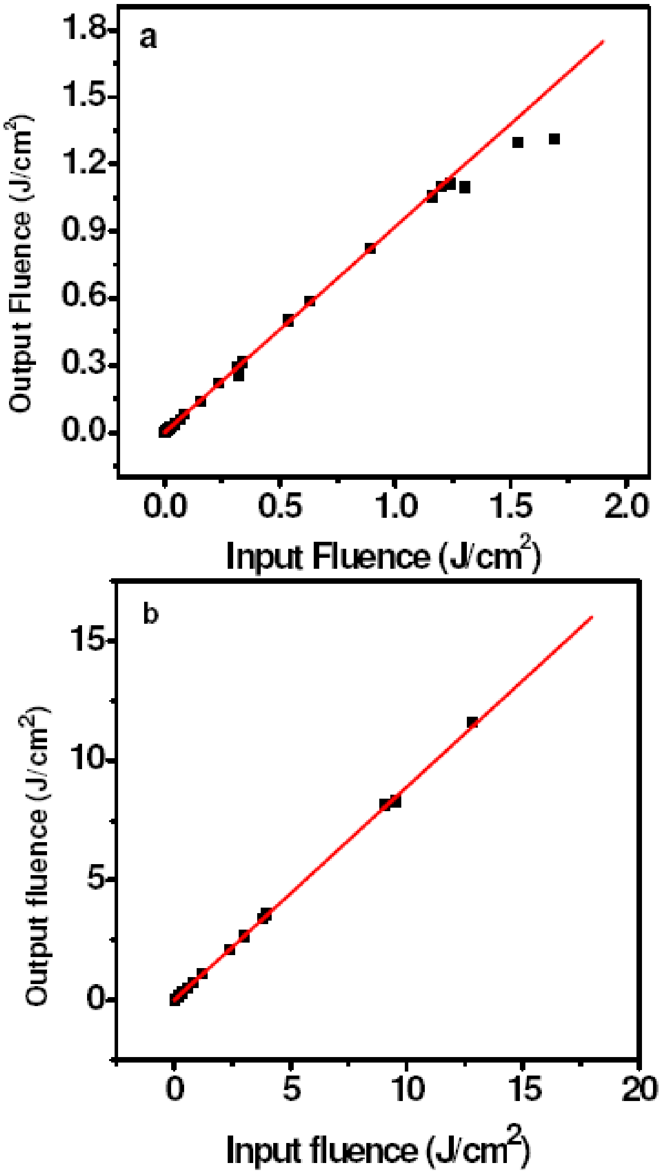

Fig. 4.8 Output energy (J/cm2) as a function of input energy (J/cm2) for citrate capped gold nanoparticles in water at (a) 532 nm (b) 1064 nm.

We have compared the optical limiting performance of the oleylamine capped gold nanoparticles in toluene with the citrate capped gold nanoparticles in water at the same experimental conditions. The citrate capped gold nanoparticles did not show any optical limiting activity at 532nm and 1064nm (see fig.4.8). The boiling points of water and toluene are quite similar. However, the thermal conductivity and heat capacity of toluene are much lower than those of water. In addition, in the oleylamine capped gold nanoparticles, gold is passivated through the -NH group with the oleylamine ligand. It has been previously demonstrated that the metal-to-solvent energy transfer is faster in NH- or SH- passivated gold nanoparticles compared to that in the citrate capped gold nanoparticles.[28-30] Optical limiting activity in amine (NH) and thiol (SH) passivated gold nanoparticles has been previously reported by a few groups.[11, 13] Therefore fast metal-to-solvent energy transfer, low thermal conductivity and low heat capacity all contribute together, leading to a quick local heating of the interface layer between the particle and solvent, which raises the temperature above a critical temperature to form the bubbles. These microbubbles act as scattering centers and result in enhanced optical limiting properties in oleylamine capped gold nanoparticles in toluene, compared to citrate capped gold nanoparticles in water.

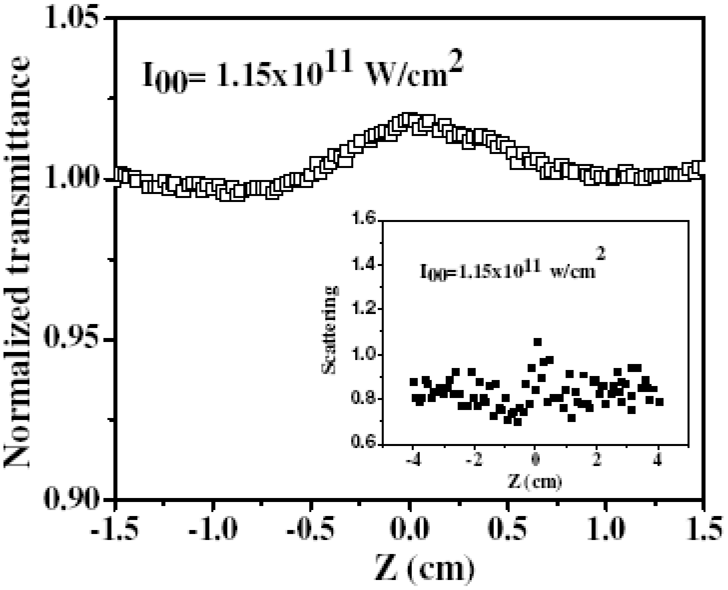

Fig. 4.9 A typical open-aperture *z* scan measurement for citrate capped gold nanoparticles in water at 780 nm with a pulse width of 300 fs. The inset shows the scattering measurement on water soluble gold nanoparticles, which suggests that there is little nonlinear scattering.

The reverse saturable absorption of gold nanoparticle under the illumination of femtosecond laser pulses at 780 nm was usually believed due to nonlinear absorption, including excited state absorption[4,31, 32] and plasmon enhanced multi-photon absorption.[33, 34] The excited state absorption includes photo-thermally induced transient absorption[31, 32] and free carrier absorption.[4] Upon the photo-excitation, the electrons are excited to energy levels higher than the Fermi level, resulting in an increased electronic temperature. The increase in the electronic temperature will lead to new transient absorption signals.[31, 32] However, we have also performed z-scan measurement for the citrate capped gold nanoparticles in water under the same experimental conditions. Saturable absorption, instead of optical limiting effect, was observed for the citrate capped gold nanoparticles (See Fig 4.9). The results suggest that the nonlinear absorption should not be the dominant factor that accounts for the reverse saturable absorption observed for the oleylamine capped gold nanoparticles since nonlinear absorption should apply similarly for gold nanoparticles dispersed in toluene and water. Considering that the major difference between the two systems is the solvent, nonlinear scattering should play very important roles for the observed optical limiting effect for femtosecond pulses at 780 nm. The scattering centers are formed mainly due to thermal-induced nonlinearity. We have performed scattering experiments for both oleylamine capped gold nanoparticles in toluene and citrate capped gold nanoparticles in water under the same experimental conditions, by placing a detector at an angle of 45 degree to the laser beam direction during the z-scan experiments. In the case of oleylamine capped gold nanoparticles in toluene, the scattering intensity increased as the sample moved towards the focus of the laser beam (see the inset of Figure 4.5a). There was nearly no increase in the scattering signal for the citrate capped gold nanoparticles (See Fig.4.9) under the same experimental conditions. These results suggest that nonlinear scattering plays a very important role in the optical nonlinearity of the oleylamine capped gold nanoparticles.

The z-scan results can be fitted well by considering both linear absorption, two-photon absorption and scattering (linear and nonlinear) as shown in Figure 4.5a by using the following equation[35, 36]

$$\frac{dI}{dz} = -\alpha_0 I - \beta I^2 - \alpha_s I \ , \qquad (1)$$

where $\alpha_s = g_s(\Delta\tilde{n})^2 \approx g_s(\Delta n_0 + \Delta n_2 I)^2$, α_0 is the ground state absorption coefficient and is taken as 2.2 cm^{-1} (80% linear transmittance), β is the two-photon absorption coefficient, and α_s is the effective scattering coefficient; g_s is a parameter that is independent of laser intensities but depends on the size, shape, and concentration of particles and wavelength of light, $\Delta\tilde{n}$ is the difference in the effective refractive indices of both linear and nonlinear components, Δn_0 is the difference between the linear refractive indices of gold nanoparticles and toluene, Δn_2 is the difference in nonlinear refractive indices between gold nanoparticles and toluene. Using the Runge-Kutta fourth order method,[37] the solution to the above equation can be obtained by integrating over time and transverse space of laser pulses. The β and Δn_2 values can then be determined to be 9.7 x 10^{-11} cm/W and 9.5 x 10^{-12} cm^2/W, respectively, through least square fit of the experimental data (by taking linear refractive indices of gold and toluene as 0.17 and 1.4963 respectively at 780 nm wavelength).

4.4 Conclusion

Here we report strong broadband optical limiting properties of oleylamine capped gold nanoparticles for both femtosecond and nanosecond laser pulses. The thresholds for the optical limiting properties of the oleylamine capped gold nanoparticles with 532 nm and 1064 nm laser pulses are lower than the CNT suspension that are known as a benchmark optical limiter. Fluence dependent and angle dependent scattering measurements confirm that the nonlinear scattering plays a very important role in the exceptional optical limiting activity of oleylamine capped gold nanoparticles at 532 nm with 7-ns pulses, at 1064 nm with 7-ns pulses and at 780 nm with 300 fs pulses. Two-photon absorption also partially contributes to the observed optical limiting effects for femtosecond laser pulses at 780 nm. These nanoparticles could be a good replacement for CNTs for optical limiting applications.

4.5 References:

1. Chen, P., Wu, X., Sun, X., Lin, J., Ji, W., Tan, K. L. *Phys. Rev. Lett.* **1999**, *82*, 2548.
2. He, G. S., Tan, L. S., Zheng, Q., Prasad, P. N. *Chem. Rev.* **2008**, *108*, 1245.
3. Elim, H. I., Yang, J., Lee, J. Y., Mi, J., Ji, W. *Appl. Phys. Lett.* **2006**, *88*, 083107.
4. Polavarapu, L., Xu, Q. H., Dhoni, M. S., Ji, W. *Appl. Phys. Lett.,* **2008**, *92*, 263110.
5. Liu, Z. B., Tian, J. G., Guo, Z., Ren, D. M., Du, T., Zheng, J. Y., Chen, Y. S. *Adv. Mater.* **2008**, *20*, 511.
6. Wang, J., Blau, W. J. *J. Phys. Chem. C* **2008**, *112*, 2298.
7. Mansour, K., Soileau, M. J., Vanstryland, E. W. *J. Opt. Soc. Am. B,* **1992**, *9*, 1100.
8. Chen, Y., Fujitsuka, M., O'Flaherty, S. M., Hanack, M., Ito, O., Blau, W. J. *Adv. Mater.* **2003**, *15*, 899.
9. Calvete, M., Yang, G. Y., Hanack, M. *Synth. Met.* **2004**, *141*, 231.
10. Francois, L., Mostafavi, M., Belloni, J., Delaire, J. A. *Phys. Chem., Chem. Phys.* **2001**, *3*, 4965.
11. Ispasoiu, R. G., Balogh, L., Varnavski, O. P., Tomalia, D. A., Goodson, T. *J. Am. Chem. Soc.* **2000**, *122*, 11005.
12. Pan, H., Chen, W. Z., Feng, Y. P., Ji, W., Lin, J. Y. *Appl. Phys. Lett.,* **2006**, 88, 223106.

13. Philip, R., Kumar, G. R., Sandhyarani, N., Pradeep, T. *Phys. Rev. B* **2000**, *62*, 13160.

14. Porel, S., Venkatram, N., Rao, D. N., Radhakrishnan, T. P. *J., Nanosci. Nanotechnol.* **2007**, *7*, 1887.

15. Sun, W. F., Dai, Q., Worden, J. G., Huo, Q. *J. Phys. Chem. B* **2005**, *109*, 20854.

16. Sun, Y. P., Riggs, J. E., Rollins, H. W., Guduru, R. *J. Phys. Chem. B,* **1999**, *103*, 77.

17. Wang, G., Sun, W. F. *J. Phys. Chem. B* **2006**, *110*, 20901.

18. Qu, S. L., Gao, Y. C., Jiang, X. W., Zeng, H. D., Song, Y. L., Qiu, H. R., Zhu, C. S., Hirao, K. *Opt. Commun.* **2003**, *224*, 321.

19. Francois, L., Mostafavi, M., Belloni, J., Delouis, J. F., Delaire, J., Feneyrou, P. *J. Phys. Chem. B* **2000**, *104*, 6133.

20. Sinani, V. A., Gheith, M. K., Yaroslavov, A. A., Rakhnyanskaya, A. A., Sun, K., Mamedov, A. A., Wicksted, J. P., Kotov, N. A. *J. Am. Chem. Soc.* **2005**, *127*, 3463.

21. Ganeev, R. A., Baba, M., Ryasnyansky, A. I., Suzuki, M., Kuroda, H. *Opt. Commun.* **2004**, *240*, 437.

22. Scalora, M., Dowling, J. P., Bowden, C. M., Bloemer, M. J. *Phys. Rev. Lett.* **1994**, *73*, 1368.

23. Nair, S. S., Thomas, J., Sandeep, C. S. S., Anantharaman, M. R., Philip, R. *Appl. Phys. Lett.* **2008**, *92*, 171908.

24. Wang, J., Hernandez, Y., Lotya, M., Coleman, J. N., Blau, W. J. *Adv. Mater.* **2009**, *21*, 2430.

25. Halder, A., Ravishankar, N. *Adv. Mater.* **2007**, *19*, 1854.

26. Lu, X. M., Tnan, H. Y., Korgel, B. A., Xia, Y. N. *Chem.sEur. J.* **2008**, *14*, 1584.

27. He, G. S., Yong, K. T., Zheng, Q. D., Sahoo, Y., Baev, A., Ryasnyanskiy, A. I., Prasad, P. N. *Opt. Express* **2007**, *15*, 12818.
28. Jain, P. K., Qian, W., El-Sayed, M. A. *J. Am. Chem. Soc.* **2006**, *128*, 2426.
29. Melinger, J. S., Kleiman, V. A., McMorrow, D., Grohn, F., Bauer, B. J., Amis, E. *J. Phys. Chem. A* **2003**, *107*, 3424.
30. Polavarapu, L., Xu, Q. H. *Nanotechnology* **2009**, *20*, 185606.
31. Lee, Y. H., Yan, Y. L., Polavarapu, L., Xu, Q. H. *Appl. Phys. Lett.,* **2009**, *95*, 023105.
32. Hartland, G. V. *Annu. Rev. Phys. Chem.* **2006**, *57*, 403.
33. Farrer, R. A., Butterfield, F. L., Chen, V. W., Fourkas, J. T. *Nano Lett.* **2005**, *5*, 1139.
34. Eichelbaum, M., Schmidt, B. E., Ibrahim, H., Rademann, K., *Nanotechnology* **2007**, *18*, 355702.
35. Venkatram, N., Rao, D. N., Akundi, M. A. *Opt. Express* **2005**, *13*, 867.
36. Joudrier, V., Bourdon, P., Hache, F., Flytzanis, C. *Appl. Phys. B: Lasers Opt.* **1998**, *67*, 627.
37. Butcher, J. C., Cash, J. R., Vanderhouwen, P. J. *J. Comput. Appl. Math.* **1993**, *45*, 1.

CHAPTER 5

NONLINEAR OPTICAL PROPERTIES OF GLUTATHIONE CAPPED GOLD CLUSTERS AND APPLICATION TO BIOIMAGING

5.1 Introduction

Recent developments in optical imaging techniques, in particular multi-photon excitation microscopy that allows studies of biological interactions at a deep cellular level, has motivated intensive research in developing multi-photon absorption fluorophores.[1–10] Biological tissues are optically transparent in the near-infrared (NIR) region.[4,11] Fluorophores that can absorb light in the NIR region by multi-photon absorption are particularly useful in bio-imaging.[4,6] Many organic dyes have been synthesized for multi-photon imaging, but their applications are limited by their small two-photon absorption (TPA) cross sections and rapid photo-bleaching.[2,9,10] Quantum dots have been known to be a good alternative for multi-photon imaging due to their large two-photon absorption cross sections.[6,12–15] However, their applications in bio-imaging have been restricted due to their cyto-toxicity and fluorescence blinking behavior.[16–23] Photoluminescence (PL) from noble metals was first observed in 1969 by Mooradian et al.[24] In 1986 Boyd et al.[25] observed strong photoluminescence from metal films with rough surfaces, in which local field enhancement was believed to be responsible for the observed strong PL. Farrer et al.[26] reported highly efficient multi-photon induced luminescence from gold nanoparticles of sizes ranging from 2.5–125 nm. Various metal nanoparticles with different shapes have been proposed as contrast agents for bio-imaging.[1,3,27–32] Among different metal nanoparticles, gold nanorods have been widely used for multiphoton cellular imaging due to their easy preparation of different sizes and aspect ratios.[3,27,29–31,33–36] However, their relatively large sizes limit their applications for intracellular imaging. In addition, gold nanorods are not suitable for one-photon imaging due to their low quantum yields. Recently a lot of research attention has been paid to fluorescent gold clusters.[28,37–47] Gold nanoparticles with sizes close to the Fermi wavelength (<1 nm) of the electron possesses molecule like properties and are denoted as gold clusters.[42,45,48] Gold clusters have many attractive features, such as strong fluorescence (quantum yields of 0.1-3 %), excellent biocompatibility, water solubility, long term stability, and low toxicity, which make them promising candidates in many biological applications. So far most of the research has focused on developing various synthetic methods to fine control the number of atoms in a cluster.[37,46,47,49–51] There are few investigations on their nonlinear optical properties[45,48] and applications in bio-imaging.[43] Ramakrishna et al.[45] recently investigated two-photon absorption properties of quantum sized gold clusters dispersed in toluene, which showed extremely high TPA cross sections at 800 nm. However, those gold clusters are only soluble in organic solvents such as toluene, which makes it difficult to functionalize them with other biomolecules, and limits their application in biological systems. These studies motivated us to investigate the two-photon properties of water soluble gold clusters and their applications in bioimaging. Among various water soluble gold clusters, glutathione capped gold clusters were known able to be further functionalized for biological applications.[39,42,51] Their linear optical properties have been well characterized.[39,42,51] However, their nonlinear optical properties and applications as fluorescence imaging contrast agents have yet to be explored. In this work we have investigated linear and nonlinear optical properties of glutathione capped gold clusters. These gold clusters display strong one- and two-photon excitation emissions. We have successfully demonstrated their applications as fluorescence contrast agents for live cell imaging. In addition, they displayed very good photostability and bio-compatibility. These gold clusters were found to have very low toxicity to live cells even at high concentrations. These exceptional properties make them promising materials for bio-imaging and other nonlinear optical applications.

5.2 Experimental section

5.2.1 Preparation and characterizations of glutathione capped gold clusters

The glutathione capped gold clusters were prepared by using a method modified from the one reported previously for the synthesis of mercaptosuccinic acid monolayer protected gold clusters by Murray et al.[50] Briefly, 80 ml of $1.25\text{x}10^{-2}$ M $HAuCl_4$ methanol solution and 40 ml of 0.075 M glutathione aqueous solution were mixed under stirring. 10 ml of 1.0 M NaBH4 aqueous solution was quickly added into the mixture. The solution immediately turned a brown colour and the stirring was continued for one hour. The solvent was evaporated at 43^0C to concentrate the solution and excess methanol was added to precipitate the clusters. The precipitate was then filtered, dissolved in~2 ml of distilled water and precipitated with methanol again to remove any impurities. The obtained gold clusters precipitate was finally dispersed in 100 ml of water for further characterizations. UV–Vis and emission spectra of the gold clusters were measured by using a Shimadzu UV 2450 spectrometer and a Perkin Elmer L55 fluorimeter, respectively. The TEM images were taken by using a JEOL2010 electron microscope.

5.2.2 Two-photon photoluminescence (TPL) measurement

The excitation source for two-photon photoluminescence (TPL) measurement was a Spectra Physics femtosecond Ti:sapphire oscillator (Tsunami), which gives output laser pulses with a tunable central wavelength from 770 to 830 nm and a repetition rate of 80 MHz. The samples were excited by directing a tightly focused laser beam onto the sample. The emission from the sample was collected at a 90^0 angle, perpendicular to the incoming excitation beam. The fluorescence signal was directed into a monochromator (Acton, Spectra Pro 2300i) coupled CCD (Princeton Instruments, Pixis 100B) with an optical fiber. A short pass filter with a cut-off wavelength at 750 nm was placed before the spectrometer to minimize the light scattering from the excitation beam.

5.2.3 Two-photon absorption (TPA) cross section measurement using z-scan method

The femtosecond z-scan measurements were performed by using a mode-locked Ti:sapphire oscillator seeded regenerative amplifier, which gives output laser pulses with a central wavelength at 800 nm and a repetition rate of 1 kHz. The laser beam was focused onto the gold cluster solution ($1 \text{ X } 10^{-6}$ M) samples contained in a 1 mm thick quartz cuvette, with a beam waist of ~20 mm. The pulse duration of the laser pulse at the sample is ~200 fs. The sample was moved along the z axis towards and away from the focus point while the transmitted signal was monitored with a lock-in amplifier. The experiment was done with an open aperture configuration. The TPA coefficient (β) was obtained by fitting the Z-scan data with a two-photon absorption model and then the TPA cross section (σ) was calculated by using the following equation.[9,28]

$$\sigma = \frac{\beta h\upsilon \times 10^3}{N_A d}$$

Where N_A is the Avogadro constant, h is the plank constant; d is the concentration of the gold cluster solution and ν is the frequency of the incident laser.

5.2.4 Cell culture and incubation for imaging

SH-SY5Y neuroblastoma (ATCC, USA) cells were grown at 37^0C in Dulbecco's Modified Eagle's Medium (DMEM/F12 (1 : 1); Gibco, USA) supplemented with 10% fetal bovine serum (FBS; Gibco, USA) and 1% antibiotic (penicillin streptomycin, Gibco, USA). The cells were placed in a 8-well chamber with a 0.17 mm coverslip bottom (Nunc, Denmark) one day prior to the addition of the gold clusters. The cells were washed with HBSS/HEPES buffer and incubated with 50 μgml^{-1} gold clusters for 24 h. Cells were then washed three times again with the same buffer solution and suspended in indicator free DMEM for imaging.

5.2.5 One- and two-photon fluorescence imaging

5.2.5.1 One-photon imaging. The imaging was performed on an Olympus FV300 inverted confocal microscope. A 633 nm He–Ne laser (Melles Griot, Singapore) with an excitation power of 100 μW was directed by a long pass dichroic mirror and scanning mirrors to a water immersion objective (60X, NA1.2, Olympus, Singapore), which focuses the light onto the samples. The fluorescence signal was then collected by the same objective and detected by the photomultiplier tube (PMT) after passing through a 660 nm long pass filter.

5.2.5.2 Two-photon imaging.

The two-photon imaging was performed on a Olympus IX70 conofcal microscope using a femtosecond Ti:sapphire laser (Mira 900, Coherent, Santa Clara, CA) as the excitation source. The output laser pulse has a wavelength of 800nm, repetition rate of 76 MHz and the pulse duration of 200 fs. The laser beam was directed into a confocal microscope, with the excitation power of 140 μW on the cells. The 60x water-immersion objective was used to focus the laser beam onto the gold cluster incubated live cells. The TPL was collected through the same objective, separated from the excitation laser by a dichroic mirror. The signal was directed to a photomultiplier tube (PMT) placed in the back port of the microscope. A 565 nm longpass filter was placed before the PMT to collect the TPL of gold clusters. All the imaging experiments were performed at 37^0C using a temperature controller.

5.2.6 Toxicity assay

In order to test the toxicity of the glutathione capped gold clusters on SH-SY5Y neuroblastoma (ATCC, USA) cells, the MTT [3-(4,5-dimethylthiazol-2-yl)-2,5-diphenyltetrazolium bromide] assay kit (Invitrogen, Singapore) was used. The MTT stock solution was prepared according to the protocol supplied by the kit.[60] The cells were seeded in a 24 well plate in 1 ml of culturing medium 24 h prior to nanoparticle incubation. The cells were subsequently incubated with different concentrations of glutathione capped gold clusters (50, 100, 200 and 400 mg ml^{-1}) for 24 h. Cells were then washed three times with HBSS/HEPES buffer followed by addition of 10 mL MTT solution to each well and incubated for 2 h at 37^0C. Then 100 mL of SDSHCl solution was added to each well and further incubated for 4 h at 37^0C. The entire content of each well was then mixed thoroughly and finally the absorbance of the resulting solution was measured at 570 nm using a UV 2450 spectrometer.

5.3 Results and discussion

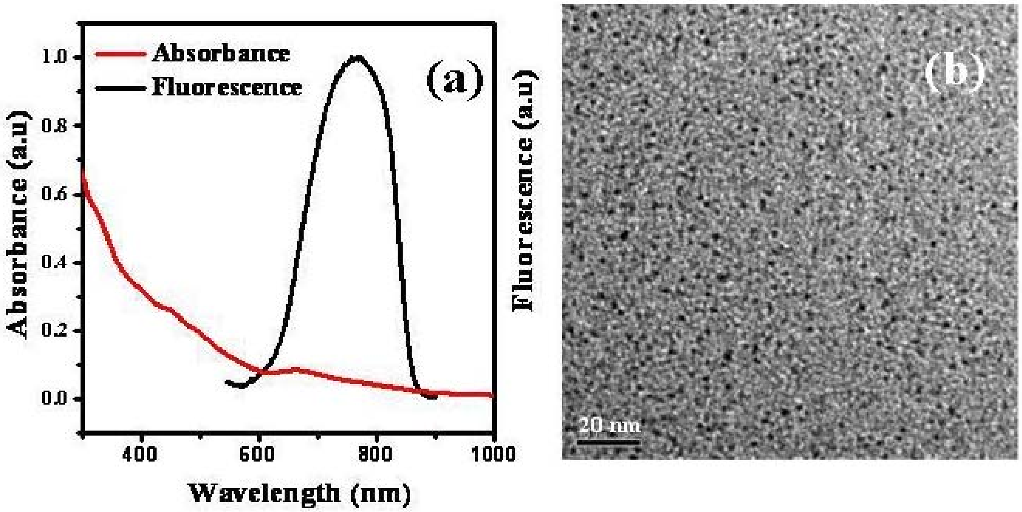

Fig. 5.1 (a) Absorption and emission spectra, and (b) TEM image of the glutathione capped gold clusters.

The glutathione capped gold clusters were prepared by using a modified method from one previously reported for the synthesis of mercaptosuccinic acid monolayer protected gold clusters by Murray et al.[50] The preparation procedures are described in the Experimental section **(5.2.1)**. Fig. 5.1 shows the UV-Vis absorption and emission spectra of the prepared glutathione capped gold clusters as well as their transmission electron microscopic (TEM) images. The TEM images were taken by drop casting a dilute gold-cluster solution onto a copper grid. The particles are quite monodisperse with sizes of 1–1.1 nm, which corresponds to approximately 25 atoms per cluster.[45]The UV-Vis spectrum of glutathione capped gold clusters shows an optical absorption maximum at 665 nm and a strong continuous band on the higher energy side. The band at 665 nm arises from intra-band (sp–sp) transition, which is expected for 25-atom gold clusters.[45,51] The absorption at the higher energy region arises from inter-band (sp–d) transition. The surface plasmon resonance was not observed in the UV-vis spectrum, suggesting that the sizes of the clusters are less than 2 nm.[45] The emission spectrum of the gold clusters under one-photon excitation at 650 nm has a dominant contribution in the near IR region with a band maximum at 780 nm. Their absorption and fluorescence spectra are consistent with the previously reported results.[50]

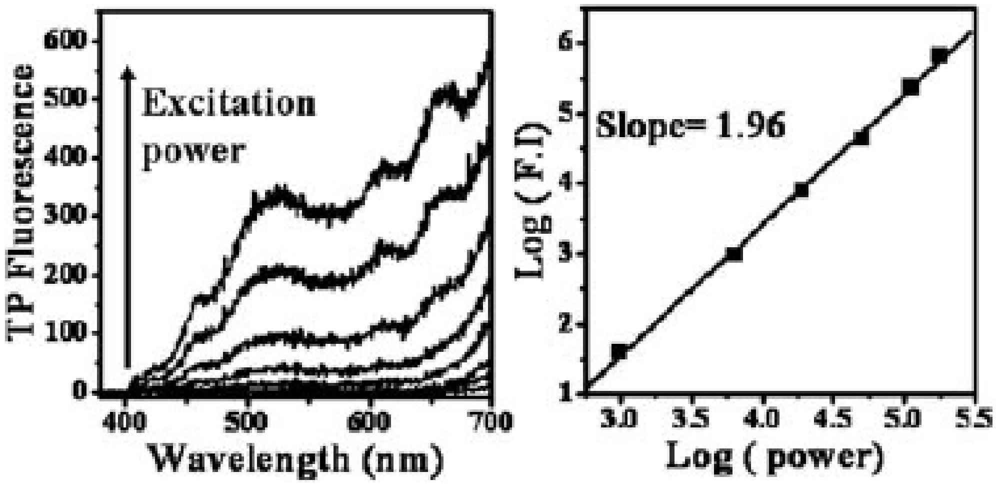

Fig. 5.2 (a) Excitation intensity dependent TPL spectra of glutathione capped gold clusters under excitation at 800 nm. (b) log–log plot of excitation intensity dependence of their TPL emission at 500 nm.

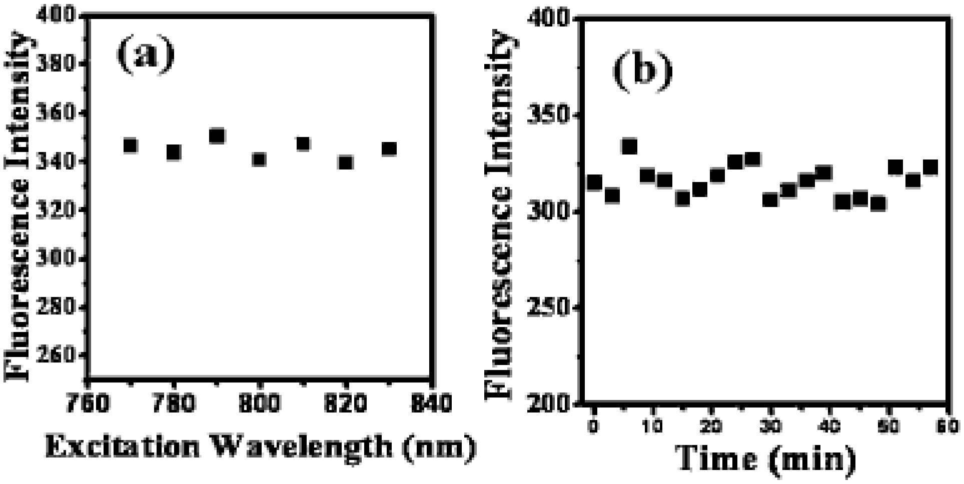

Fig. 5. 3 (a) TPL intensity of glutathione capped gold clusters at 500 nm under different excitation wavelengths and (b) under 800 nm for different periods of illumination time.

The gold clusters also show strong two-photon excitation photoluminescence (TPL). Fig. 5.2 shows TPL spectra of the gold clusters under excitation at 800 nm by using femtosecond laser pulses of different excitation intensities. A 750 nm short pass filter was used to block the scattering from the excitation source. The obtained TPL spectra of the gold clusters are very broad spanning over from 400 to 650 nm. The near-IR portion was not presented due to strong contamination from the scattering of the excitation beam. The log–log plot excitation power dependent emission intensities at 500 nm (Fig. 5.2) give a slope of ~2, confirming that the emission is due to a two-photon excitation process. When the gold clusters were irradiated with a continuous wave (CW) beam of the same wavelength and same power, the emission signal disappeared down to the background noise level, which further confirms the emission is due to a two-photon excitation process. It has been previously reported that the TPL of gold nanoparticles can be strongly enhanced by their surface plasmon resonance.[30,52] For example, gold nanorods with a longitudinal plasmon band at 800 nm emit strong TPL compared to spherical gold nanoparticles at an excitation wavelength of 800 nm, which was ascribed to plasmon resonance enhancement.[30,53] The TPL intensity of these gold nanorods was reported to be strongly dependent on the excitation wavelength.[30,53] We have measured the TPL of gold clusters over an excitation wavelength range from 770 to 830 nm, and little excitation wavelength dependence was observed (Fig. 5.3a). In addition, the TPL of these glutathione capped gold clusters in water showed very good photostability. The TPL intensity of these gold clusters in aqueous solution remained nearly constant during continuous irradiation with femtosecond laser pulses with power of 230 mW (Repetition rate of the laser is 76 MHz and the focus point is 20μM) for one hour (Fig. 5.3b). The good photostability of nanoparticles is a very important factor for their applications as fluorescence contrast agents for bio-imaging.

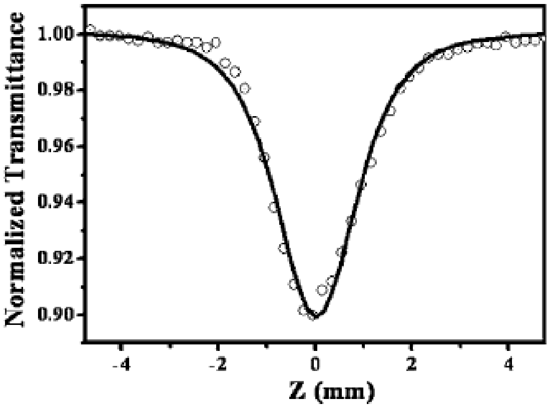

Fig. 5.4 z-Scan measurement results on the gold clusters under femtosecond laser excitation at 800 nm. The solid line is the best fit based on a two photon absorption model. The concentration of gold cluster is 1 x10^{-6} M and the pulse energy is 180 nJ.

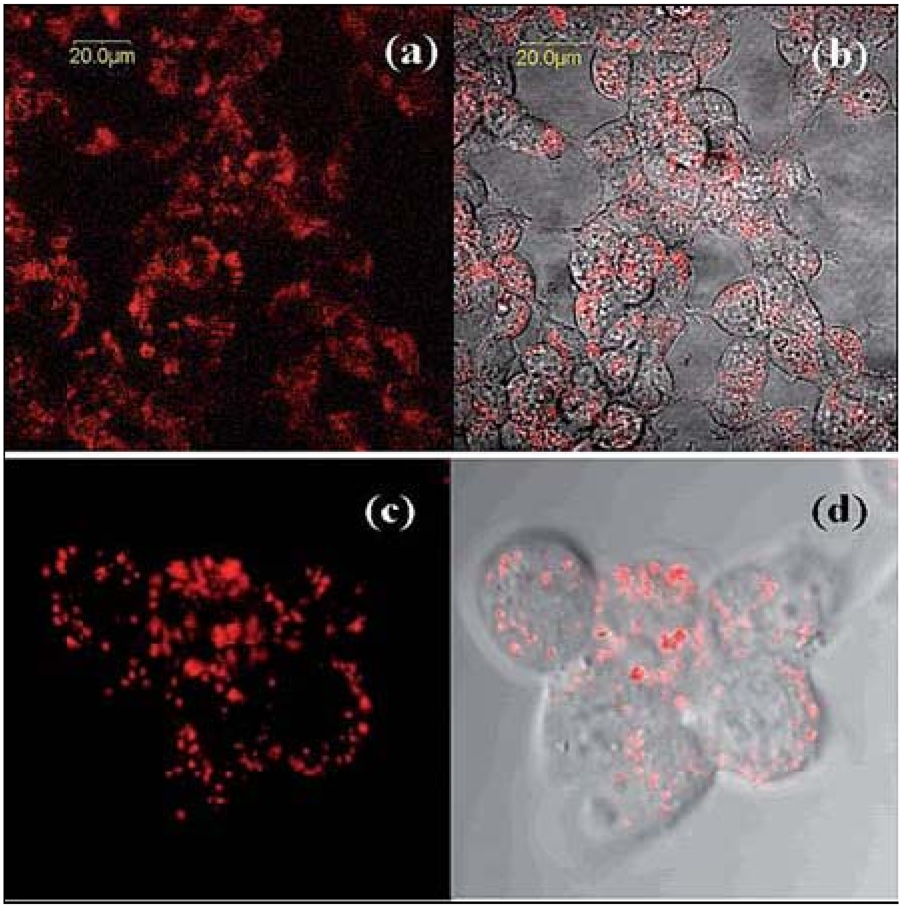

Fig. 5.5 One-photon (a) and two-photon (c) excitation fluorescence images of SH-SY5Y neuroblastoma cells that were incubated with the gold clusters. The excitation wavelength is 633 nm. The images on the right (b & d) are the overlaid pictures of the fluorescence images and the corresponding differential interference contrast (DIC) images.

I have also investigated the two-photon absorption (TPA) properties of the glutathione monolayer protected gold clusters by using a z-scan technique. Fig. 5.4 shows the z-scan measurement results using 800 nm femtosecond laser pulses as the excitation source with a pulse energy of 180 nJ. The data can be well fit using a two-photon absorption model[14,15,54] and the TPA cross section of the gold clusters was calculated to be ~189 740 GM, which is much higher compared to those of typical organic fluorescent dyes and quantum dots.[9,14,15] The obtained large TPA cross section value for glutathione monolayer protected gold clusters is on the same order of magnitude as the previous results obtained by Ramakrishna et al.,[45] who reported a TPA cross section of 427 000 GM for the Au25 clusters in toluene. The huge TPA cross section and exceptional photostability makes these gold clusters promising candidates for many nonlinear optical applications.

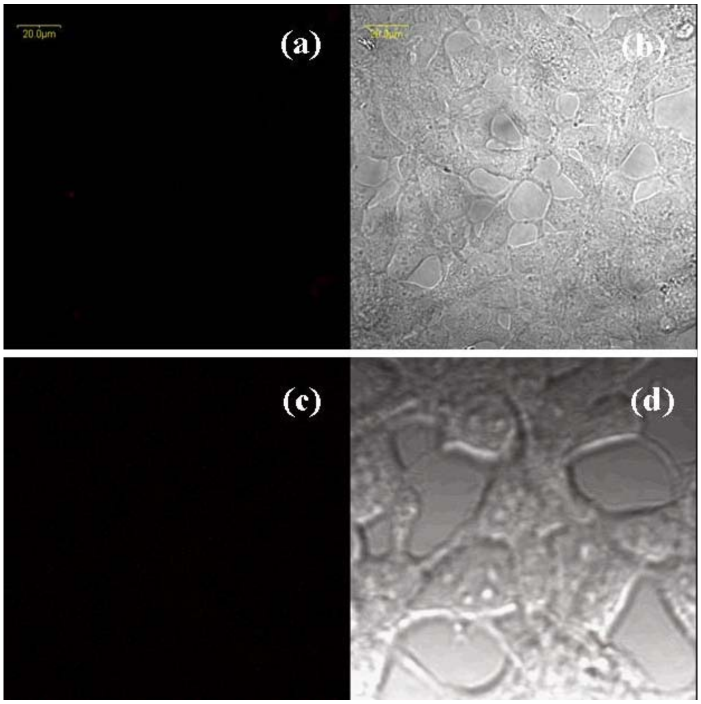

Fig. 5.6. One-photon (a) and two-photon (c) excitation fluorescence images of SH-SY5Y neuroblastoma cells without the incumbated of gold clusters**.** The excitation wavelength is 633 nm. The images on the right (b&d) are the overlaid pictures of the fluorescence images and the corresponding differential interference contrast (DIC) images.

I have tested the capability of gold clusters for both one- and two-photon excitation cell imaging on SH-SY5Y human neuroblastoma cells (human cancer cells). The cells were incubated with 50 μg ml^{-1} of gold clusters for 24 h and then subjected to confocal imaging. Fig. 5.5a shows one-photon excitation (633 nm) fluorescence image of SH-SY5Y human neuroblastoma cells using gold clusters as fluorescence contrast agents. It can be clearly seen that the particles are mainly located at the cytoplasm of the cells. To make sure that the observed fluorescence was indeed from gold clusters, we also performed a control experiment at the same experimental conditions without addition of gold clusters. We did not observe any fluorescence from the cells without incubation with the gold clusters (See fig.5.6). The control experiment confirms that the observed fluorescence was due to the gold clusters attached to those cells instead of autofluorescence of the cells. Fig. 5.5c shows the two-photon excitation fluorescence image of SH-SY5Y human neuroblastoma cells incubated with gold clusters under excitation of femtoseond laser pulses at 800 nm with an excitation power of 140mW. Similar to the one-photon excitation results, the particles inside the cells can be clearly seen and no auto-fluorescence from the cells was observed under the same experimental conditions (See fig.5.6). The cells were also imaged with a different z-position using a XYZ scanning mode[29] under two-photon excitation (Fig. 5.7). The z-stack sectioning clearly confirms that the glutathione capped gold clusters were internalized inside the cells. Many nanomatereials generally have strong cytotoxcity. Biocompatibility is a critical issue for their biological applications such as bio-imaging.[28,55–57]

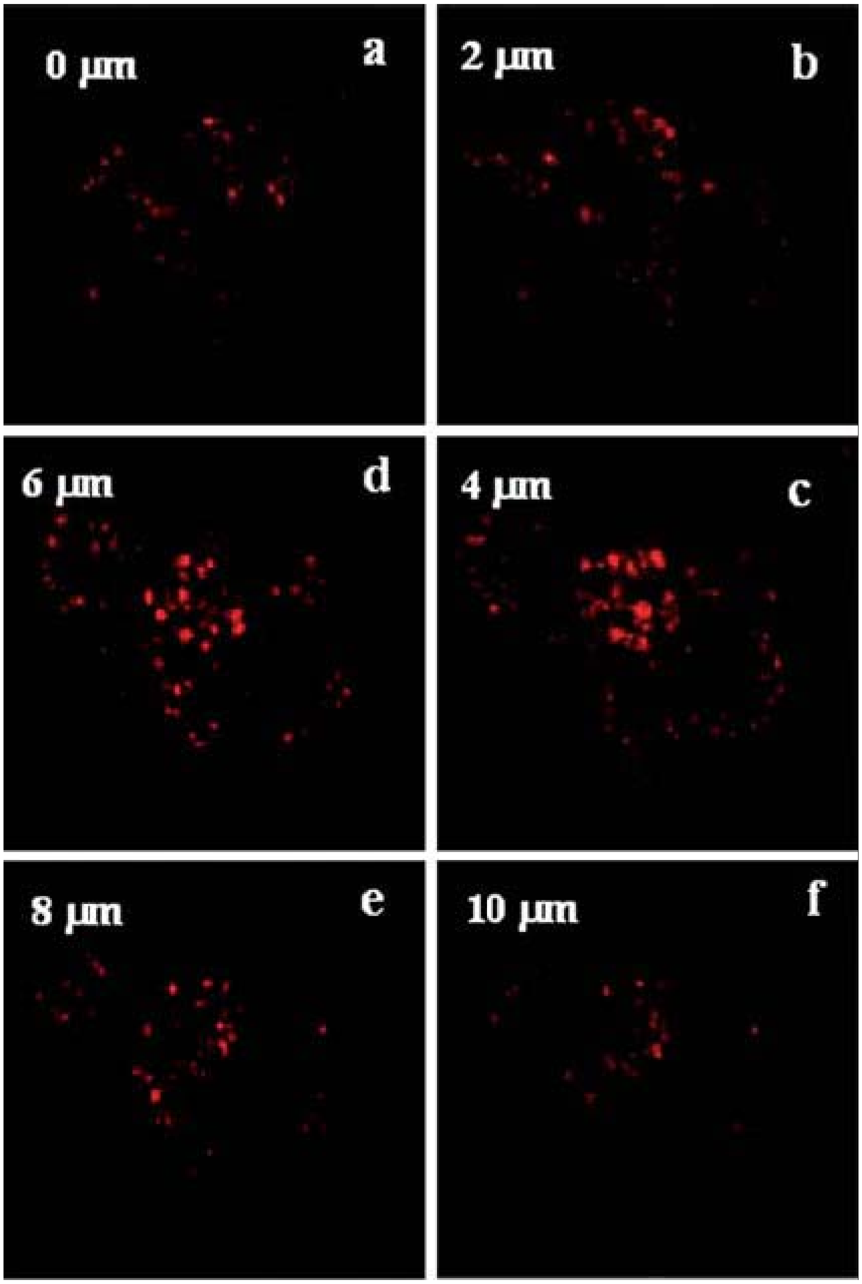

Fig. 5.7 z-Sectioning of SH-SY5Y neuroblastoma cell images obtained using gold clusters as two-photon fluorescence contrast agents under excitation of 800 nm femtosecond laser pulses.

I have examined the toxicity of the glutathione capped gold clusters on the SH-SY5Y human neuroblastoma cells using an MTT test (Fig. 5.8). The results clearly indicate that the cells are viable even at very high concentrations (400 mg ml^{-1}) of these glutathione capped gold clusters. Glutathione is a known antioxidant[58] that helps protect cells from reactive oxygen species such as free radicals and peroxides.[58,59] The glutathione capped gold clusters showed quite low toxicity toward the cells.

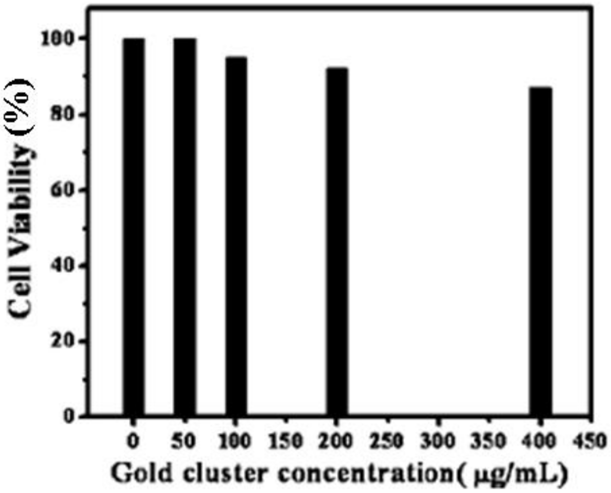

Fig. 5.8 The cell viability results obtained using MTT test after overnight incubation with different concentrations of glutathione capped gold clusters.

These gold clusters have unique advantages compared to the previously reported bio-imaging nanomaterials. Previously Wu et al.[31] have shown that gold nanorods are very good materials for two-photon imaging. However, gold nanorods are not proper for one-photon imaging due to it low quantum yields. Quantum dots are known as good imaging agents for both one-photon and two-photon excitation imaging. However, their cytotoxicity have limited their applications in bio-imaging. In addition, quantum dots typically show photo-blinking behavior.[20,23] It has been reported that Au clusters do not have this problem.[26] Most importantly, compared to gold nanorods and quantum dots, these gold clusters have much smaller sizes, which is particularly important for bio-imaging. Their small sizes make them easy to be introduced into cells and able to target the inside portions of the cells using these gold clusters, which may not be possible using larger size nanoparticles. These gold clusters are capable of acting as both one-photon and two-photon excitation imaging agents, which give similar imaging effects for conventional situations. However, their extra two-photon imaging capability allows them to penetrate deeper into the biological tissues and enable in vivo imaging with larger depths. In addition to their low toxicity and good biocompatability, the glutathione protected gold clusters can be further functionalized with biomolecules using the COOH group in glutathione for further applications.

5.4 Conclusions

In summary, one- and two-photon emission properties of glutathione capped gold clusters were investigated. The two-photon absorption properties of these monolayer protected quantum size gold clusters were studied by using two-photon excitation photoluminescence measurements and femtosecond z-scan technique. The TPA cross section of these glutathione capped gold clusters was measured to be ~189 740 GM in water, which is much larger compared to those of organic fluorescent dyes and quantum dots. In addition, these gold clusters show exceptional photo-stability. The gold clusters also displayed very low toxicity to cells even at high concentrations of gold clusters. We have successfully demonstrated their applications in both one- and two-photon excitation live cell fluorescence imaging. The exceptional properties of these gold clusters make them a good alternative for bio-imaging and other nonlinear optical applications.

5.5 References

1. L. Bickford, J. Sun, K. Fu, N. Lewinski, V. Nammalvar, J. Chang and R. Drezek, Nanotechnology, 2008, **19**, 315102.
2. Z. Cheng, J. Levi, Z. M. Xiong, O. Gheysens, S. Keren, X. Y. Chen and S. S. Gambhir, Bioconjugate Chem., 2006, **17**, 662–669.
3. N. J. Durr, T. Larson, D. K. Smith, B. A. Korgel, K. Sokolov and A. Ben-Yakar, Nano Lett., 2007, **7**, 941–945.
4. J. O. Escobedo, O. Rusin, S. Lim and R. M. Strongin, Curr. Opin. Chem. Biol., 2009, **14**, 64–70.
5. A. Hoshino, K. Hanaki, K. Suzuki and K. Yamamoto, Biochem.Biophys. Res. Commun., 2004, **314**, 46–53.
6. R. Hu, K. T. Yong, I. Roy, H. Ding, W. C. Law, H. X. Cai, X. H. Zhang, L. A. Vathy, E. J. Bergey and P. N. Prasad, Nanotechnology, 2010, **21**, 145105.
7. X. H. Huang, I. H. El-Sayed, W. Qian and M. A. El-Sayed, J. Am.Chem. Soc., 2006, **128**, 2115–2120.
8. D. Nagesha, G. S. Laevsky, P. Lampton, R. Banyal, C. Warner, C. DiMarzio and S. Sridhar, Int. J. Nanomedicine, 2007, **2**, 813–819.
9. G. S. He, L. S. Tan, Q. Zheng and P. N. Prasad, Chem. Rev., 2008, **108**, 1245–1330.
10. B. A. Reinhardt, L. L. Brott, S. J. Clarson, A. G. Dillard, J. C. Bhatt, R. Kannan, L. X. Yuan, G. S. He and P. N. Prasad, Chem. Mater., 1998, **10**, 1863–1874.

11. A. Petrovsky, E. Schellenberger, L. Josephson, R. Weissleder and A. Bogdanov, Cancer Res., 2003, **63**, 1936–1942.

12. V. Biju, T. Itoh, A. Anas, A. Sujith and M. Ishikawa, Anal. Bioanal. Chem., 2008, **391**, 2469–2495.
13. D. R. Larson, W. R. Zipfel, R. M. Williams, S. W. Clark, M. P. Bruchez, F. W. Wise and W. W. Webb, Science, 2003, **300**, 1434–1436.
14. G. C. Xing, W. Ji, Y. G. Zheng and J. Y. Ying, Appl. Phys. Lett., 2008, **93**, 2411143.
15. Y. L. Qu and W. Ji, J. Opt. Soc. Am. B, 2009, **26**, 1897–1904.
16. A. M. Derfus, W. C. W. Chan and S. N. Bhatia, Nano Lett., 2004, **4**, 11–18.
17. R. Hardman, Environ. Health Perspect., 2006, **114**, 165–172.
18. C. Kirchner, T. Liedl, S. Kudera, T. Pellegrino, A. M. Javier, H. E. Gaub, S. Stolzle, N. Fertig and W. J. Parak, Nano Lett., 2005, **5**, 331–338.
19. N. Lewinski, V. Colvin and R. Drezek, Small, 2008, **4**, 26–49.
20. C. H. Crouch, O. Sauter, X. H. Wu, R. Purcell, C. Querner, M. Drndic and M. Pelton, Nano Lett., 2010, **10**, 1692–1698.
21. R. T. Sibatov and V. V. Uchaikin, Opt. Spectrosc., 2010, **108**, 761– 767.
22. M. Kuno, D. P. Fromm, H. F. Hamann, A. Gallagher and D. J. Nesbitt, J. Chem. Phys., 2000, **112**, 3117–3120.
23. K. T. Shimizu, R. G. Neuhauser, C. A. Leatherdale, S. A. Empedocles, W. K. Woo and M. G. Bawendi, Phys. Rev. B: Condens. Matter Mater. Phys., 2001, **63**, 205316–205321.
24. A. Mooradia, Phys. Rev. Lett., 1969, **22**, 185–187.

25. G. T. Boyd, Z. H. Yu and Y. R. Shen, Phys. Rev. B: Condens. Matter, 1986, **33**, 7923–7936.

26. R. A. Farrer, F. L. Butterfield, V. W. Chen and J. T. Fourkas, Nano Lett., 2005, **5**, 1139–1142.

27. P. K. Jain, I. H. El-Sayed and M. A. El-Sayed, Nano Today, 2007, **2**, 18–29.

28. C. L. Liu, M. L. Ho, Y. C. Chen, C. C. Hsieh, Y. C. Lin, Y. H. Wang, M. J. Yang, H. S. Duan, B. S. Chen, J. F. Lee, J. K. Hsiao and P. T. Chou, J. Phys. Chem. C, 2009, **113**, 21082–21089.

29. J. Park, A. Estrada, K. Sharp, K. Sang, J. A. Schwartz, D. K. Smith, C. Coleman, J. D. Payne, B. A. Korgel, A. K. Dunn and J. W. Tunnell, Opt. Express, 2008, **16**, 1590–1599.

30. H. F. Wang, T. B. Huff, D. A. Zweifel, W. He, P. S. Low, A. Wei and J. X. Cheng, Proc. Natl. Acad. Sci. U. S. A., 2005, **102**, 15752–15756.

31. X. Wu, T. Ming, X. Wang, P. N. Wang, J. F. Wang and J. Y. Chen, ACS Nano, 2009, **4**, 113–120.

32. L. Tong, C. M. Cobley, J. Y. Chen, Y. A. Xia and J. X. Cheng, Angew. Chem., Int. Ed., 2010, **49**, 3485–3488.

33. T. B. Huff, M. N. Hansen, Y. Zhao, J. X. Cheng and A. Wei, Langmuir, 2007, **23**, 1596–1599.

34. W. S. Kuo, C. N. Chang, Y. T. Chang, M. H. Yang, Y. H. Chien, S. J. Chen and C. S. Yeh, Angew. Chem., Int. Ed., 2010, **49**, 2711– 2715.

35. L. Tong, Y. Zhao, T. B. Huff, M. N. Hansen, A. Wei and J. X. Cheng, Adv. Mater., 2007, **19**, 3136–3141.

36. T. Ming, L. Zhao, Z. Yang, H. J. Chen, L. D. Sun, J. F. Wang and C. H. Yan, Nano Lett., 2009, **9**, 3896–3903.

37. C. J. Ackerson, P. D. Jadzinsky and R. D. Kornberg, J. Am. Chem. Soc., 2005, **127**, 6550–6551.
38. O. M. Bakr, V. Amendola, C. M. Aikens, W. Wenseleers, R. Li, L. Dal Negro, G. C. Schatz and F. Stellacci, Angew. Chem., Int. Ed., 2009, **48**, 5921–5926.
39. C. T. Chen, W. J. Chen, C. Z. Liu, L. Y. Chang and Y. C. Chen, Chem. Commun., 2009, 7515–7517.
40. C. A. J. Lin, T. Y. Yang, C. H. Lee, S. H. Huang, R. A. Sperling, M. Zanella, J. K. Li, J. L. Shen, H. H. Wang, H. I. Yeh, W. J. Parak and W. H. Chang, ACS Nano, 2009, **3**, 395–401.
41. S. Link, A. Beeby, S. FitzGerald, M. A. El-Sayed, T. G. Schaaff and R. L. Whetten, J. Phys. Chem. B, 2002, **106**, 3410–3415.
42. S. Link, M. A. El-Sayed, T. G. Schaaff and R. L. Whetten, Chem. Phys. Lett., 2002, **356**, 240–246.
43. M. A. H. Muhammed, P. K. Verma, S. K. Pal, R. C. A. Kumar, S. Paul, R. V. Omkumar and T. Pradeep, Chem.–Eur. J., 2009, **15**, 10110–10120.
44. S. A. Patel, C. I. Richards, J. C. Hsiang and R. M. Dickson, J. Am. Chem. Soc., 2008, **130**, 11602–11603.
45. G. Ramakrishna, O. Varnavski, J. Kim, D. Lee and T. Goodson, J. Am. Chem. Soc., 2008, **130**, 5032–5033.
46. L. Shang and S. J. Dong, Chem. Commun., 2008, 1088–1090.
47. M. Z. Zhu, H. F. Qian and R. C. Jin, J. Am. Chem. Soc., 2009, **131**, 7220–7221.
48. O. Varnavski, G. Ramakrishna, J. Kim, D. Lee and T. Goodson, J. Am. Chem. Soc., 2010, **132**, 16–17.

49. A. C. Dharmaratne, T. Krick and A. Dass, J. Am. Chem. Soc., 2009, **131**, 13604–13605.

50. T. Huang and R. W. Murray, J. Phys. Chem. B, 2001, **105**, 12498– 12502.

51. R. C. Jin, Nanoscale, 2010, **2**, 343–362.

52. S. Nah, L. J. Li and J. T. Fourkas, J. Phys. Chem. A, 2009, **113**, 4416– 4422.

53. D. S. Wang, F. Y. Hsu and C. W. Lin, Opt. Express, 2009, **17**, 11350– 11359.

54. Y. H. Lee, Y. L. Yan, L. Polavarapu and Q. H. Xu, Appl. Phys. Lett., 2009, **95**, 023105.

55. A. Verma and F. Stellacci, Small, 2010, **6**, 12–21.

56. Y. Pan, S. Neuss, A. Leifert, M. Fischler, F. Wen, U. Simon, G. Schmid, W. Brandau and W. Jahnen-Dechent, Small, 2007, **3**, 1941–1949.

57. C. J. Murphy, A. M. Gole, J. W. Stone, P. N. Sisco, A. M. Alkilany, E. C. Goldsmith and S. C. Baxter, Acc. Chem. Res., 2008, **41**, 1721– 1730.

58. O. Blokhina, E. Virolainen and K. V. Fagerstedt, Ann. Bot., 2003, **91**, 179–194.

59. M. Valko, C. J. Rhodes, J. Moncol, M. Izakovic and M. Mazur, Chem.-Biol. Interact., 2006, **160**, 1–40.

60. Invitrogen: http://products.invitrogen.com/ivgn/product/V13154.

CHAPTER 6

SELF ASSEMBLY OF GOLD NANOPARTICLES AND APPLICATIONS TO NONLINEAR OPTICS AND SURFACE ENHANCED RAMAN SCATTERING

6.1. Introduction

Metal nanoparticles, such as silver and gold, have attracted a great deal of attention because of their unique optical and electronic properties and potential applications in biological, optoelectronic, and photonic technology.[1, 2, 3] In particular the interactions of metal nanoparticles with optical fields will result in collective oscillations of conduction electrons within the nanoparticles, which is the "particle plasmon" resonance. The plasmon resonance energy of metal nanoparticles depends on the sizes and shapes of the particles and their dielectric environment for isolated nanoparticles and the interactions between the particles in aggregated structures.[4, 5, 7] The coupling of the plasmon resonance of metal nanoparticles with molecules could result in enhanced linear and nonlinear optical properties such as surface-enhanced Raman scattering (SERS) signals.[8-11] To optimize and extend the applications of metal nanoparticles, recently there has been strong interest in the self-assembly of metal nanoparticles into 1-D, 2-D, and 3-D structures. The coupling of gold nanoparticles has been demonstrated by using surfactants,[12, 13] bifunctional organic molecules,[5, 14, 15] DNA duplex formation,[16] biorecognition systems,[17, 18] and polymers.[19] The optical properties of metal nanoparticles in self-assembled structures could be tailored to different applications.

Lin *et. al.*[20] and Zhang *et. al.*[14] demonstrated one-dimensional plasmon coupling by self-assembly of gold nanospheres into branched chain networks using 2-mercaptoethanol as a coupling agent. Dai *et. al.*[21] reported synthesis of nanonecklace from mono- functionalized gold nanoparticles. Besides self-assembly of nanoparticles into planar higher order structures through bottom-up approach, several groups have also reported the synthesis of nanochains by spontaneous self-assembly of nanoparticles with electric and magnetic dipoles.[22] Spontaneous self assembly of CdTe nanoparticles into nanochains have been reported by partial removal of the stabilizer molecules.[23] Halder *et. al.*[24] recently reported preparation of ultrafine gold nanowire arrays by oriented attachment. In their experiment, multi-step reactions were used and gold nanoparticles were aged for several hours to a few days to form the arrays.

Selvakannan *et. al.*[25, 26] reported tryptophan and Lysine capped gold nanoparticles by spontaneous reduction of the $HAuCl_4$ solution directly with amino acid at higher temperatures as well as reduction by $NaBH_4$ and aged for few hours in the amino acid solution to cap the particles with amino acid. They found that use of amino acid can result in some degree of cross-linking of the gold nanoparticles during the reduction processes. Because of strong additional field enhancement in the gap regions between the particles (the “hot spot”), local field effects could be enhanced by several orders of magnitude in the metal aggregates or assembled nanoparticles, which are responsible for the much stronger SERS response compared to that of isolated nanoparticles.[9, 27] The

SERS signals has been found to be enhanced on the order of 10^{14} in the presence of “hot particles”, which allows SERS studies to be performed at the single-molecule level.[28]

In this chapter, I demonstrated two simple methods to prepare gold nanochains. In the first method, a simple single-step facile synthesis of gold nanochains within a few minutes by using amino acid (glutamic acid and histidine) as a capping agent is demonstrated. It was showed that the gold nanochains were formed via the nanospheres fusing into one another by an oriented attachment mechanism. The z-scan measurements on Au nanochains showed transition from saturable absorption to reversible saturable absorption at higher pump intensities. In the second method, I demonstrate a simple method to assemble citrate-stabilized gold nanoparticles into nanochains within a few seconds by using water-soluble conjugated polymers. The formation of nanochains resulted in the appearance of a new longitudinal plasmon band. The longitudinal plasmon band associated with the gold nanochains can be continuously tuned from visible to near-infrared by the addition of different amounts of conjugated polymers into the Au nanosphere solutions. I have also demonstrated the application of these assembled gold nanochains as a substrate for surface enhanced Raman scattering (SERS), which gave huge, reproducible SERS signals~400 times better than that when the isolated Au nanospheres were used as a substrate.

6.2. Experimental section

6.2.1 Chemicals

Chloroauric acid ($HAuCl_4 \cdot 3H_2O$), L-histidine and L-glutamic acid, tri sodium citrate, were purchased from Aldrich. Sodium borohydride ($NaBH_4$, 98%) was obtained from

Fluka. poly[(9,9-di(3,3′-*N*,*N*′-trimethylammonium)-propyl-fluorenyl-2,7-diyl)-*alt-co*-(1,4-phenylene)] diiodide salt (PFP) was purchased from American dye source. All chemical reagents were used as received without further purification. Water used in the preparation of all samples was purified with cartridges from Millipore (NANOPure, Barnstead, USA) to a resistivity of 18.0 MΩ·cm.

6.2.2. Synthesis of amino acid capped gold nanoparticles

In a typical experiment, 1.0 ml of 5.0 mM $HAuCl_4$ was dissolved in 25 ml of water. $HAuCl_4$ was reduced by quickly adding 0.5 ml of 30 mM freshly prepared ice cold solution of $NaBH_4$ in the presence of different amounts (0.5 ml, 1.5 ml, 2.0 ml) of 30 mM glutamic acid while stirring the solution. When 0.5 ml of 30 mM glutamic acid was used (the obtained sample will be referred as Sample hereafter), the $HAuCl_4$ was immediately reduced to gold nanoparticles upon addition of $NaBH_4$, manifested by immediate solution color change from colorless to red. No further color change was observed when the solution was kept stirring for another 5 minutes. The situations were different when a larger amount (thus a higher concentration) of glutamic acid solution was used. When 1.5 ml of 30 mM glutamic acid was used in the reaction (Sample b), the color of the solution appeared red initially upon addition of $NaBH_4$ to the $HAuCl_4$ solution, and then gradually changed into violet within 15 minutes. When 2.0 mL of glutamic acid solution was used (Sample c), the color changed from red to pink and then black-grey upon addition of $NaBH_4$. All the solutions were homogeneous and clear. Similar experiments were also performed by replacing glutamic acid with histidine as a capping agent and similar results were obtained.

6. 2.3 Synthesis of citrate capped gold nanoparticles

In a typical experiment, 10 mL of a 38.8 mM sodium citrate solution was quickly injected into 100mLof 1mM boiling HAuCl4 in a 250mLround-bottomed flask under vigorous stirring. The solution quickly changed color from pale yellow to dark red. The solution was continuously heated at ~100 °C for 10 min and was then kept stirring for another 15 min while cooling. The TEM images showed that the obtained Au nanoparticles have an average particle size of 13 nm. The UV-vis extinction spectra of the prepared gold nanoparticles display a strong extinction band with a maximum at 520 nm, which is a characteristic plasmon resonance band of isolated spherical gold nanoparticles (see fig.6.8).

6.2.4. Characterization of gold nanoparticles

These materials were characterized by using UV-visible spectroscopy, Infrared spectroscopy, transmission electron microscope (TEM) and femtoseond z-scan measurements.

UV-Visible spectra of the nanoparticles were measured using a Shimadzu UV 2450 spectrometer. FTIR spectra of amino acid capped gold nanoparticles were recorded from the nanoparticle powders. These nanoparticles were first centrifuged with a speed of 14000rpm to remove the excess amino acid in the solution, and were subsequently dried in a rotavapour to remove the water fully. The power was then mixed with KBr to make pellet and the spectrum was measured by using a Bio-rad Excalibur FTIR spectrometer.

TEM images were taken from a Philips CM10 electron microscope at an accelerating voltage of 100 kV and A JEOL JEM3010 field emission transmission electron microscope was used to obtain high resolution TEM (HR-TEM) images.

6.2.5 Nonlinear optical properties of gold nanochains prepared by using amino acid as capping agent

The nonlinear optical properties of the prepared Au nanochains were characterized using femtosecond z-scan measurements at 800nm. The laser pulses were generated by a mode-locked Ti: Sapphire oscillator seeded regenerative amplifier with a repetition rate of 1 kHz. The laser beam was focused onto the Au nanoparticle solution samples contained in a 1-mm-thick quartz cuvette, with a beam waist of ~ 20 μm. The pulse duration of the laser pulse at the sample is around 200fs. The linear transmission of the Au nanowire sample was adjusted to b3 ~70% at 800nm when the sample was off the focus. The sample was moved along the z- axis towards and away the focus point and the transmitted signals were monitored with a lock-in amplifier. The experiment was done with an open –aperture configuration.

6.2.6 SERS measurements using gold nanochains prepared by conjugated polymer induced self assembly

The prepared gold nanochains were also used as a substrate for surface-enhanced Raman scattering (SERS). The SERS measurements were performed by using a Renishaw micro-Raman spectrometer with an excitation wavelength of 532 nm and power of 40mW.The substrates for SERS measurements were prepared by immersing trimethoxy-[3-(methylamino) propyl] silane (APS)- modified quartz substrates into the aggregated or isolated nanoparticle solutions for 12 h, followed by rinsing with water. The sample was prepared by drop casting 10 μL of 5 nM rhodamine 6G (R6G) ethanol solution onto a gold nanochainmodified quartz substrate or 10 μL of 0.1 μMR6G solution onto an isolated gold nanosphere-modified quartz substrate. The reference sample was prepared by drop casting 10 μL of 100 mM R6G ethanol solution onto a quartz substrate and allowing the solvent to evaporate.

6.3. Results and Discussion

6.3.1 Synthesis of gold nanochains using amino acid as capping agent

Figure 6.1 shows the typical TEM images of the gold nanoparticles prepared using different concentrations of glutamic acid, as well as the corresponding UV-visible extinction spectra of these nanoparticles. When 0.5 ml of glutamic acid was used (Sample a), the obtained nanoparticles are mainly nanospheres with diameters of around 10-15 nm. The extinction spectrum of the sample showed a sharp peak at 520 nm, which is a typical Plasmon resonance band of Au nanospheres.[20] At a 1:9 molar ratio of HAuCl4/glutamic acid (sample B), the obtained nanoparticles have a chain-like appearance with branching, in which small gold spheres with diameters of 10–15 nm are connected in a chain of various lengths. The particles are connected like a necklace and the particles are fused into each other. Compared to the extinction spectrum of sample A, the plasmon peak at 520 nm decreases in intensity and new bands appeared in the longer wavelength range. The broadened absorption spectra are consistent with the formation of the anisotropic nature of gold nanoparticles in the solution.[20] At a 1:12 molar ratio of HAuCl4/glutamic acid (sample C), the thickness of the chain increases. Careful inspection of their TEM images indicated that the nanowires were formed from small particles with diameters of ~20 nm. Their extinction spectra became even broader. In addition to the 520 nm band, another new peak at 700 nm can be clearly seen.

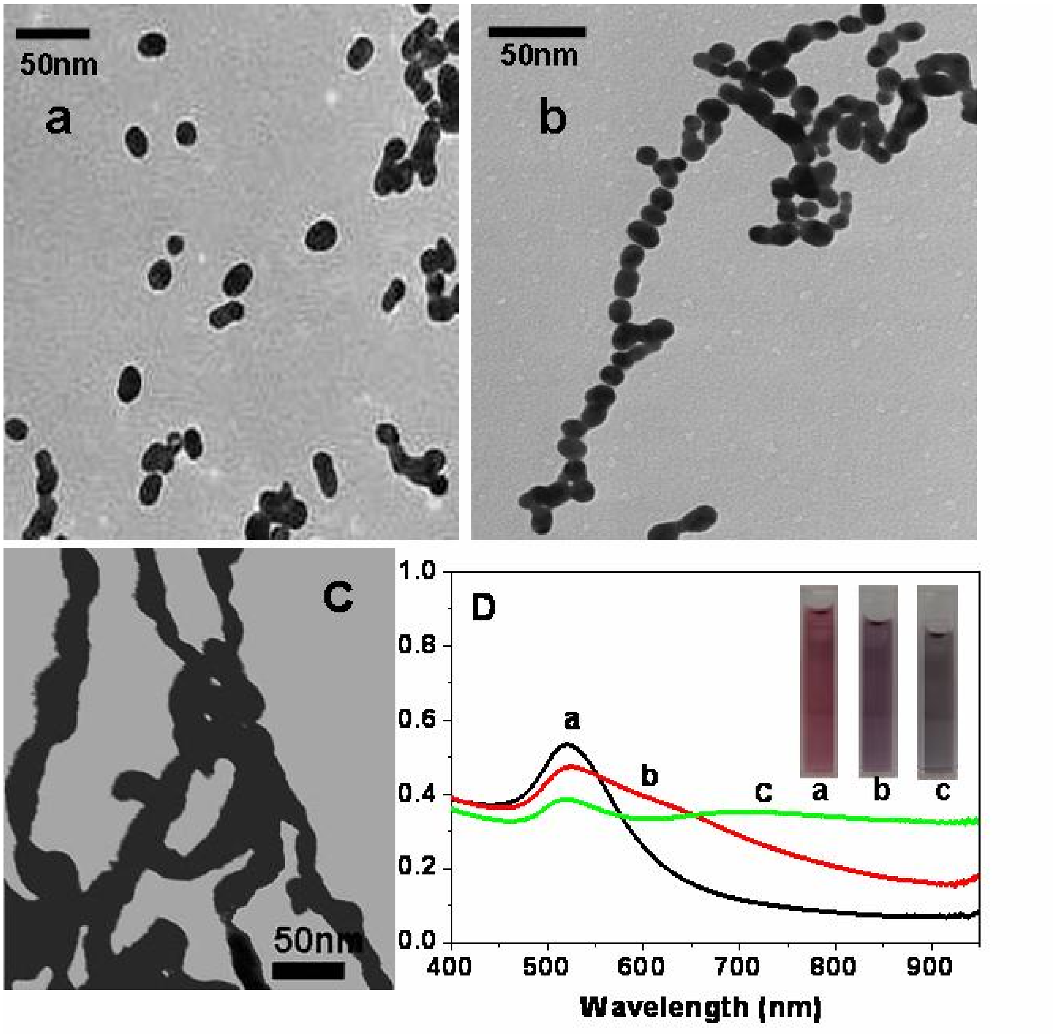

Fig. 6.1 TEM images and extinction spectra of glutamic acid capped gold nanoparticles for different amounts of 30 mM glutamic acid solution used in the synthesis (the molar ratio of HAuCl4/glutamic acid is 1:3 for A, 1:9 for B and 1:12 for C, respectively). The inset shows the picture of the three solution samples.

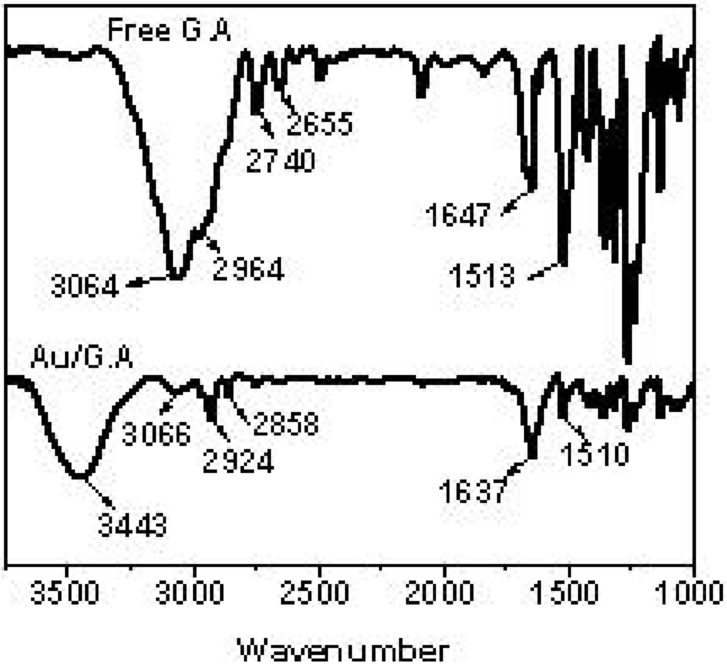

Fig. 6.2 FTIR spectra of pure glutamic acid (upper panel) and glutamic acid (G.A) capped gold nanoparticles (lower panel).

Figure 6.2 shows the FTIR spectra for pure glutamic acid and glutamic acid-capped gold nanoparticles. The symmetrical NH_3^+ bending mode at 1510 cm^{-1} decreases in intensity in glutamic acid capped gold nanoparticle, compared to that of pure glutamic acid. The asymmetric stretching mode of NH_3^+ has a broad band with a maximum at 3064 cm^{-1}. The 3064 cm^{-1} band decreases in intensity due to the binding of NH_3^+ to the gold surface. A new broad band with a maximum at 3443 cm^{-1} appears which is likely due to reduction of some of the carboxylic acid groups into primary alcohol by $NaBH_4$. In the final nanochains solution, the surface of the gold particles might be covered by OH groups. It has been previously reported that bifunctional molecules containing NH_2 and

OH groups might be responsible for the formation of linearly assembled Titania nanostructures [38], though the exact mechanism is still under debate.

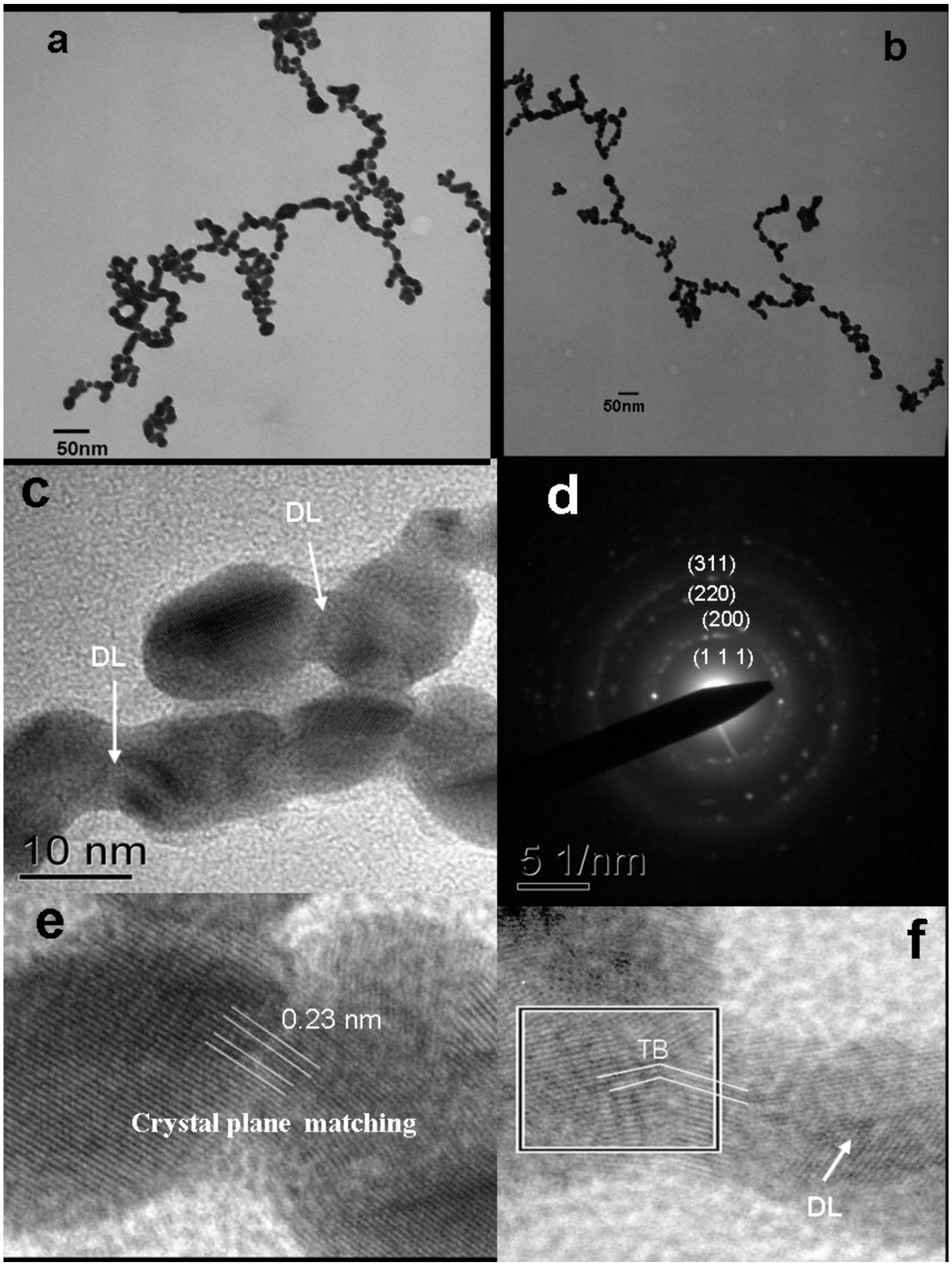

Fig. 6.3 More TEM (3a, 3b) images, HRTEM (3c, 3e, 3f) images and SAED (3d) pattern of nanochains synthesized at a moderate concentration of glutamic acid (Sample b). The enlarged version of c is also available in the supporting information. "DL" and "TB" stand for "dislocation" and "twin boundary", respectively.

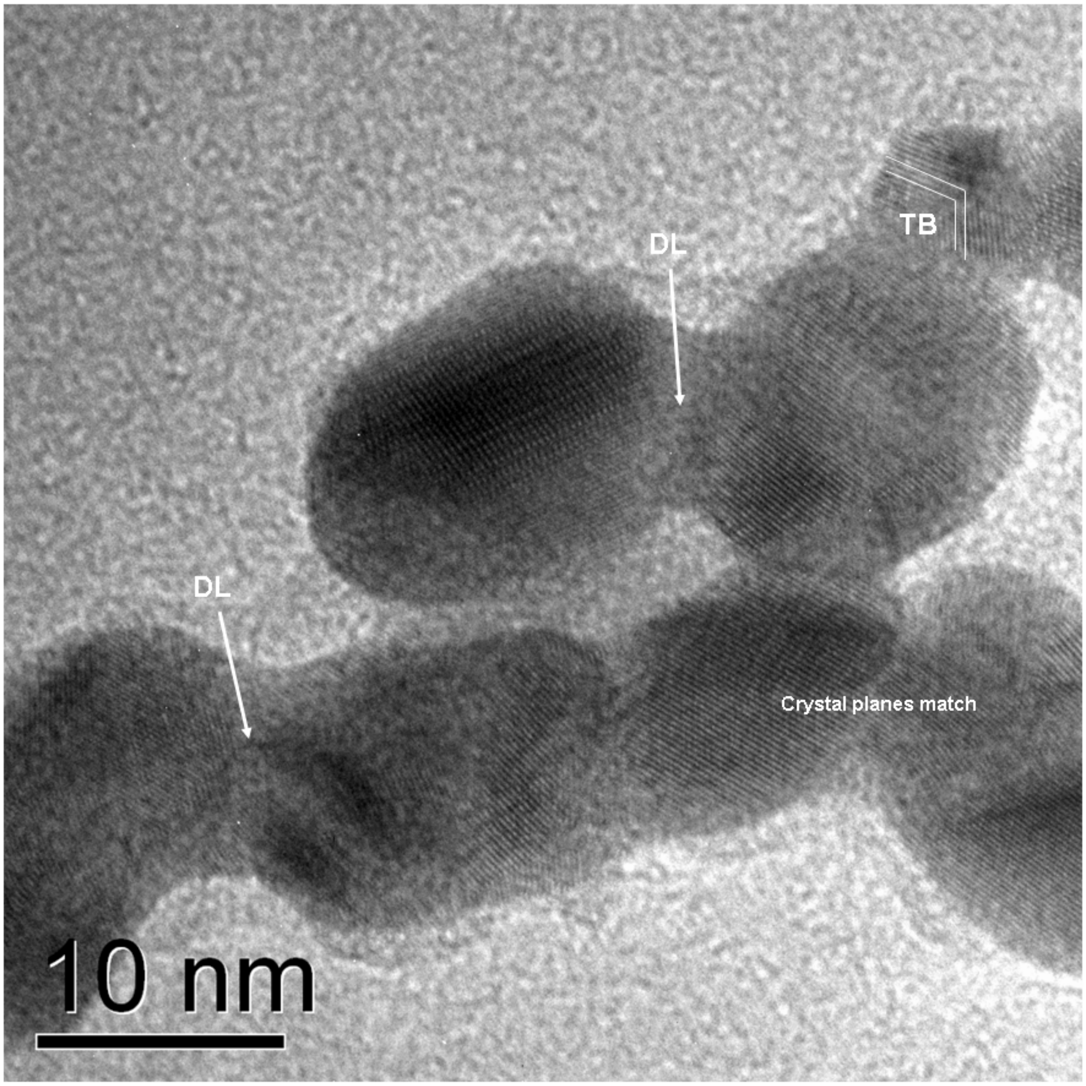

Fig. 6.4 The enlarged version of Figure 3c of the main text. “DL” and “TB” stand for “dislocation” and “twin boundary”, respectively.

More TEM images and high resolution TEM (HRTEM) images of gold nanochains (Sample b) are shown in Figure 6.3. The HR-TEM images clearly show that the particles are fused into one another. The lattice fringe spacing is 0.23 nm, which corresponds to (111) facet (see the fig.6.4 for the enlarged image). Figure 6.3d shows selected area electron diffraction (SAED) pattern of the nanochains shown in Figure 6.3c. Careful examination of Figure 6.3e reveals that the particles are fused in a way such that the lattice planes of those two particles exactly match each other and appear like a single crystal. The SAED pattern showed single crystal features. Twin boundaries and dislocations also have been identified as shown in Figure 6.3e and 6.3f. The driving force for formation of dislocations at attachment interfaces is chemical bond formation between structurally similar surfaces of the particles when they approach each other.

Based on the HRTEM images, I proposed the formation of Au nanochains by an oriented attachment mechanism.[29] The oriented attachment mechanism describes the spontaneous self-organization of adjacent particles, which make them share a common crystallographic orientation, followed by joining of these particles at a planar interface. During the materials preparation processes, the nanoparticle solution first appeared as color of red and then slowly changed the color to violet, which suggest that spheres were formed first, followed by linear aggregation of those particles into nanochains slowly by the oriented attachment mechanism. The gold nanoparticles were stabilized by the amine group that is bound to gold surface. The binding ability between the amine group and Au surface is different for different facets. The binding of amino acid molecules to the (111) facet might be relatively weaker compared to other facets, [30] as revealed by the fact that fusion of nanoparticles occurred along (111) facet. The preferential removal of the capping agent from these facets and zwitterionic nature of amino acids allows the particles to fuse into each other by dipole-dipole interactions. The dipole-dipole interactions are thermodynamically favorable by the reduction of the particle surface energy when the interface is eliminated. There is also some possibility for attachment of particles on other (111) facets, which leads to formation of branched nanowires as shown in the TEM images. Other possible interactions that might be responsible for particle attachment include hydrogen bonding and weak van der Waals interactions between the capping agent molecules. These interactions are usually weak and not strong enough to hold a large number of particles together.

Oriented attachment mechanism has been recently proposed to explain the formation of various anisotropic structures of semiconductor nanowires[23, 31, 32] such as ZnTe, CdTe, PbSe, metal nanowires such as Au [24] and metal oxides.[33] Polleux *et. al.*[34] reported ligand-directed assembly of TiO_2 nanoparticles into nanochains using 2-amino-2-(hydroxymethyl)-1,3-propanediol. They showed that formation of anisotropic structure was favorable with a higher ligand concentration and polydentate ligand played a major role in the oriented attachment mechanism. Banfield el. al.[29] also showed that the nanoparticles can act as building blocks for formation of highly ordered structures by oriented attachment. Yeadon *et. al.*[35] gave an alternative possible explanation for this behaviour. They proposed the alignment of nanoparticles on the substrate by “contact epitaxy”. This is not likely to be the dominant mechanism for the formation of nanochains in our studies. The broad UV/visible extinction spectra of the solution supported formation of nanowires-like structure in solution, which is more likely due to dipole-dipole interactions, similar to the case of CdTe nanowires formation.[23] The linear assembly of colloidal particles might take place in the presence of an intrinsic or induced dipole moment once the dipole-dipole interaction was strong enough to overcome the thermal energy and the electrostatic repulsion between the colloidal particles.[36] These dipole-dipole interactions among amino acid capped gold nanoparticles are strong due to the zwitterionic nature of amino acids.[37] The amino acids create net dipole moment on the nanoparticle surface. The strong dipole-dipole interactions might be the dominant driving force for the particles fusing into wires at higher concentration of glutamic acid since the net dipole moment is high at higher concentration of amino acid on the nanoparticle surface.

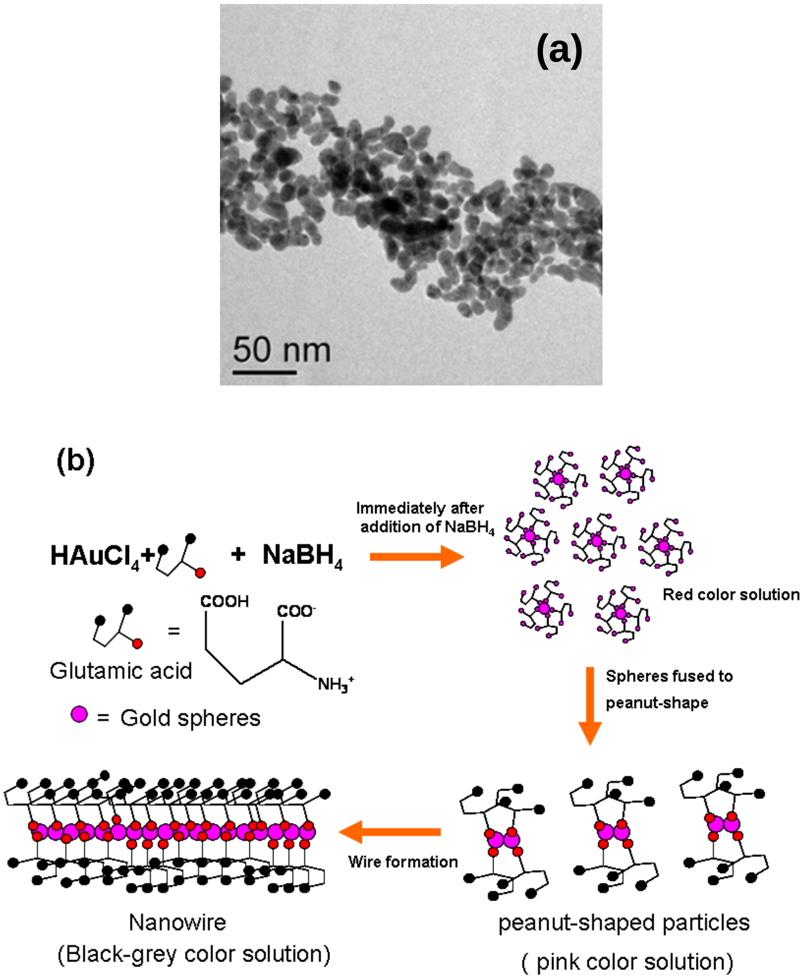

Fig. 6.5 (a) TEM image from the intermediate product formed after one minute of the reaction when 2.0ml of glutamic acid solution was used. (b) Based on the experimental observations the shape transformation of gold nanoparticles while the reaction progress at 30mM, 2.0mL of glutamic acid

Selvakannan *et. al.*[25] have observed random aggregates of gold nanoparticles when they first reduced the gold salt with $NaBH_4$ and then capped with lysine by aging for several hours. They clearly observed a slight gap at the contact of nanoparticles which shows that the particles are not fused into one another. They proposed that hydrogen bonding is responsible for the aggregation of particles. In another paper[26] they showed that there was no attachment between the particles when they capped the particles with tryptophan after the reduction of gold salt with $NaBH_4$. Though there are a few reports on the aggregation of gold nanoparticles with amino acid, the mechanism of nanochain and nanowire formation is still not very clear. Here I observed the formation of Au nanochains and nanowires, and proposed that the weak binding of the NH_2 group to the (111) facet is one of the possible mechanisms in this oriented attachment process.

To understand the mechanism of nanowire (Fig. 6.1c) formation when 2.0ml of glutamic acid solution was used, the TEM image of an intermediate product was taken as shown in Figure 6.5a. To obtain the intermediate product, the reaction was slowed down by using a slower stirring speed. One drop of reaction mixture was extracted for TEM images after the reaction proceeded for 1 minute when the solution was pink in color. The reaction stopped when the sample was dried for TEM images. Figure 6.5a shows that the obtained products were mainly peanut-shaped nanocrystals and some nanospheres with a diameter of ~20nm. This observation support that these peanut-shaped nanoparticles were formed first from small spheres, which were subsequently transformed into wire-like structures (shown in Fig. 6.1c) when the reaction proceeds. The shape transformation of gold nanoparticles while reaction progress is shown in Fig. 6.5b based on the TEM observation of the intermediate product in the nanowire formation. I hope that the zwitterionic nature amino acids induce a net dipole moment and these dipole-dipole interactions are responsible for the assembly of nanospheres into 1D-dimentional nanostructures.

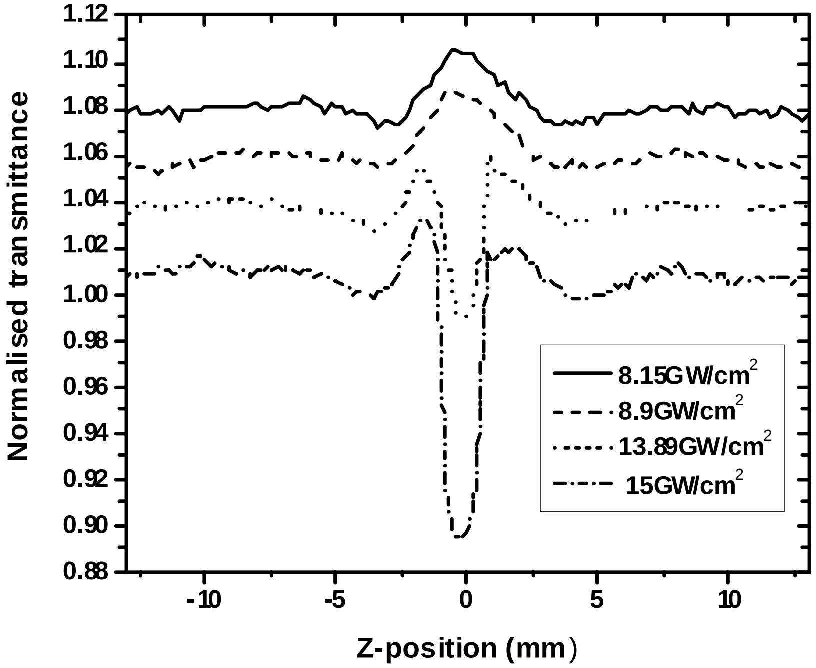

Fig. 6.6 Z-scan measurements of gold nanowires at 800 nm with different excitation intensities. The Au nanowires was prepared when 2.0 ml of glutamic acid was used (sample c).

The proposed mechanism is shown in Fig. 6.5b. Because of the weak binding of NH_2 group to the (111) facet, amino acid molecules were preferentially removed from the facet and that allows the particles aggregate linearly, which is supported by the observation of peanut shaped nanoparticles in the beginning of the reaction. When the reactions further proceeded, the diffusion of particles into one another may result in formation of nanowires with nanoparticles fully fused into each other, as shown in Figure 6.1c.

Figure 6.6 shows the open aperture z-scan measurement of gold nanowires prepared when 2.0 ml of glutamic acid was used (Sample c). It was found that the sample display saturable absorption at low excitation intensities (8.15 GW/cm^2 and 8.9 GW/cm^2). As the pump intensity increased, the z-scan results display a reverse saturable absorption behavior, at higher pump intensity, e.g. 15 GW/cm^2. The transition from saturable absorption at low pump intensity to reverse saturable absorption indicated that another nonlinear process took place and became dominant at high pump intensities. Such an effect has potential application in optical pulse compressor, optical switching and optical limiting.[38] A similar transition behavior was also reported by Elim at al.[39] in their studies on gold nanorods and they ascribed its origin to free carrier absorption. Other possible mechanism responsible for such transition in anisotropic Au nanoparticles at high pump intensities include surface Plasmon enhanced multi-photon absorption.[40]

Furthermore, the synthesis of gold nanochains can also be performed using other amino aids as capping agents. For example, the reaction was performed using histidine as capping agent, which results the network like structures and the extinction spectrum broadens with the increase of histidine concentration in the reaction. The TEM images of the histidine capped gold nanoparticles are shown in fig. 6.7 and it shows that the nanoparticles of 4nm in size fused into one another to form network like structures. No obvious longitudinal band was observed in the histidine capped gold nanoparticles due to week interparticle coupling between small size (4nm) particles.

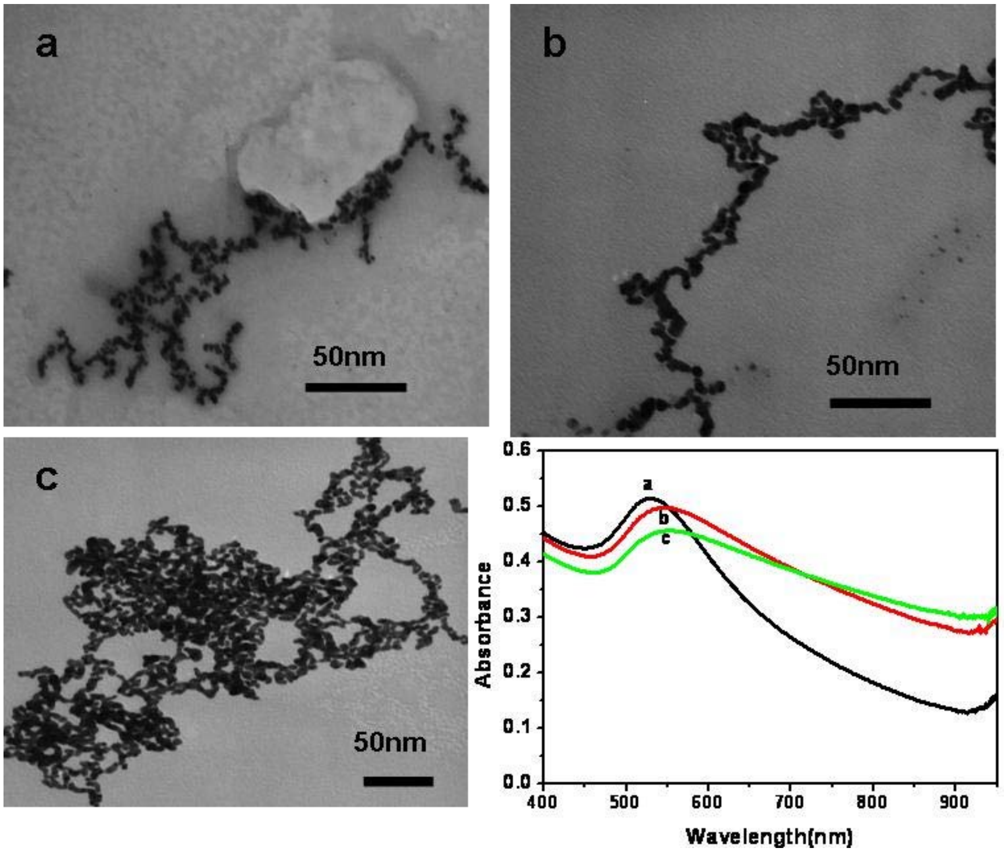

Fig. 6.7 TEM images and extinction spectra of histidine capped gold nanoparticles for different amounts of 30 mM histidine solution used in the synthesis (a: 0.5 ml; b: 1.5 ml; c: 2.0 ml).

6.3.2 Water-Soluble Conjugated Polymer-Induced Self-Assembly of Gold Nanoparticles

Here, I have investigated the interactions between Au nanoparticles and cationic conjugated polymers. Previous studies on interactions between conjugated polymers and metal nanoparticles focused on the quenching effects of metal nanoparticles on conjugated polymers,[41] which could be used to develop applications as biological and chemical sensors. So far, there has been no report on the effects of conjugated polymers on the metal nanoparticles. In this work, I found that a cationic conjugated polymer, poly[(9,9-di(3,3′-*N*,*N*′-trimethylammonium)-propyl-fluorenyl-2,7-diyl)-*alt*-*co*-(1,4-phenylene)] diiodide salt (PFP), can induce the self-assembly of gold nanoparticles to form gold nanochains. The PFP stock solution (1×10^{-5} M in repeat units) was prepared by dissolving in a 1:1 DMF/H_2O solvent mixture. When PFP was added to a 3.66×10^{-11} M (in particles) gold nanoparticle solution, the solution immediately changed color from red to blue or violet. The extent of aggregation and sizes of the nanochains were strongly dependent on the amount of PFP added. When a smaller amount of PFP was added, such as with a PFP/Au molar ratio (PFP in terms of repeat units and Au in terms of particles) of 9400:1, the TEM images (Figures 6.8 and 6.9) clearly show the aggregation of gold nanoparticles and the formation of gold nanochains. The aggregated sample mainly consisted of short linear nanochains with lengths of 75-150 nm (Figures 6.8 and 6.9), equivalent to 5-10 isomeric 13 nm Au nanoparticles. When a larger amount of PFP was added, such as with a PFP/Au molar ratio of 27 000:1, the solution immediately changed color to violet. The TEM pictures showed the formation of 3-D random aggregates, and a polymer coating was even formed on the particle surface. Figure 6.10 shows the UV-vis extinction spectra of Au nanoparticle aggregates after the addition of different amounts of PFP. Upon addition of PFP, the intensity of the transverse band at 520 nm decreased, and a new plasmon band (600-1000nm) appeared on the red side of the transverse band of the isolated gold nanoparticles. The appearance of this long-wavelength plasmon band is a clear indication of the formation of aggregated nanostructures. When the nanoparticles form aggregates, their plasmon modes interact and form a new plasmon band that is associated with the longitudinal mode of the plasmon oscillation along the long axis of the gold nanoparticle chains. As the PFP concentration increased, the new band became further broadened and red-shifted into the near-IR region, indicating a stronger extent of aggregation and a larger distribution in the size of the aggregated nanoparticles. In addition to these spectral changes, another band with a peak wavelength at 380 nm also appeared at higher polymer concentrations. This additional band at 380 nm arises from the absorption of conjugated polymer PFP.

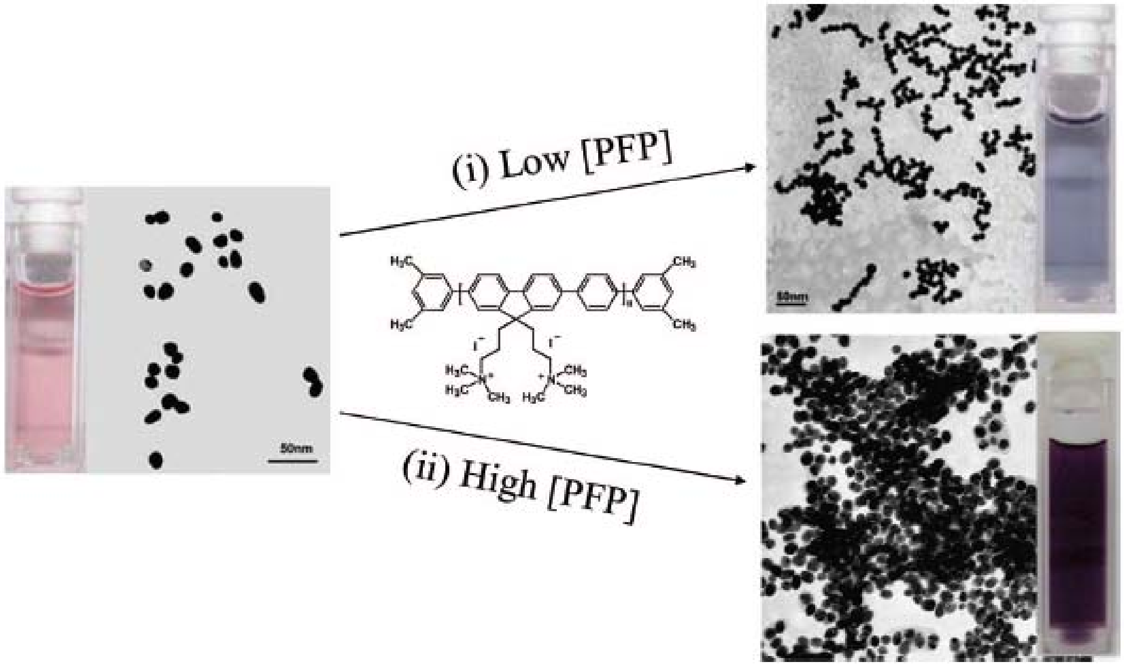

Fig. 6.8 Conjugated polymer-induced aggregation of gold nanoparticles: sample pictures and corresponding TEM pictures of nanoparticles before and after the addition of different amounts of PFP. The PFP/Au molar ratios (PFP in repeat units and Au in particles) are (i) 9400:1 and (ii) 27 000:1.

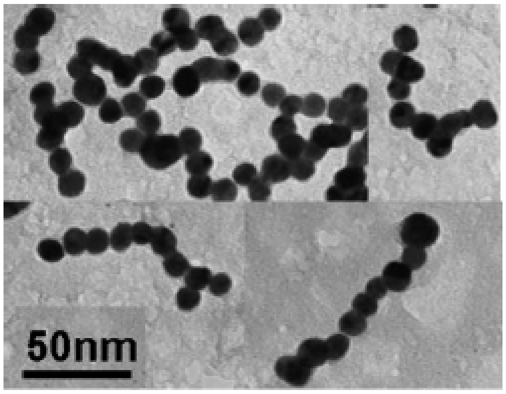

Fig. 6.9 TEM images of some 1-D nanochains formed with a PFP/Au molar ratio of 9400:1.

It has been previously reported that the self-assembly of gold nanoparticles into chainlike structures can be induced by using a surfactant such as CTAB or 2-mercaptoethanol (MEA).[5, 12] In these previous reports, it usually took several hours to assemble the gold nanoparticles fully. In our experiment, the assembly of gold nanoparticle using cationic conjugated polymers was rapid, and the assembled product was stable. I observed an immediate color change from red to blue or violet upon addition of conjugated polymer, indicating the immediate formation of the aggregated structures. The aggregated solution was generally very stable and could be stored for weeks without the observation of any precipitation, except at very high polymer/Au molar ratios. Because the cationic conjugated polymers are soluble in aqueous solvents and bear positive charges, they can easily bind to the negatively charged surface of the Au nanoparticles through electrostatic interactions, which induces the self-assembly of nanoparticles and the formation of nanochains or complicated nanostructures. The prepared gold nanochains were also used as a substrate for surface-enhanced Raman scattering (SERS).

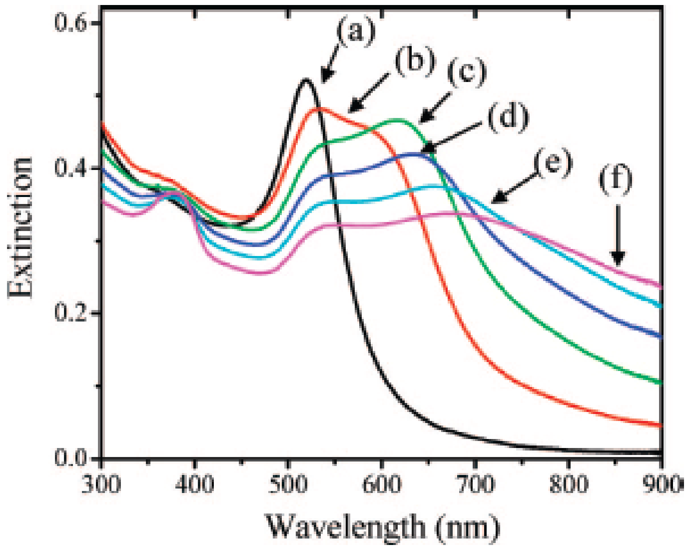

Fig. 6.10 UV-vis extinction spectra of Au nanoparticles upon addition of different amounts of PFP with PFP/Au molar ratios (PFP in repeat units and Au in particles) of (a) 0:1, (b) 4700:1, (c) 9400:1, (d) 14 100:1, (e) 18 800:1, and (f) 27 000:1.

Figure 6.11 shows the far-field SERS spectra of R6G on the quartz substrate modified with gold nanospheres and nanochains prepared with a polymer/Au molar ratio of 9400:1. The R6G on the quartz substrate gave very weak signals, and R6G on the Au nanosphere-modified substrate gave a moderate SERS signal. The gold nanochain-modified substrate gave a much stronger SERS response compared to that of the gold nanosphere-modified substrate. The Raman signal observed at 1180 cm^{-1} is associated with C-C stretching vibrations, and bands at 1308, 1360, 1506, 1572, and 1648 cm^{-1} are due to the aromatic C-C stretching vibrations. The Raman spectra agree well with the previously reported results.[10] The surface enhancement factors for gold nanospheres and nanochains were calculated from $(I_{sig}/C_{sig})/(I_{ref}/C_{ref})$, where I_{sig} and I_{ref} represent the intensities of the 1648 cm^{-1} band for the R6G adsorbed on the gold nanosphere- or nanochain-modified substrate and the quartz substrate, respectively, whereas C_{sig} and *C*ref represent the corresponding concentrations of R6G on these substrates. The enhancement factors for the gold nanospheres and gold nanochains were roughly estimated by comparing the peak intensity at 1648 cm^{-1} to 2.1×10^7 and 8.4×10^9, respectively. The SERS signal of R6G on the gold nanochain-modified substrate is about 400 times stronger than that on the isolated gold nanosphere substrate. These enhancement factors are excellent for an ensemble-averaged measurement.[8] Considering the fact that only a small fraction of aggregates are SERS-active[8, 9] the actual enhancement factor could be 10-100 times higher.

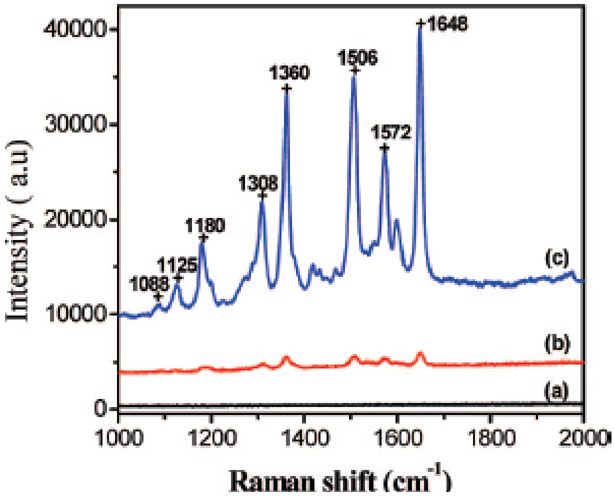

Fig. 6.11 Raman spectra of (a) 100mMrhodamine 6G (R6G) adsorbed on quartz, (b) 0.1 μM R6G adsorbed on a gold nanosphere-modified quartz substrate, and (c) 5.0 nM R6G adsorbed on a gold nanochain modified quartz substrate.

The SERS mechanism was believed to be due to a combination of an electromagnetic field enhancement and a chemical effect.[8] The chemical effect usually contributes a factor of 10^2, and the enhanced electromagnetic field contributes dominantly with an enhancement factor of up to 10^7-10^{12}. In the present study, the SERS signals on the gold nanochain-modified substrates were much stronger than those of nanospheres. I believe that SERS enhancement is mainly due to the local electromagnetic field enhancement. The conjugated polymers induced the assembly of gold nanospheres into nanochains, which created many hot spots at the junctions of the nanochains. The plasmon coupling of gold nanospheres at these hot spots will produce a very intense local electromagnetic field and consequently strong SERS signals. In our experiments, we still observed a reasonable SERS signal for R6G on the isolated gold nanosphere substrate, probably as a result of the fact that some of the Au nanospheres will also self-aggregate on the quartz substrate to form hot spots for SERS enhancement, though they will be much weaker than that when conjugated polymers were used. Schwartzberg et al.[9] reported that Na_2S-induced gold aggregates gave a SERS enhancement factor of 10^7-10^9 by assuming that only about 1% of the aggregates were actually SERS-active. Recently, Lin et al.[11] reported an enhancement factor of 5.6×10^9 by using Au pearl-necklace nanomaterials as a SERS substrate. In our current study, the cationic conjugated polymers were used to induce the aggregation of gold nanoparticles to form gold nanochains, which can serve as a good SERS substrate and gave a raw SERS enhancement factor of 8.4×10^9.

6.4. Conclusions

I have developed two simple methods assemble the gold nanoparticles into gold nanochains for nonlinear optical and surface enhanced Raman scattering applications. In the first method, a simple single step synthesis of gold nanochains by reducing aqueous $HAuCl_4$ with $NaBH_4$ in the presence of different concentration of amino acids as a capping agent was demonstrated. Those gold nanochains display saturable absorption at lower intensities and reverse saturable absorption at higher intensities of 800nm femtosecond laser pulses. In the second method, I self assembled the spherical gold nanoparticles into gold nanochains using water soluble conjugated polymers. A longitudinal plasmon resonance band was formed as a result of the plasmon coupling of gold nanoparticles and can be tuned from visible to near infrared by adjusting the polymer/Au molar ratio. The gold nanochains were used as a SERS substrate with a enhancement factor ~400 times larger than that on the isolated gold nanosphere substrate.

6.5 References

1. Nam, J. M., Thaxton, C. S., Mirkin, C. A., *Science,* 2003, **301**, 1884–1886.
2. Seker, F., Malenfant, P. R. L., Larsen, M., Alizadeh, A., Conway, K., Kulkarni, A. M., Goddard, G., Garaas, R., *Adv. Mater.,* 2005, **17**, 1941–1945.
3. Reece, P. J., *Nat. Photonics,* 2008, **2**, 333–334.
4. El-Sayed, M. A., *Acc. Chem. Res.,* 2001, **34,** 257–264.
5. Lin, S., Li, M., Dujardin, E., Girard, C., Mann, S., *AdV. Mater.,* 2005, **17**, 2553–2559.
6. Feldstein, M. J., Keating, C. D., Liau, Y. H., Natan, M. J., Scherer, N. F., *J. Am. Chem. Soc.,* 1997, **119,** 6638–6647.

7. Ramakrishna, G., Dai, Q., Zou, J. H., Huo, Q., Goodson, T. *J. Am. Chem. Soc.,* 2007, **129**, 1848–1849.

8. Kneipp, K., Kneipp, H., Itzkan, I., Dasari, R. R., Feld, M. S., *Chem. Rev.,* 1999, **99**, 2957–2976.

9. Schwartzberg, A. M., Grant, C. D., Wolcott, A., Talley, C. E., Huser, T. R., Bogomolni, R., Zhang, J. Z. *J., Phys. Chem. B,* 2004, **108**, 19191–19197.

10. Shao, M. W., Lu, L., Wang, H., Wang, S., Zhang, M. L., Ma, D. D. D., Lee, S. T., *Chem. Commun.,* 2008, 2310–2312.

11. Lin, Z. H., Chang, H. T., *Langmuir,* 2008, **24**, 365–367.

12. Yang, Y., Nogami, M., Shi, J. L., Chen, H. R., Ma, G. H., Tang, S. H., *Appl. Phys. Lett.,* 2006, **88,** 081110.

13. Yang, Y., Matsubara, S., Nogami, M., Shi, J. L., Huang, W. M., *Nanotechnology,* 2006, **17**, 2821–2827.

14. Zhang, S. Z., Kou, X. S., Yang, Z., Shi, Q. H., Stucky, G. D., Sun, L. D., Wang, J. F., Yan, C. H., *Chem. Commun.,* 2007, 1816–1818.

15. Polavarapu, L., Xu, Q. H., *Nanotechnology,* 2008, **19**, 075601.

16. Lazarides, A. A., Schatz, G. C. *J., Phys. Chem. B,* 2000, **104**, 460–467.

17. Caswell, K. K., Wilson, J. N., Bunz, U. H. F., Murphy, C. J., *J. Am. Chem. Soc.,* 2003, **125**, 13914–13915.

18. Chang, J. Y., Wu, H. M., Chen, H., Ling, Y. C., Tan, W. H., *Chem. Commun.,* 2005, 1092–1094.

19. Sardar, R., Shumaker-Parry, J. S., *Nano Lett.,* 2008, **8**, 731–736.

20. Lin S, Li M, Dujardin E, Girard C and Mann S, *Adv. Mater.*, 2005, **17,** 2553

21. Dai Q, Worden J G, Trullinger J and Huo Q, *J. Am. Chem. Soc.,* 2005, **127,** 8008

22. Tlusty T and Safran S A, *Science,* 2000, **290,** 1328

23. Tang Z Y, Kotov N A and Giersig M, *Science,* 2002, **297,** 237

24. Halder A and Ravishankar N, *Adv. Mater.,* 2007, **19,** 1854

25. Selvakannan P R, Mandal S, Phadtare S, Pasricha R and Sastry M, *Langmuir,* 2003, **19,** 3545

26. Selvakannan P, Mandal S, Phadtare S, Gole A, Pasricha R, Adyanthaya S D and Sastry M, *J. Colloid Interface Sci.,* 2004, **269,** 97

27. Kawamura, G., Yang, Y., Nogami, M., Appl. Phys. Lett., 2007, **90**, 261908.

28. Nie, S. M., Emery, S. R., *Science* 1997, **275**, 1102–1106.

29. Banfield J F, Welch S A, Zhang H Z, Ebert T T and Penn R L, *Science,* 2000, **289,** 751

30. Pong B K, Lee J Y and Trout B L, *Langmuir,* 2005, **21,** 11599

31. Yong K T, Sahoo Y, Zeng H, Swihart M T, Minter J R and Prasad P N, *Chem. Mater.,* 2007, **19,** 4108

32. Lu W G, Gao P X, Bin Jian W, Wang Z L and Fang J Y, *J. Am. Chem. Soc.,* 2004, **126,** 14816

33. Zeng H C, *J. Mater. Chem.,* 2006, **16,** 649

34. Polleux J, Pinna N, Antonietti M and NiederbergerM, *Adv. Mater.,* 2004, **16,** 436

35. Yeadon M, Ghaly M, Yang J C, Averback R S and Gibson J M, *Appl. Phys. Lett.,* 1998, **73,** 3208

36. Liao J H, Zhang Y, Yu W, Xu L N, Ge C W, Liu J H and Gu N, *Colloids Surf.* A, 2003, **223,** 177

37. Xu S J, Nilles M and Bowen K H, *J. Chem. Phys,* 2003,. **119,** 10696

38. Band Y B, Harter D J and Bavli R, *Chem. Phys. Lett.* 1986, **126,** 280

39. Elim H I, Yang J, Lee J Y, Mi J and Ji W, *Appl. Phys. Lett,.* 2006, **88,** 083107

40. Mohamed M B, Volkov V, Link S and El-Sayed M A, *Chem. Phys. Lett.,* 2000, **317,** 517

41. Fan, C. H., Wang, S., Hong, J. W., Bazan, G. C., Plaxco, K. W., Heeger, A. J. *Proc. Natl. Aca. Sci. U.S.A.,* 2003, ***100***, 6297–6301.

CHAPTER 7

ALKYLAMINE CAPPED METAL NANOPARTICLE “INKS” FOR PRINTABLE SERS SUBSTRATES, ELECTRONICS AND BROADBAND PHOTODETECTORS

7.1 Introduction

Noble metal nanoparticles are of great interest owing to their unique properties and potential wide applications.[1-8] These noble metal nanoparticles display an interesting phenomenon called surface plasmon resonance (SPR), which arises from the collective oscillations of conductive electrons induced by incident electromagnetic radiation.[9] The SPR depends on the size and shape of the metal nanoparticles. Various methods have been developed to prepare metal nanoparticles of different morphologies in the past two decades.[10-13] The application of metal nanoparticles in plasmonics,[14] photonics,[15] electronic devices[16-21] and surface enhanced Raman substrates[22-28] have been under intensive study.

Surface-enhanced Raman scattering (SERS) spectroscopy have been demonstrated as being useful in ultrasensitive chemical and biological detections.[25] Various physical methods such as electron beam lithography,[22] sputtering,[26] chemical vapor deposition,[29,30] nanosphere lithography[31] and focused ion beam pattering[32] have been used to fabricate SERS substrates by controlling the assembly of silver or gold nanoparticles into specific structures. Although, the substrates fabricated using above mentioned techniques showed large Raman enhancements with good SERS reproducibility, they are of high cost and difficult to extend to large area device fabrication. Solution-processing methods are attractive because of their advantages of ease of fabricating a large area device, physical flexibility, and most importantly, low cost.

Metal nanoparticles have also found applications in efficient photon detection owing to plasmon enhanced photo-response.[18,33] Most of the previous works utilize plasmon resonance to enhance the photocurrent efficiency of semiconductor devices via electric field enhancement.[34] However, the photo-response bandwidths of these semiconductor devices are usually limited by their band-gap energies. There are a few reports on the photoconductivity of gold nanoparticle films.[8, 35] Silver nanoparticles have been rarely studied in this regard. As silver is much cheaper than gold, it is attractive to use silver nanoparticles films as an alternative for photo detection and other optoelectronic applications.

Another related important active research area is to explore simple and cost effective methods to prepare conductive metal nanoparticles with high stability and solubility.[19-21, 36-38] These metal nanoparticles could be used as an "ink" for solution processed printable conductors,[21] circuits,[20] micromechanical systems,[39] and electrodes.[40] The nanoparticle solutions with high concentrations are usually called "inks". It should be noted that nanoparticles "inks" are different from nano pastes that are not printable due to high viscosity. The ligand protected metal nanoparticle "inks" can be used to prepare conductive metal films at ambient temperatures. So far most metal nanoparticle "inks" were prepared by using thiol capping agents,[21, 36, 39] which are toxic and expensive. Moreover, thiols have strong tendency to etch the nanoparticles, which have negative effects on the long term stability. In general, the thiol capped metal nanoparticle "inks" were usually prepared via a two-step process,[21, 41] in which the gold ions were first phase-transferred from water to toluene using surfactants followed by reduction of gold ions with $NaBH_4$ in the presence of alkanethiols. Although this method has been demonstrated to be successful in preparing gold nanoparticles, it cannot be used to prepare the silver nanoparticles.

Here I demonstrated a facile and general method to prepare low cost, highly soluble and stable alkylamine capped gold and silver nanoparticle "inks" with particle size of 3-5 nm. In our method, alkylamine was used as the capping agent, which is less toxic and cheaper compared to the conventionally used thiol-type capping agents for the preparation of "inks". In contrast to previously reported physical methods,[22,26,29-32] we present a facile solution processed method for the fabrication of highly efficient SERS substrates, which can detect analytes down to a few nM and flexible plastic substrates are demonstrated for the first time using metal nanoparticle "inks". The metal nanoparticle films were found to undergo insulator-to-metal transformations under annealing, with transition temperature mainly dependent on the capping agent. I have demonstrated the application of alkylamine capped metal nanoparticle inks as printable electrodes for graphene based field-effect transistors (FET). The metal nanoparticle films prepared by using these nanoparticle "inks" also displayed broadband (400-1100 nm) photo-response.

7.2 Experimental Section

7.2.1 Materials: Silver nitrate ($AgNO_3$, 99%) and gold (III) chloride trihydrate ($HAuCl_4{\cdot}3H_2O$, 99.9%), Oleylamine, Dodecylamine, octylamine were purchased from

Aldrich. All chemicals were used as received without further purification.

7.2.2 Preparation of alkylamine capped gold and silver nanoparticle "inks"

In a typical synthesis of silver nanoparticle "ink', 100 mg $AgNO_3$ was first dissolved in 50 mL of toluene containing 2 mL of oleylamine in a round bottom flask. The mixture was sonicated about 20 min until all $AgNO_3$ was totally dissolved. $AgNO_3$ was reduced by quickly adding 10 mL of 10 mg/ml freshly prepared $NaBH_4$ solution under vigorous stirring condition. The addition of $NaBH_4$ resulted in an immediate color change from colorless to dark yellow. The mixture was kept stirring for another 5 min. The nanoparticles containing organic layer was separated from the aqueous layer in the reaction mixture and then filtered to remove any undissolved impurities. The nanoparticles were then purified by a series of procedures. First, the toluene solvent was removed by using a rotavap. 100 mL of ethanol was then added into remaining solution to precipitate out the nanoparticles. The precipitate was separated by centrifugation (5000 rpm for 15 min) and then washed with ethanol two more times to wash off the remaining uncapped oleylamine and other impurities. The precipitate was then dissolved in toluene after being dried for ~10 min. The solution was again filtered to remove any undissolved impurities. Ag nanoparticle "ink" (in toluene solvent) with a concentration of 50mg/ml were then prepared. The same steps were done to synthesize oleylamine-capped gold nanoparticle ink using $HAuCl_4$ as a precursor. Unlike silver salt, the gold salt dissolves in toluene in the presence of oleylamine very easily by sonicating the solution for 2-3 min. The similar procedures can be used to prepare any alkylamine capped gold or silver nanoparticle "inks".

7.2.3 Synthesis of silver nanoparticle ink is shown in photographs

Ag NO_3 + Oleylamine+ Toluene mixture was sonicated until Ag NO_3 dissolved

$NaBH_4$ was added into the mixture

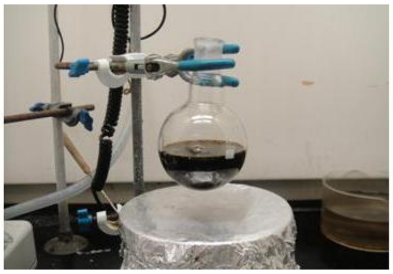

Silver nanoparticle ink after reduction

Aqueous layer was separated

The organic layer was filtered to remove any undissolved impurities

Purification

The toluene was fully evaporated from the filtered solution

Ag nanoparticles+ unreacted oleylamine

Ethanol was added

Ethanol was added to precipitate the nanoparticles and remove the un-reacted oleylamine

Centrifuged

Nanoparticle precipitate was separated by centrifugation

Nanoparticle precipitate after remove the ethanol and unreacted oleylamine

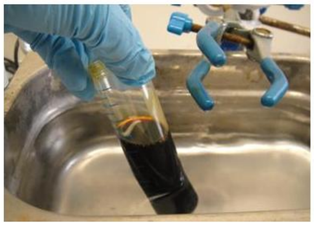

The purified precipitate was dissolved in toluene.

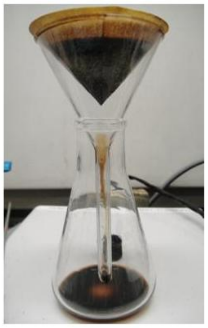

The solution was filtered to remove any further un-dissolved impurities.

Toluene was fully removed to measured the weight of the particles

The nanoparticles were dispersed in toluene with the required concentration

7.2.4 Preparation of SERS substrates using gold and silver nanoparticle “inks”

The glass substrates were first sonicated in aqua regia for 30 min followed by rinsing with water and ethanol. The glass plates were subsequently washed with acetone and dried in an oven. The SERS substrates were prepared by spin coating the oleylamine capped Ag or Au ink of concentration 30mg/ml with a spin speed of 600rpm for 60 seconds. Four substrates were then annealed at different temperatures (100, 150, 200, and 250 ^{o}C) for 20 min. 10 μL of 1μM Rhodamine6G solution was dropped onto each SERS substrate using a micropipette. The SERS measurements were performed by using a Renishaw micro-Raman spectrometer with an excitation wavelength of 514 nm.

7.2.5 Conductivity measurement using four-probe configuration

The conductivities of the nanoparticle ink at different annealing temperatures were measured by using a four-probe substrate. The four-probe substrate was prepared by thermal evaporation of four aluminium electrodes on glass substrate in a line with a spacing of 4 mm. The nanoparticle ink was dropped onto these four probe substrates with a thickness of ~200 nm and the substrate was annealed to different temperatures with an increasing rate of 5^{o}C per minute and maintained for 5 minutes at each temperature. The conductivity was calculated by measuring the resistance of the nanoparticle film by using GS 610 source measurement unit (Yokogawa).

7.2.6 Measurement of Electron relaxation dynamics of gold nanoparticle film annealed at different temperatures

The ultrafast relaxation dynamics of the gold nanoparticle film annealed at 50, 180 and 250^{o}C in air were measured by using reflection pump–probe experiments, which were performed using a femtosecond Ti:sapphire laser system (Spectra Physics). The laser pulses were generated from a mode-locked Ti:sapphire oscillator seeded regenerative amplifier with a pulse energy of 2 mJ at 800 nm and a repetition rate of 1 kHz. The 800 nm laser beam was split into two portions. The larger portion of the beam was passed through a BBO crystal to generate the 400 nm pump beam by frequency-doubling. A small portion of the 800 nm pulses was used to generate white light continuum in a 1 mm sapphire plate. The white light continuum was split into two beams, a probe and a reference beam. The reference beam and reflected probe beam from the sample was directed to photodiodes that were connected to lock-in amplifiers and a computer. The intensity of the pump beam was attenuated with the neutral density filter. The pump beam is focused onto the sample with a beam size of 300 μm and overlaped with the smaller-diameter (100 μm) probe beam. The delay between the pump and probe pulses was varied by a computer-controlled translation stage. The pump beam was modulated by an optical chopper at a frequency of 500 Hz. The decay dynamics of the gold nanoparticle film was monitored at their surface plasmon resonance by exciting the film with 400 nm pump laser at pulse energy of 0.2nJ.

7.2.7 Synthesis of Graphene Oxide (GO): GO was synthesized from graphite via a modified Hummers and Offeman’s method.[50] 1.5g graphite flakes (Asbury Carbons Ltd.) and 1.0g $NaNO_3$ were placed in 500 mL round bottom flask. 45 mL of concentrated H_2SO_4 was subsequently added into the flask. The mixture was stirred overnight at room temperature. 6.0g $KMnO_4$ was then slowly added into the mixture at ice bath to avoid rapid heat evaluation. After 4 hours the flask was shifted to an oil bath and reaction mixture was stirred at 35 °C for 2 hrs. The temperature was slowly increased to 60 °C and stirred for 4 hrs. Finally, the reaction mixture was added into 40 mL of water and stirred at 90 °C for 5 hrs. The reaction was ended by adding 10 mL of 30% H_2O_2, which resulted change of colour from yellow to brown. The warm solution was then filtered and washed with 5% HCl and water. The obtained solid was then dissolved in water sonicated to exfoliate oxidized graphene. The oxidized graphene was centrifuged at 1000 rpm for 2 min. After removing all visible graphite particles, it was again centrifuged at 15,000 rpm for 2 hrs. This washing procedure was repeated till the pH became 4-5. For complete oxidation, the above dried GO was further treated with 70% HNO_3 (10 mL of HNO_3/100 mg of GO). The mixture was sonicated for 8 hrs at 60 °C and the sediment was dispersed in water. The obtained GO was purified by washing multiple times with ethanol and water. The product was spin coated onto the silica substrate for AFM image measurements. The AFM images showed that most of the GO sheets are single layer and there are some GO with a few layers. The topographic heights of these GO sheets are 1-2 nm. (See fig. 7.9 for AFM image)

7.2.8 Preparation of nanoparticle films for broadband photoresponse measurements:

Oleylamine capped gold or silver nanoparticles were dissolved in toluene with a concentration of 30 mg/ml and spin-coated on ITO/PEDOT electrode with spin speed of 800rpm for 60 sec and annealed at $120^{o}C$ for 10 min under N_2 atmosphere. Subsequently Al electrode (100 nm thickness) was preparation by using evaporation method at 1x10^{-6} bar vacuum to complete the device fabrication. Active layer film (Au or Ag nanoparticles) thicknesses were measured to be 80 nm using surface profiler. The device has a structure of ITO/PEDOT:PSS (40nm)/Au or Ag nano particles (80nm)/Al (100nm). All photocurrent and electric (I-V) measurements were carried out using an Autolab PGSTAT30 potentiostat (EcoChemie, The Netherlands). The photocurrent response of Au and Ag nanoparticle films were measured by exciting with diode lasers of different wavelengths (400, 532, 980 and1064 nm) ranging from visible to near-infrared range under an ITO voltage 0V.

7.3 Results and Discussion

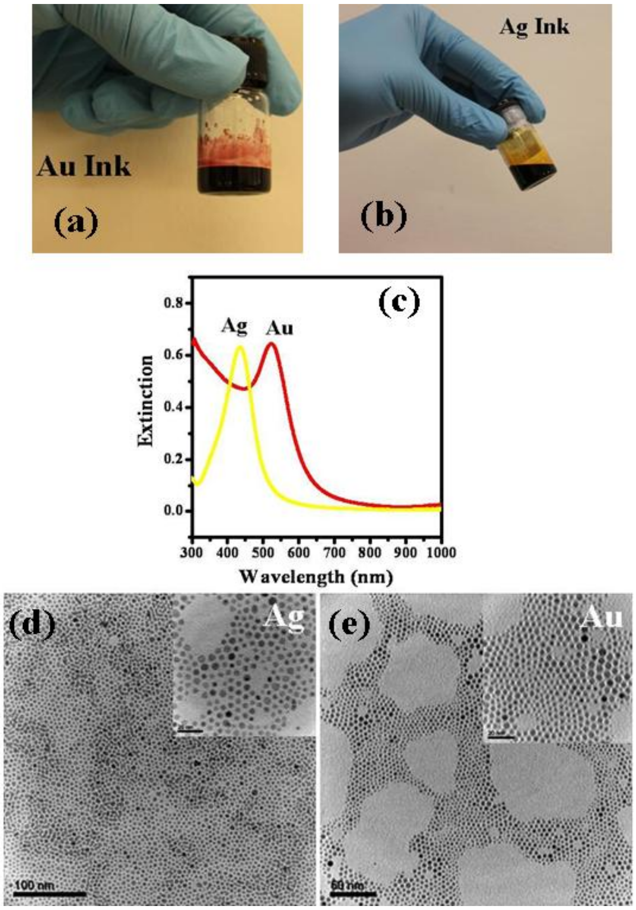

Fig. 7.1 Pictures (a-b) and extinction spectra (c) of oleylamine capped gold and silver “inks”; d-e) TEM images of the silver and gold nanoparticles.

In this work, gold or silver nanoparticle "inks" were prepared by simply mixing $AgNO_3$ or $HAuCl_4$ and oleylamine in a toluene solvent, followed by reduction with aqueous $NaBH_4$. The nanoparticles were purified by precipitating with ethanol (See the experimental section). I found that any alkylamine can be used to dissolve the metal salts in organic solvents directly by sonication without any phase transfer from aqueous to organic phase, which is simpler and more advantageous compared to those method using phase transfer agents.[42] Figure 7.1a-c shows gold and silver nanoparticle inks in toluene solution with a concentration of 50mg/ml and their extinction spectra. The gold and silver nanoparticles show surface plasmon resonances at 530 and 420 nm respectively. The TEM images of the silver and gold nanoparticles (Fig. 7.1d&7.1e) show that the "inks" contains 3-5 nm spherical nanoparticles. Previously, Chen et al.[43] and Wang et al.[44] have reported the synthesis oleylamine capped gold and silver nanoparticles at higher temperatures by using oleylamine as solvent and reducing agent. Compared to those reported method, our current method is a general and simple method for rapid and large scale preparation of any alkyl amine capped Au or Ag nanoparticles at room temperature in high concentration and high purity, which is essential for solution processed applications. The prepared nanoparticles are very stable in highly concentrated solutions or powder form. No degradation was observed after storing concentrated solution or powder for more than one and half year at room temperature. This method uses toluene and ethanol solvents as the solvent, which can be easily recycled. The nanoparticles prepared by this method have much reduced cost and the method is environmentally friendly. The alkylamine capped nanoparticle "inks" thus prepared have high solubility up to 80mg/ml in toluene, which is good for printable electronics and many other solution processed applications.

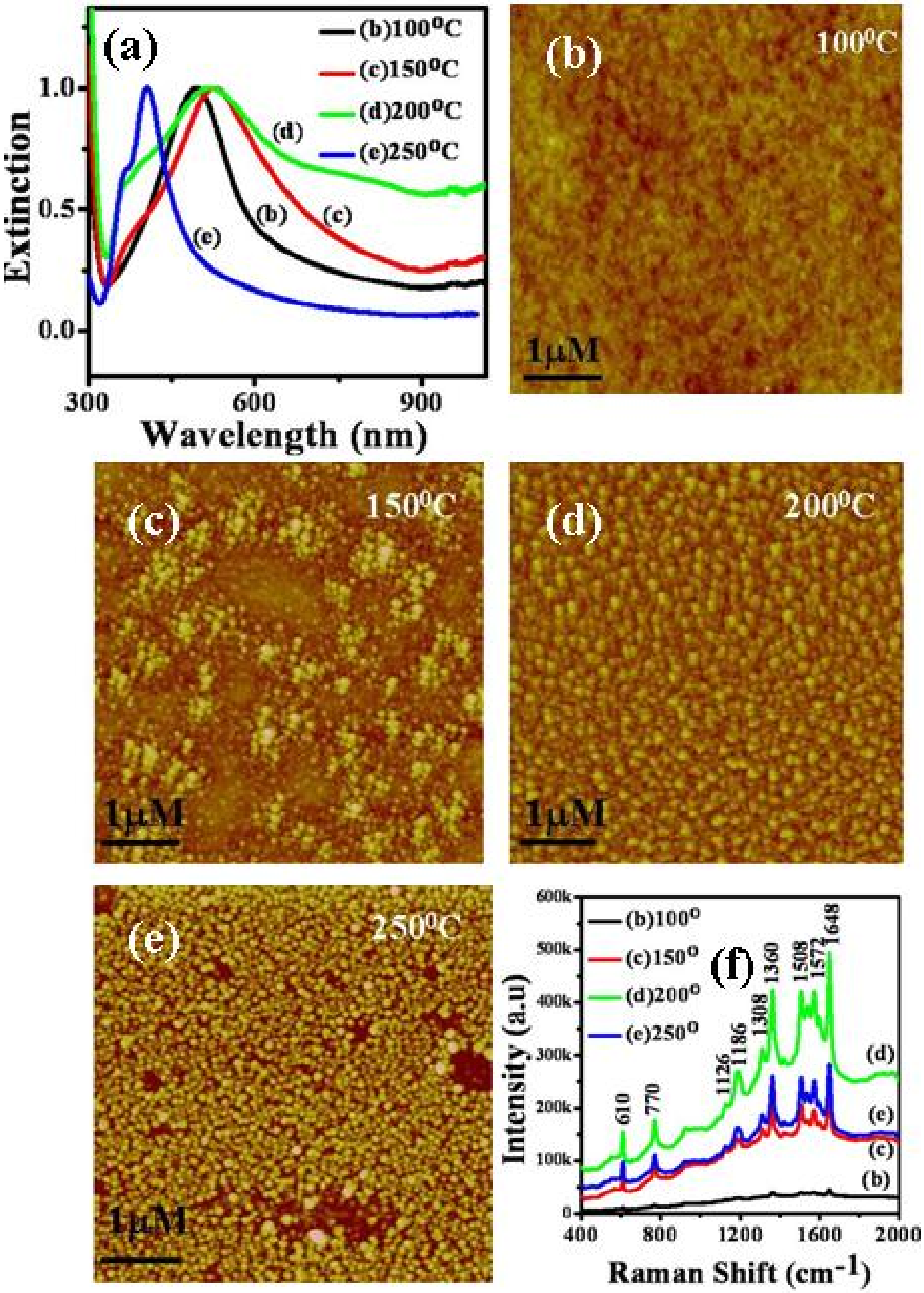

Fig. 7.2 a) Extinction spectra, **b-e)** AFM images of the Ag nanoparticle films annealed at 100, 150, 200, and 250°C, respectively, and **f)** SERS spectra of R6G (1μM) on these Au nanoparticle films.

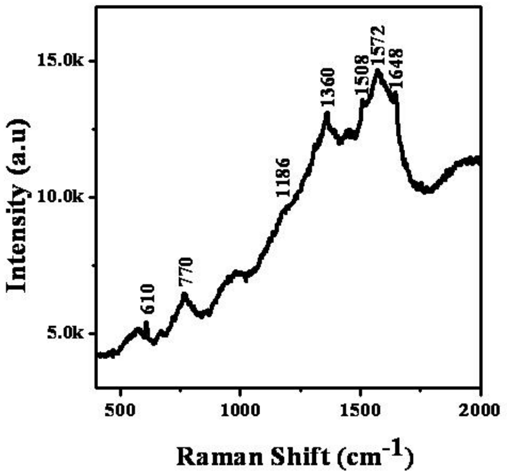

Fig. 7.3 SERS signals of 1nM Rhodamine 6G on oleylamine capped silver nanoparticle substrate annealed at 200°. I did not observed any signals from the other three substrates prepared by annealing at 100, 150 and 250°C with this concentration of R6G under same experimental conditions.

The prepared metal nanoparticle "inks" were used to fabricate SERS substrates via solution processing, which have many advantages over conventional physical methods.[22,26,29-32] The nanoparticles were first spin coated onto four clean glass substrates under same conditions followed by annealing the substrates. Figure 7.2a shows the extinction spectra of the spin coated silver nanoparticle films after annealing the substrates at different temperatures (See the experimental section for the detailed preparation procedures). The silver nanoparticles have an extinction maximum at 420 nm in toluene solution (Figure 7.1c). When the film was annealed at 100°C, the band maximum of extinction spectrum shifted to 490 nm. Its AFM image (Figure 7.2b) shows that 5 nm silver nanoparticles are closely packed and form a smooth film. The red shift in the extinction maximum of the nanoparticle film compared to that of pure particles in solution suggest strong coupling between the nanoparticles on the film. When the nanoparticle film was annealed at 150^{o}C, the initial 5 nm silver nanoparticle film partially transforms into nanoparticles of ~50-80 nm in size (Figure 7.2c). When the nanoparticle film was heated up to 200^{o}C, the nanoparticle film fully transforms into larger aggregated nanoparticles of ~70-90nm in size (Figure 7.2d). The extinction spectra of the silver nanoparticles films annealed at 150 and 200^{o}C exhibit extinction maxima at 520 nm, consistent with the strongly coupled larger particles as observed by AFM. The extinction spectrum became broadened as the annealed temperature increased. When the nanoparticle film was heated to 250^{o}C, the extinction spectrum of the nanoparticle film became blue shifted, resembling that of individual spherical nanoparticles. At higher temperature the oxidation of the nanoparticle surface could reduce the plasmon coupling between the nanoparticles, which results in a blue shift in the extinction spectrum. The AFM image (Figure 7.2e) shows that the nanoparticles became less aggregated and the particles appeared more spherical in shape. The film morphology change at 250 ^{o}C might be due to oxidation of the nanoparticle film at the elevated temperatures. The results show that the substrates annealed at 200^{o}C produce large aggregated Ag nanoparticles, which are expected to generate hotspots and give huge SERS signals due to enhanced electromagnetic field.[27]Gold nanoparticles films were also prepared under the same experimental conditions. The gold nanoparticles were also found to grow in size as the annealing temperature increased up to 150^{0}C, but further increase of annealing temperature resulted in formation of smooth films due to the coalescence of gold nanoparticles. The extinction spectra of the oleylamine capped gold nanoparticle films annealed at different temperatures are shown in Figure 7.4a. The extinction spectrum became broader as the annealing temperature increased. When the film was annealed to 200 °C and above, the nanoparticle was found to form on the substrate with close contact with each other and the films appears as smooth compared to the film prepared at 150 °C (Figure 7.4d&7.4e) due to the coalescence of gold nanoparticles at higher temperatures. The extinction spectrum became broad due to the strong coupling between nanoparticles. When the gold nanoparticle film was annealed at 250°C, the extinction spectrum showed the bulk like properties, which is different from the temperature dependent extinction spectrum of the silver film.

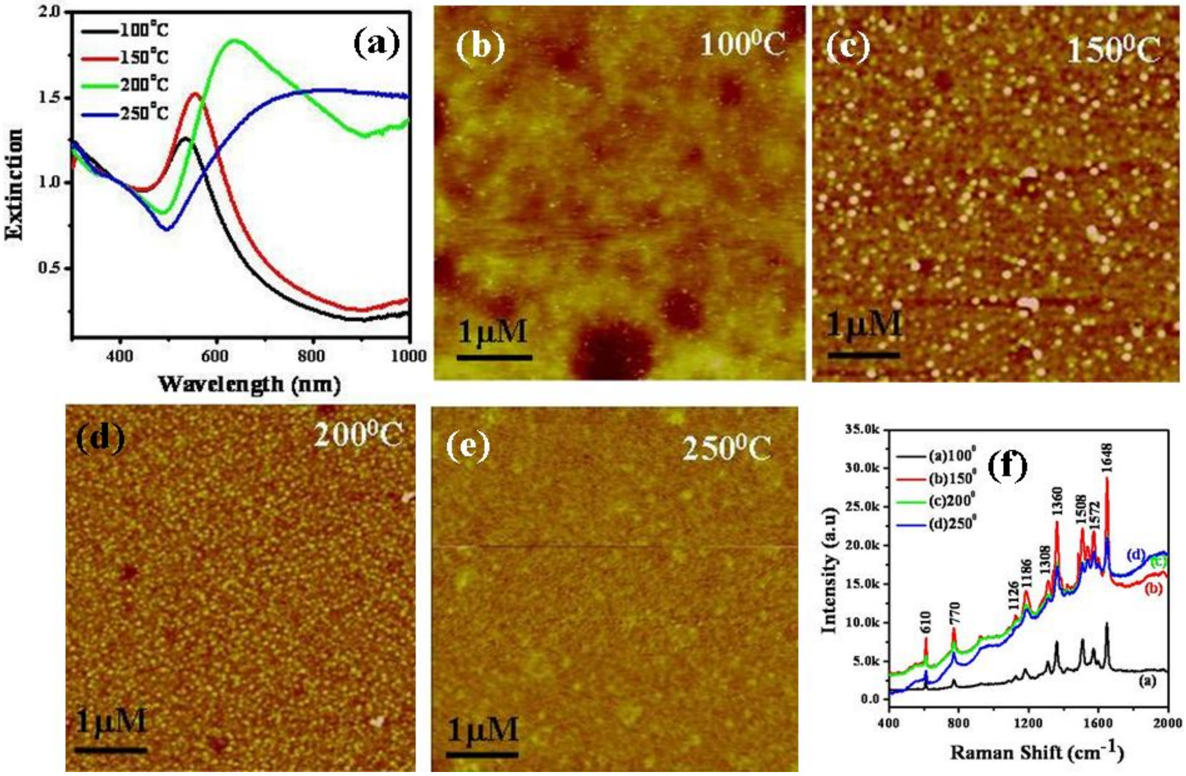

Fig. 7.4 Extinction spectra (a) and AFM images (b-e) of the oleylamine capped gold nanoparticle film annealed at 100, 150, 200, and 250°C and f) SERS spectra of R6G (1µM) on these Au nanoparticle films.

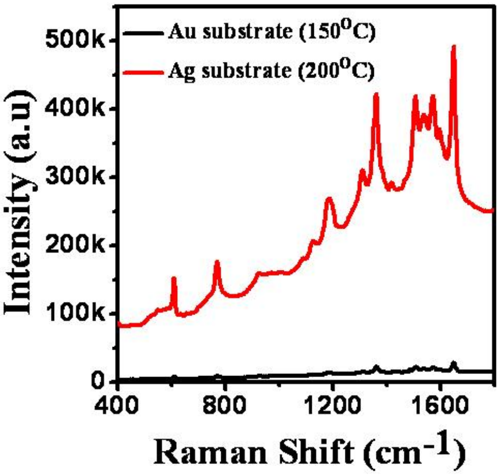

Figure 7.5. SERS spectra of R6G (1μM) on the oleylamine capped Ag and Au nanoparticle substrates prepared by annealing the Ag substrate at 200°C and Au substrate at 150°C. Ag nanoparticle substrate gave SERS signals 17 times larger than the Au nanoparticle substrate.

The performance of the SERS substrates were examined by using 6G (R6G) as a probe and 514 nm laser as the excitation source. The sample was prepared by drop casting 10 μL of 1μM R6G ethanol solution onto the four nanoparticle modified glass substrates and allowing the solvent to evaporate under different temperatures. Figure 7.2f shows the SERS spectra of R6G on four nanoparticle films that were annealed at 100, 150, 200, and 250°C, respectively. The Raman spectra agree well with the previously reported results.[45] The Raman signal observed at 1186 cm^{-1} is associated with C-C stretching vibrations, and bands at 1308, 1360, 1508, 1572, and 1648 cm^{-1} are due to the aromatic C-C stretching vibrations. The SERS signal is weakest for the nanoparticle film prepared at annealing temperature of 100 °C. The SERS signal intensity increases as the annealing temperature increases until 200°C, where the strongest SERS signal was observed. Further increase in the annealing temperature cause the decease of the SERS intensity, which is consistent with the AFM images. The SERS signal intensity 200^{o}C could detect very low concentrations of R6G. Analytes with concentration as low as a few nM could be detected by using these Ag nanoparticle films (See Fig 7.3). The SERS experiment was also performed on the gold nanoparticle films prepared under similar experimental conditions. The SERS spectra of Rhodamine6G measured on the four gold nanoparticle substrates are shown in Figure 7.4f. The maximum SERS enhancement was observed on the film prepared by annealing at 150^{o}C. The gold nanoparticle film for the substrate prepared by annealing at 200 ^{o}C is ~22 times higher than that for the substrate prepared by annealing at 100^{o}C. It was found that I could use the SERS substrate annealed at 200^{o}C to detect very low concentrations of R6G. Analytes with concentration as low as a few nM could be detected by using these Ag nanoparticle films (See Fig. 7.3). The SERS experiment was also performed on the gold nanoparticle films prepared under similar experimental conditions (See Fig. 7.4). The gold nanoparticle film prepared by annealing at 150 ^{o}C gave the largest enhancement among all the substrates. However, the maximum SERS signal given by Au nanoparticle substrates is 17 times smaller compared to that of Ag nanoparticle film (See Fig. 7.5). Fewer enhancements by the gold nanoparticle films compared to Ag nanoparticle films could be due to strongly damped plasmons in the gold when excited with green laser because of the coupling to interband transitions.[46]

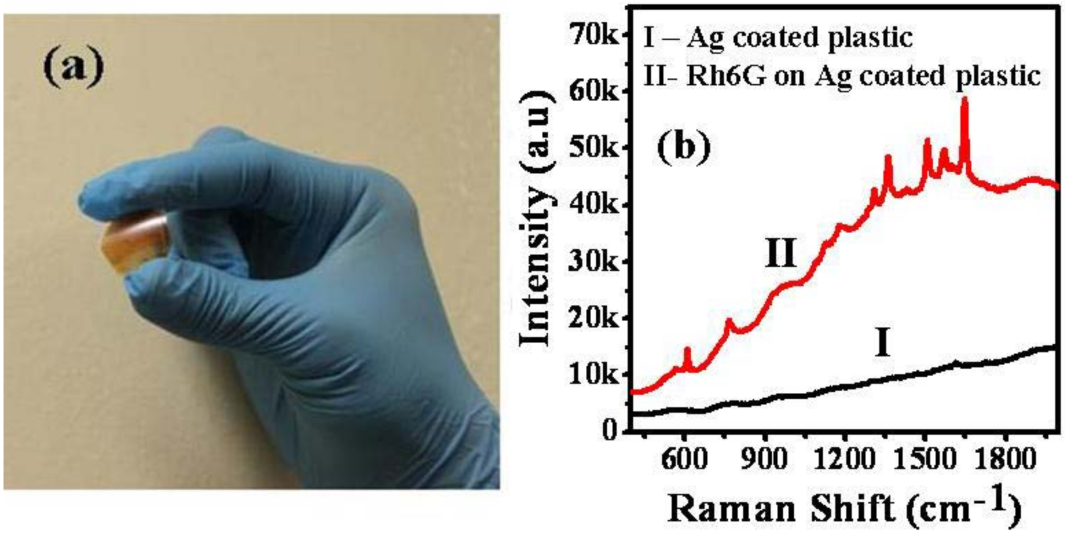

Fig. 7.6 a) Ag nanoparticles coated on flexible plastic substrate by dipping the substrate into the Ag nanoparticle ink and then air dried; B) SERS spectra of R6G (1μM) on the plastic substrate. No signals were observed from Ag coated plastic substrate without R6G.

I have also fabricated plastic flexible SERS substrates by using these metal nanoparticles (Figure 7.6), which was prepared by dipping the plastic substrate into the nanoparticle ink. These plastic SERS substrates could be used to detect μM concentration of analytes without annealing the substrate considering the thermal instability of the plastic substrate. Recently Liz-Marzán and co-workers have developed SERS substrates for broad excitation wavelengths using silver nanoparticle films prepared by the layer-by-layer technique[27] or templated approach.[47] Bartosz[28] and co-workers have also demonstrated that the self-assembled nanotriangles displayed excellent SERS sensitivity with an order of magnitude enhancement compared to the individual nanotriangles. However, these methods are not convenient for large scale fabrication of SERS substrates. Here I have demonstrated a facile fabrication of SERS substrates using simple solution processing. This method could be further extended to fabricate SERS substrates by ink-jet printing using nanoparticle "inks". The detection limit can be improved to nM if the substrate is thermally treated

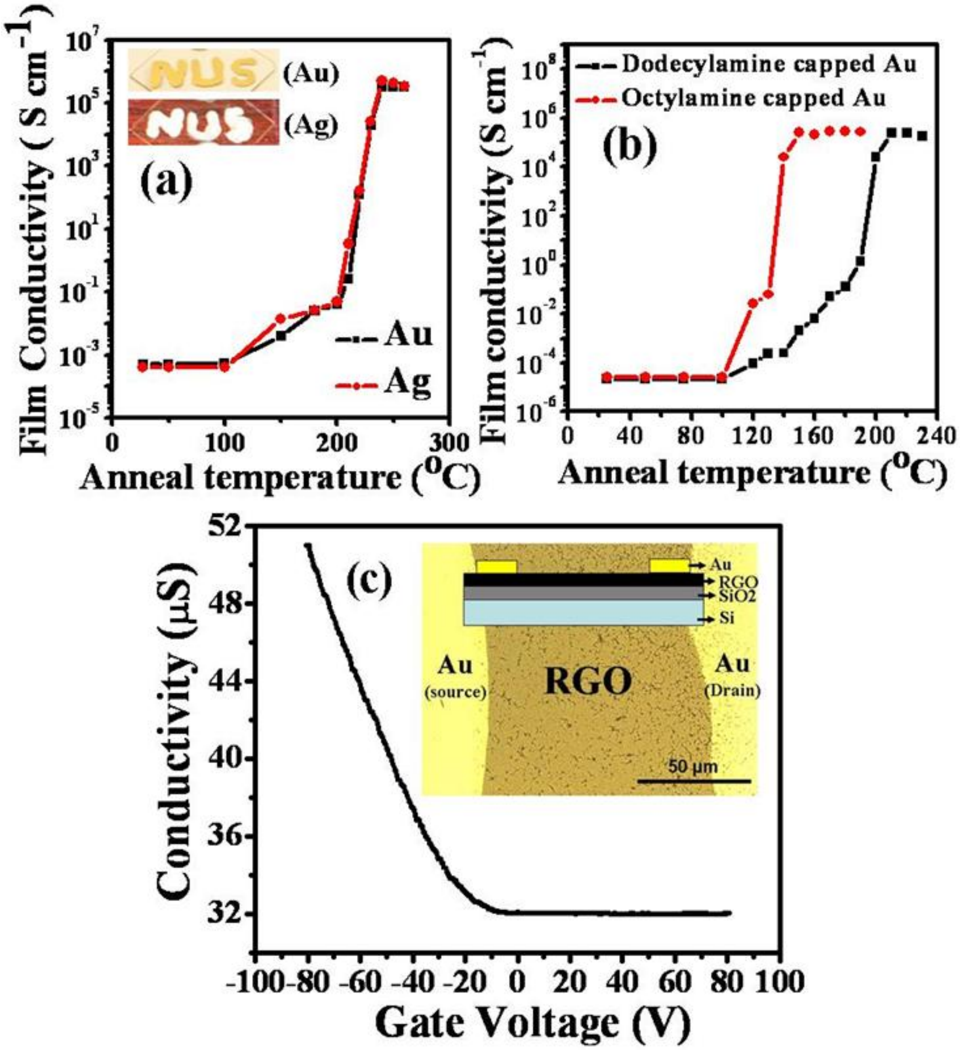

Fig. 7.7 a) Conductivity of the oleylamine capped Au and Ag nanoparticle films measured as a function of anneal temperature in four-probe configuration. The inset shows the colors of the Au and Ag nanoparticle films after annealing at 250^{o}C. b**)** Conductivity of the dodecylamine (DDA) and octylamine capped Au nanoparticle films measured as a function of annealing temperature in a four-probe configuration. The transition temperatures for DDA and octylamine are 190-200^{o}C and 130-140^{o}C, respectively. **c)** Graphene based filed-effect transistor. Inset shows the optical microscope image of the prepared FET and schematic representation of the reduced GO thin film FET.

I have also explored the potential applications of these metal nanoparticle "inks" in printable electronics by examining their insulator-to-metal transition properties. The conductivity was measured on vacuum evaporated four-in-line probe substrates. Figure 7.7a shows the conductivity of the drop casted oleylamine capped Au and Ag nanoparticle films annealed at different temperatures at atmospheric conditions. The Au and Ag nanoparticle films as deposited without annealing behaved like an insulator with very low conductivity of 10^{-3}-10^{-4} S·cm^{-1}. The insulator behavior of the nanoparticle films is because the oleylamine monolayer on the nanoparticle surface hinders the charge tunneling between the nanoparticles. The conductivity of the metal nanoparticles started to increase as the annealing temperature increased above 100^{o}C and jumped rapidly at annealing temperatures above 200^{o}C. The conductivity reaches maxima at 250^{o}C, 3.1x10^{5} S·cm^{-1} for the Au film and 3.3 x10^{5} S·cm^{-1} for the Ag film, which are quite close to the bulk conductivity of Au (~4.5x10^{5} S·cm^{-1}) and Ag (~6.3x10^{5} S·cm^{-1}). At 250^{o}C, the oleylamine sublimes and interconnected conducting paths will rapid transition of the black color nanoparticle films into a gold color Au film and white color Ag film, accompanied by a sublimation of the oleylamine in the form of a black smoke. The inset in the Figure 7.7a shows the color of the nanoparticle film after annealing to 250 ^{o}C. The optical microscopic image and AFM image of the Au nanoparticle films shows that there were no cracks in the film after annealing at 250 ^{o}C (see Fig. 7.9). The temperature dependent conductivities of both Au and Ag films follow a similar trend, which suggests that the insulator-to-metal transformation mainly depends on the capping agent. I have also prepared dodecylamine and octylamine capped gold nanoparticles and measured their annealing temperature dependent conductivities. Their insulator-metal transition temperatures were observed to be 190-200°C and 130-140°C for dodecylamine and octylamine capped Au nanoparticles respectively (See Figure 7.7b). The transition temperatures can thus be tailored to the plastic compatible temperatures by using proper alkylamine as the capping agent.

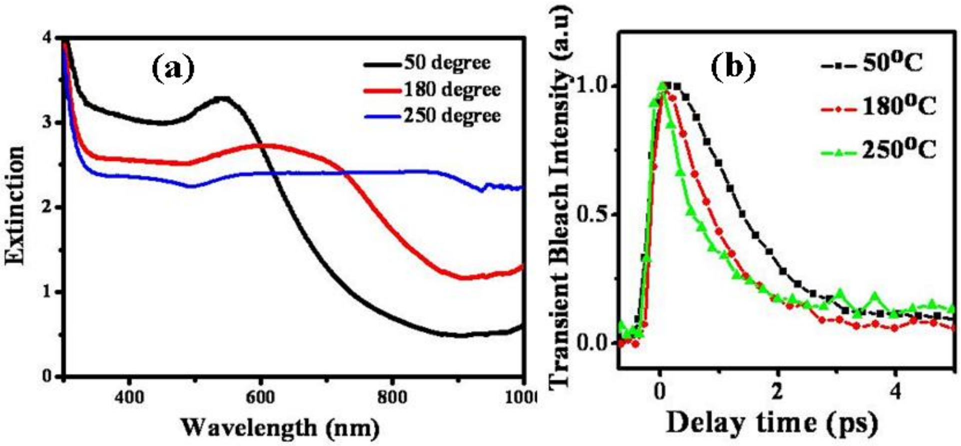

Fig. 7.8 a) UV-visible spectra of oleylamine capped gold nanoparticle film annealed at different temperatures. **b)** Electron relaxation dynamics of the oleylamine capped Au nanoparticle films annealed at 50, 180 and 250°C.

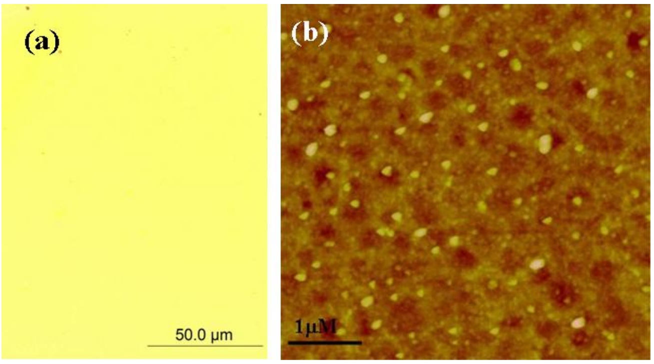

Fig. 7.9 a) Optical microscope image of the conductive gold nanoparticle film prepared from oleylamine capped gold nanoparticle ink. b) AFM image of the conductive nanoparticle film. The AFM image shows that the nanoparticles were interconnected to form conductive film after annealing at 250^{o}C.

The insulator-to-metal transformation of oleylamine capped gold nanoparticle film was monitored by using UV-vis spectroscopy (Figure 7.8a). The broad extinction spectra of the annealed nanoparticle film at raised annealing temperatures suggest the formation of 3D-interconnected structures. Furthermore, the electron relaxation dynamics of the nanoparticle film at different annealing temperatures were investigated by using femtosecond pump-probe experiment. The femtosecond laser pulses with central wavelength at 400 nm and pulse energy of 0.2 nJ were used as the pump beam. Figure 7.8b shows the electron relaxation dynamics of oleylamine capped gold nanoparticle film annealed at 50, 180 and 250^{o}C with probe wavelength at their SPR band maximum at 540, 600 and 600 nm respectively (Figure 7.8a). The electron relaxation time becomes faster as the annealing temperature increases. The film annealed at 50 °C exhibited a relaxation time of 1.4 ps. The relaxation time becomes 0.8ps for annealing temperature of 250 °C, which is very close to the relaxation time of bulk gold.[48] When the film was annealed above the transition temperature, the nanoparticles in the film interconnect each other and provide an extra electron relaxation pathway, which results in a faster electron relaxation time. These results suggest that the there is strong coupling within the nanoparticles after annealing the film above the transition temperatures, which is responsible for the dramatic increase of conductivity of the film above the transition temperature.[9]

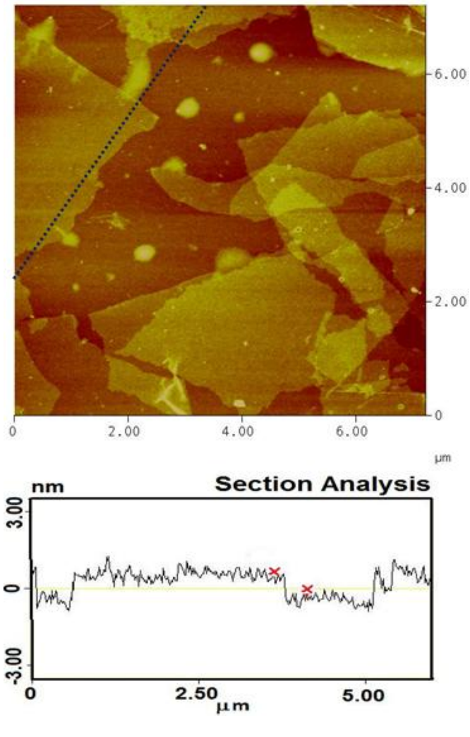

Fig. 7.10 AFM image of the graphene oxide nanosheets as prepared.

We have recently demonstrated the promise of chemically processed graphene in printed electronics.[49] Here I employed gold nanoparticles as printable electrodes for source and drain contacts on a multi-layer graphene film field-effect transistor (MLG-FET) with layer thickness of ~ 15 nm (Figure 7.7c). Graphene oxide (GO) was synthesized from graphite via a modified method used by Hummers and Offeman [50] (see experimental section). The AFM image of the GO is presented in fig.7.10. GO film derived from small-sized GO flakes with a typical lateral dimension of ≤ 10 μm was drop-casted uniformly onto a SiO_2/Si substrate and annealed at 1000 ^{o}C in vacuum to restore the π – electron network. The source and grain were prepared by depositing gold nanoparticles onto the GO film using micropipette followed by annealing the film at 250^{o}C for 5 min. The two-point probe configuration was used to determine the back-gated transistor response. The gate leakage current was limited to 100 pA.

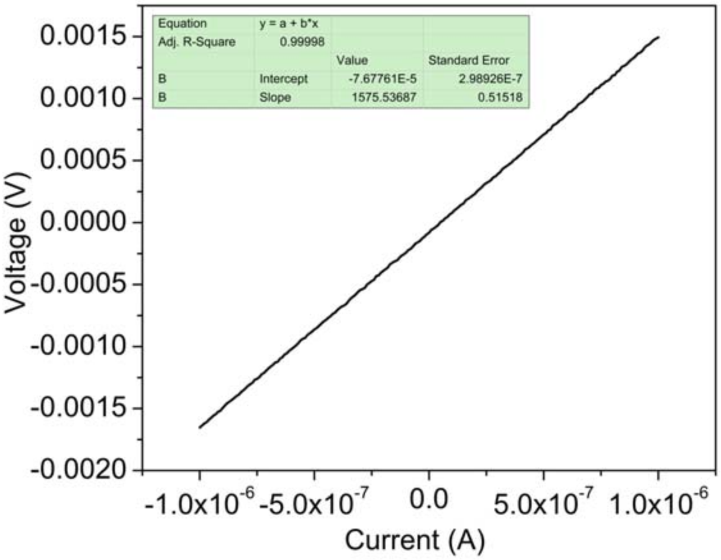

Equation	y = a + b*x		
Adj. R-Square	0.99998		
		Value	Standard Error
B	Intercept	-7.67761E-5	2.98926E-7
B	Slope	1575.53687	0.51518

Fig. 7.11 Resistance measurement of the reduced graphene film prepared on Si/SiO_2 substrate for FET measurements.

The graphene film gave a film conductivity of 2116 S/m (see Fig. 7.11 for the I-V curve) after normalizing geometrical factors. Carrier mobility can be extracted from the linear regime of the transfer characteristics, using $\mu = [(\Delta I_{ds}/V_{ds})(L/W)]/C_{ox}\ \Delta V_g$ where L and W are channel length (~ 100 μm) and width (~ 2 mm) respectively, C_{ox} is silicon oxide gate capacitance (which is 1.21×10^{-8} F/cm^2 for a gate oxide thickness of 285 nm), I_{ds}, V_{ds}, and V_g are drain-source current, drain-source voltage (fixed at 1 V) and gate voltage, respectively. Figure 7.7c shows the transfer characteristics of a typical FET device. P-Type response was reproducibly observed for all devices with a maximum hole mobility of 26.4 cm^2/(V·s). The absence of an ambipolar response of the MLG film might be due to residual hydroxyl groups acting as electron traps.[51] We have previously shown that the n-type behaviour could be restored by optimizing several key steps in film processing and device fabrication.[50] These experiments demonstrated these gold nanoparticle "Inks" could act as attractive materials for printable electrodes and be extended to applications in organic electronics.

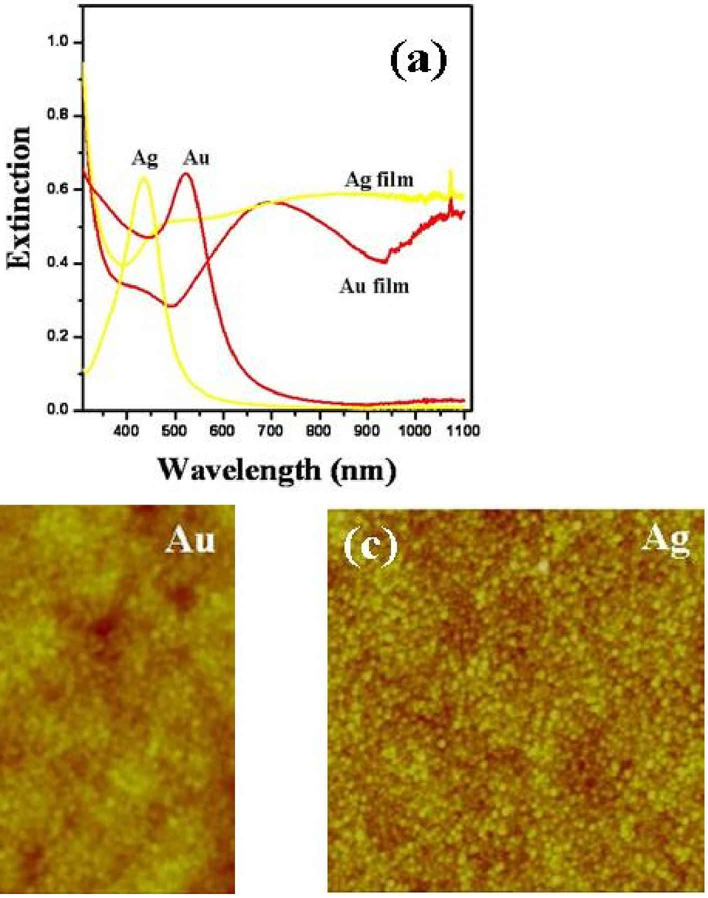

Fig. 7.12 a) Extinction spectra of the gold and silver nanoparticle films on the ITO substrates after annealing the substrate at 120°C in comparision with the nanoparticles in toluene solution. b-c) The corresposning AFM images

The photo-response of the solution processed metal nanoparticle films has also been investigated. Broad range of wavelengths of light can be detected by using these nanoparticle films, owing to the broad extinction spectra of the film as shown in figure 7.12a. The photo-responses of the Au and Ag films prepared from oleylamine capped Au and Ag nanoparticles were studied by using different diode lasers with wavelengths at 400, 532, 980, 1064 nm. Figure 7.14A shows the schematic picture of the device fabrication and photoresponse measurements. The device was fabricated by spin coating the oleylamine capped gold or silver nanoparticles on the PSS: PEDOT modified substrate, annealing at 120°C and then followed by cathode (Aluminium) evaporation (Fig.7.14A). The extinction spectra of the prepared Au and Ag nanoparticle films on the ITO substrate (Figure 7.12a) are very broad, spanning from visible to near-infrared wavelengths. The AFM images (Figure 7.12b&c) of the nanoparticle films showed that 30-40 nm particles were closely packed on the entire substrates. The initial 5 nm particles were transformed into 30-40nm particles after annealing the films at 120°C. These larger particles couple each other on the entire film, which is responsible for the broad extinction spectra. Figures 7.14B and 7.14C shows the typical photoresponse of Au and Ag nanoparticle films upon alternating on/off laser illumination at 532 and 1064 nm in the air at room temperature. It can be seen that the Au and Ag nanoparticle films respond to both the visible and near-Infrared (NIR) illumination. The photocurrent generated from the silver nanoparticle film is slightly higher than that generated from the gold nanoparticle film. The higher photoconductivity of silver might be due to the high conductivity (see figure 7.13) and closely packed film morphology of the silver nanoparticle film.[8, 52] The photocurrent response showed a similar pattern to that of the carbon nanotube films, which was explained as due to low mobility of the interconnected nanotube network.[53, 54] Here in the case of nanoparticle films, the oleylamine capping agent is responsible for the low mobility, which results in slow raise and decay. The photocurrent originates from the hot electrons excited by SPR absorption, which diffuse through the organic layer barriers

on the nanoparticles. Figure 7.14D&7E show the power dependent photocurrent generation from the Au and Ag nanoparticle films with the excitation of 400, 532, 980 and 1064 nm, respectively. The maximum photocurrent was observed for laser illumination wavelength at 532 nm. The photocurrent decreased as the excitation wavelength changed from 532 to 1064 nm. For both gold and silver films, the photocurrent at different laser irradiation power displayed a linear relationship, similar to many photon detection devices.[54] The device showed very good stability. The device performances were checked three months after their initial preparation and the performance remained unaltered.

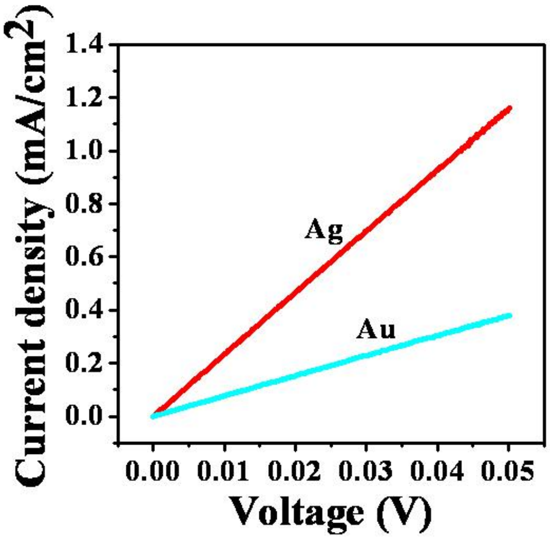

Fig. 7.13 Electric I-V characteristics of the Au and Ag nano particle films that were used for photocurrent response.

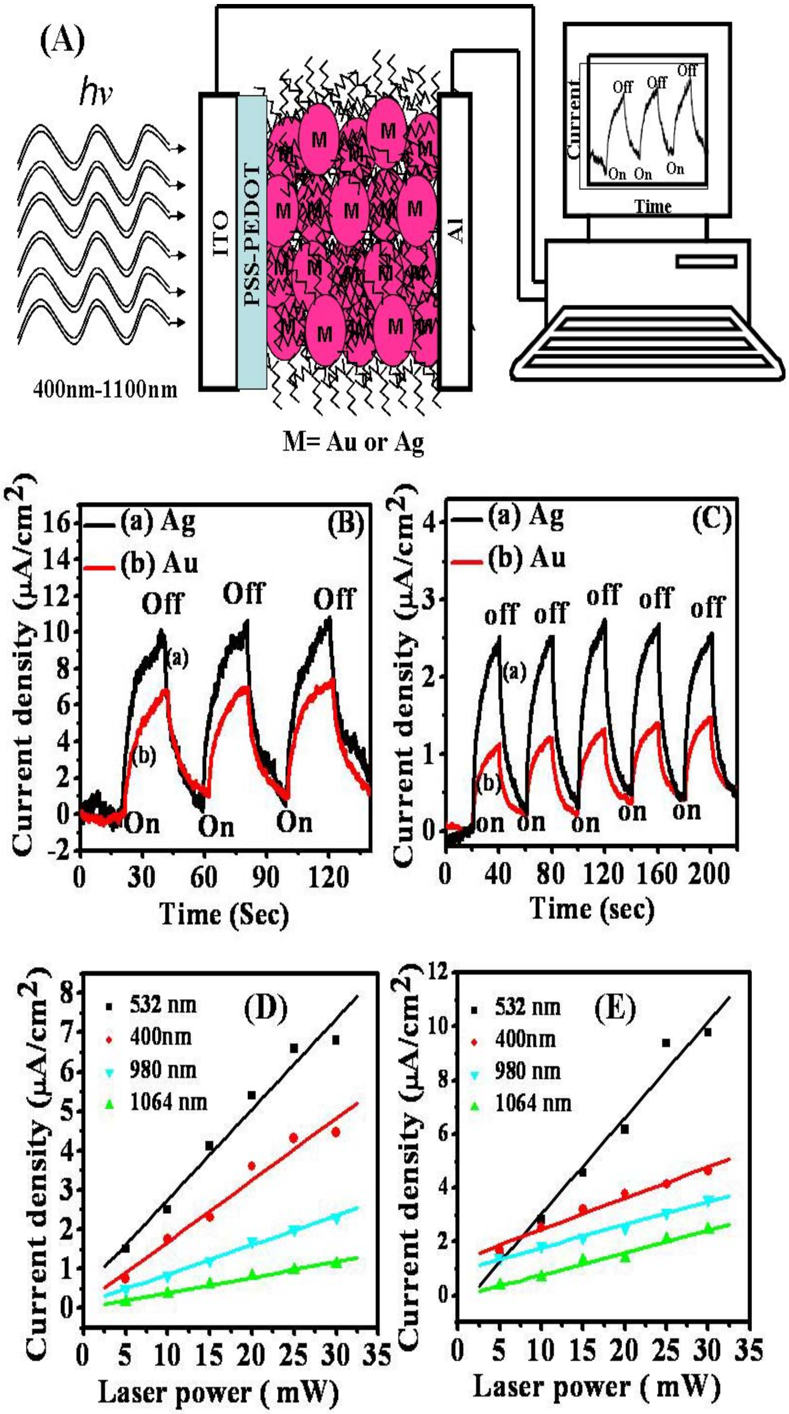

Fig. 7.14 A) Schematic representation of the photoresponse device and the experimental setup. B) Photocurrent response of Au and Ag nanoparticle films to alternating on/off 532 (B) and 1064 nm (C) laser illumination at a power of 30 mW. D, E) Laser power ependent photocurrent generation

7.4 Conclusion

Oleylamine capped gold and silver nanoparticles were prepared by a general and facile method, which can be generalized to prepare any alkylamine capped nanoparticles. Using these metal nanoparticle “inks”, I have demonstrated their applications in large scale fabrication of SERS substrates with a detection limit of nM concentration via solution processing. Silver nanoparticle films were found to give larger enhancement compared to gold nanoparticle films. Insulator-to-metal transition properties of the alkylamine capped metal nanoparticles were investigated. The transition temperatures could be tailored to the plastic compatible temperatures by using proper alkylamine as the capping agent. The ultrafast electron relaxation studies of the nanoparticle films demonstrated that faster elelctron relaxation was observed at higher annealing temperatures due to stronger electronic coupling between the nanoparticles. The application of these alkylamine capped gold nanoparticle inks to printable electronics has been demonstrated by fabrication of Graphene FET by printing the source and drain using the oleylamine capped gold nanoparticles. Furthermore, the broadband photoresponse properties of the Au and Ag nanoparticle films have also been demonstarted by using visible and IR lasers. These results demonstrate that these nanoparticle “inks” are promising for applications for low cost and large scale production of printable SERS substrates, electronics, and broadband photo-response devices.

7.5 References

1. C. Wang, H. G. Yin, R. Chan, S. Peng, S. Dai and S. H. Sun, *Chem. Mater*. 2009, **21**, 433-435.

2. D. A. Giljohann, D. S. Seferos, W. L. Daniel, M. D. Massich, P. C. Patel and C. A. Mirkin, *Angew Chem-Int. Ed.*, **49**, 3280-3294.

3. J. N. Anker, W. P. Hall, O. Lyandres, N. C. Shah, J. Zhao and R. P. Van Duyne, *Nat. Mater.,* 2008, **7**, 442-453.

4. S. Lal, S. Link and N. J. Halas, *Nat. Photonics,* 2007, **1**, 641-648.

5. R. Klajn, P. J. Wesson, K. J. M. Bishop and B. A. Grzybowski, *Angew. Chem. Int. Ed.,* 2009, **48**, 7035-7039.

6. M. S. Gudiksen, L. J. Lauhon, J. Wang, D. C. Smith and C. M. Lieber, *Nature,* 2002, **415**, 617-620.

7. S. Song, Y. Qin, Y. He, Q. Huang, C. Fan and H. Chen, Chem. Soc. Rev., 2010, DOI: 10.1039/c000682n.

8. H. Nakanishi, K. J. M. Bishop, B. Kowalczyk, A. Nitzan, E. A. Weiss, K. V. Tretiakov, M. M. Apodaca, R. Klajn, J. F. Stoddart and B. A. Grzybowski, *Nature,* 2009, **460**, 371-375.

9. P. K. Jain, W. Qian and M. A. El-Sayed, *J. Phys. Chem. B,* 2006, **110**, 136-142.

10. C. J. Murphy, T. K. San, A. M. Gole, C. J. Orendorff, J. X. Gao, L. Gou, S. E. Hunyadi and T. Li, *J. Phys. Chem. B,* 2005, **109**, 13857-13870.

11. Y. G. Sun and Y. N. Xia, *Science,* 2002, **298**, 2176-2179.

12. R. C. Jin, Y. W. Cao, C. A. Mirkin, K. L. Kelly, G. C. Schatz and J. G. Zheng, *Science,* 2001, **294**, 1901-1903.

13. T. Ming, W. Feng, Q. Tang, F. Wang, L. D. Sun, J. F. Wang and C. H. Yan, *J. Am. Chem. Soc.,* 2009, **131**, 16350-16351.

14. W. H. Ni, H. J. Chen, J. Su, Z. H. Sun, J. F. Wang and H. K. Wu, *J. Am. Chem. Soc.,* 2010, **132**, 4806-4814.

15. C. C. DuFort and B. Dragnea, in *Annu. Rev. Phys. Chem.,* 2010, **61,** 323-344.

16. T. Y. Dong, W. T. Chen, C. W. Wang, C. P. Chen, C. N. Chen, M. C. Lin, J. M. Song, I. G. Chen and T. H. Kao, *Phys. Chem. Chem. Phys.,* 2009, **11**, 6269-6275.

17. J. P. Clifford, G. Konstantatos, K. W. Johnston, S. Hoogland, L. Levina and E. H. Sargent, *Nat. Nanotech.,* 2009, **4**, 40-44.

18. P. Banerjee, D. Conklin, S. Nanayakkara, T. H. Park, M. J. Therien and D. A. Bonnell, *Acs Nano,* 2010, **4**, 1019.

19. S. Magdassi, M. Grouchko, O. Berezin and A. Kamyshny, *Acs Nano,* 2010, 4, 1943-1948.

20. J. Perelaer, B. J. de Gans and U. S. Schubert, *Adv. Mater.,* 2006, **18**, 2101-2104.

21. S. Sivaramakrishnan, P. J. Chia, Y. C. Yeo, L. L. Chua and P. K. H. Ho, *Nat. Mater.,* 2007, **6**, 149-155.

22. N. A. Abu Hatab, J. M. Oran and M. J. Sepaniak, *Acs Nano,* 2008, **2**, 377-385.

23. R. A. Alvarez-Puebla, R. Contreras-Caceres, I. Pastoriza-Santos, J. Perez-Juste and L. M. Liz-Marzan, *Angew. Chem. Int. Ed.,* 2009, **48**, 138-143.

24. D. He, B. Hu, Q. F. Yao, K. Wang and S. H. Yu, *Acs Nano,* 2009, **3**, 3993-4002.

25. R. C. Jin, *Angew. Chem. Int. Ed.,* 2010, **49**, 2826-2820.

26. A. Merlen, V. Gadenne, J. Romann, V. Chevallier, L. Patrone and J. C. Valmalette, *Nanotechnology,* 2009, **20**, 215705.

27. S. Abalde-Cela, S. Ho, B. Rodriguez-Gonzalez, M. A. Correa-Duarte, R. A. Alvarez-Puebla, L. M. Liz-Marzan and N. A. Kotov, *Angew. Chem Int. Ed.,* 2009, **48**, 5326-5329.

28. D. Walker, K. Browne, B. Kowalczyk and B. Grzybowski, *Angew. Chem. Int. Ed.*, 2010, **49**, 6760-6763.

29. T. Lopez-Rios and E. Sandre, *J. Raman Spectrosc.* 1998, **29**, 733-737.

30. X. Y. Zhang, J. Zhao, A. V. Whitney, J. W. Elam and R. P. Van Duyne, *J. Am. Chem. Soc.,* 2006, **128**, 10304-10309.

31. C. L. Haynes and R. P. Van Duyne, *J. Phys. Chem. B,* 2001, **105**, 5599-5611.

32. A. G. Brolo, E. Arctander, R. Gordon, B. Leathem and K. L. Kavanagh, *Nano Lett.,* 2004, **4,** 2015-2018.

33. T. Akiyama, K. Aiba, K. Hoashi, M. Wang, K. Sugawa and S. Yamada, *Chem. Commun.,* 2010, **46,** 306-308.

34. H. A. Atwater, A. Polman, Nature Materials, 9, 205; Y. A. Akimov, K. Ostrikov and E. P. Li, *Plasmonics,* 2009, **4**, 107-113.

35. X. N. Xie, Y. L. Xie, X. Y. Gao, C. H. Sow, A. T. S. Wee, *Adv. Mater.,* 2009, **21**, 3016-3021.

36. D. Huang, F. Liao, S. Molesa, D. Redinger and V. Subramanian, *J. Electrochem. Soc.,* 2003, 150, G412-G417.

37. Y. L. Wu, Y. N. Li and B. S. Ong, *J. Am. Chem. Soc.,* 2007, **129**, 1862-1862.

38. J. J. P. Valeton, K. Hermans, C. W. M. Bastiaansen, D. J. Broer, J. Perelaer, U. S. Schubert, G. P. Crawford and P. J. Smith, *J. Mater. Chem.,* 2010, **20**, 543-546.

39. S. B. Fuller, E. J. Wilhelm and J. M. Jacobson, *J. Microelectromech.Syst.,* 2002, **11**, 54-60.

40. W. Gaynor, J. Y. Lee and P. Peumans, *Acs Nano* 2010, **4**, 30-34.

41. M. Brust, M. Walker, D. Bethell, D. J. Schiffrin and R. Whyman, *J. Chem. Soc., Chem. Commun.,* 1994, 801-802.

42. J. Yang and J. Y. Ying, *Nat. Mater.* 2009, **8**, 683-689.

43. M. Chen, Y. G. Feng, X. Wang, T. C. Li, J. Y. Zhang and D. J. Qian, *Langmuir*, 2007, **23**, 5296-5304.

44. C. Wang, H. G. Yin, R. Chan, S. Peng, S. Dai and S. H. Sun, *Chem.Mater.*, 2009, **21**, 433-435.

45. Y. H. Sun, K. Liu, J. Miao, Z. Y. Wang, B. Z. Tian, L. N. Zhang, Q.Q. Li, S. S. Fan and K. L. Jiang, *Nano Lett.,* 2010, **10**, 1747-1753.

46. M. Rycenga, K. K. Hou, C. M. Cobley, A. G. Schwartz, P. H. C. Camargo and Y. N. Xia, *Phys. Chem. Chem. Phys.,* 2009, **11**, 5903-5908.

47. N. Pazos-Perez, W. Ni, A. Schweikart, R. A. Alvarez-Puebla, A. Fery and L. M. Liz-Marzan, *Chem. Sci.,* 2010, **1**, 174-178.

48. R. H. M. Groeneveld, R. Sprik and A. Lagendijk, *Phys. Rev. B,* 1995, **51**, 11433-11445.

49. S. Wang, P. K. Ang, Z. Q. Wang, A. L. L. Tang, J. T. L. Thong and K. P. Loh, *Nano Lett.,* 2010, **10**, 92-98.

50. W. S. Hummers and R. E. Offeman, *J. Am. Chem. Soc.,* 1958, **80**, 1339-1339.

51. V. C. Tung, M. J. Allen, Y. Yang and R. B. Kaner, *Nat. Nanotech.,* 2009, **4**, 25-29.

52. K. Kim and D. L. Carroll, *Appl. Phys. Lett.,* 2005, **87**, 203113.

53. P. Stokes, L. W. Liu, J. H. Zou, L. Zhai, Q. Huo and S. I. Khondaker, *Appl. Phys. Lett.,* 2009, **94**, 042110.

54. B. Pradhan, K. Setyowati, H. Y. Liu and D. H. Waldeck, J. Chen, *Nano Lett.,* 2008, **8**, 1142-1146.

CHAPTER 8

AQUEOUS SILVER NANOPARTICLE INK PRINTABLE AT MILD TEMPERATURE AND APPLICATION FOR PRINTABLE PLASTIC ELECTRONICS

8.1 Introduction

Recent devolopments in printable electronics has opened the doors for the manufacturing of light weight, flexible, cost-effective electronic devices that are beyond the conventional silicon-based devices.[39-41] Currently the printable electronic devices such as field effect transistors,[42] photovoltaics,[43] radio frequency identification tags,[44] displays[45] and sensors,[46] are driving the market. All these devices require electrical contacts. Various materials such as graphene,[47] carbon nanotubes,[48] polymers[49] and metals[50, 51] have been used as electrodes. Among all these conductive materials metal electrodes have been most widely used due to their high conductivity. Different physical methods, such as vaccum evoporation, photolithiography and sputtering, are usually used to fabricate conductive metal electrodes for various electronic devices. The fabrication of conductive electrodes by solution processing offers several advantages such as flexibility, low temperature nad role-to-roll processing, and reduced cost over conventional physical deposition methods.[39-41, 52, 53] Several research groups are actively enagaged in developing metal nanoparticle inks for printable electronics.[40, 43, 50, 53-57] Inkjet printing technology can be utilized to directly print metal contacts using conductive metal nanoparticle inks, overcoming the disadvantages of physical deposition methods.

The nanoparticle inks used for printing electrical contacts are either organic or aqueous dispersions of metal nanoparticles (NPs) protected by organic capping agents. The organic capping agents prevent electrons moving from one particle to another. The resistivity of the electrical contact printed by using these metal NPs is usually not high due to the presence of insulating organic capping agents on the nanoparticles. This problem can be overcome by sintering the electrical contact after printing. The sintering can be achieved by annealing the substrate to higher temperatures,[51, 54] laser irradiation,[58] microwave irradiation,[59] or chemical treatment.[53, 56] So far most of the previosuly reported methods[40, 54, 58, 60, 61] for preparation of conductive films via solution processing require further treatments after printing the nanoparticle film. However, the plastic substrates and polymer films used in flexible plastic electronics are heat sensitive. It is challenging to prepare electrical contacts on plastic substrates that have a low glass transition temperatures(T_g) since further treatment procedures that make the electrodes conductive could destroy the plastic substrates or polymer films. Over the last a few years many research groups have been making tremendous effort in reducing the sintering temperature to be compatible with plastic substrates.[51, 53, 54, 56]

Here in this work, I have prepared a silver (Ag) nanoparticle inks and demonstrated fabrication of large area conductive silver films on glass and plastic substrates at room temperature by using these Ag nanoparticle inks. These films can be made conductive by very mild annealing processes that is plastic compataible. The conductivity was achieved due to coalescence of Ag nanoparticles on the substrate after the solvent evoporation. This method is advnatgeous compared to the previously reported methods in which the substrate was usually heated above 200^0C. I have further demonstrated fabrication of P3HT-PCBM solar cell by direct deposition of cathode by using these Ag nanoparticle ink. 2.25% solar cell efficiency was achieved. The fabrication of conductive silver films on flexible plastic substrates at mild temperatures is expected to have high impact on future low-cost printable electronics.

8.2 Experimental Section:

8.2.1 Synthesis of silver nanoparticle "Ink": Ag nanoparticle ink was prepared by reducing silver nitrate ($AgNO_3$) with sodium borohydride ($NaBH_4$) in the presence of polyvinylpyrrolidone (PVP) as a stabilizer. In a typical synthesis of Ag nanoparticle ink, 0.5 g of $AgNO_3$ and 0.5 g of PVP were dissolved in 100 ml of deionised water under stirring. 8 ml of 10 mg/ml freshly prepared $NaBH_4$ solution was added dropwise to the reaction mixture, resulting in an immediate solution colour change from colorless to dark yellow. The solution was kept stirring for another 5 minutes and then filtered to remove any undissolved impurities. The resultant solution was centrifuged with a speed of 5000 rpm for 45 min to concentrate and remove the extra PVP present in the solution. The precipitate was collected and dispersed in ethanol for further studies (see ESI for photos of the synthetic procedure). The PVP stabilizer plays an important role in the formation of aqueous soluble Ag nanoparticle ink. The reaction that was performed without PVP resulted in formation of an insoluble power with micron size Ag nanoparticles (fig.8.1).

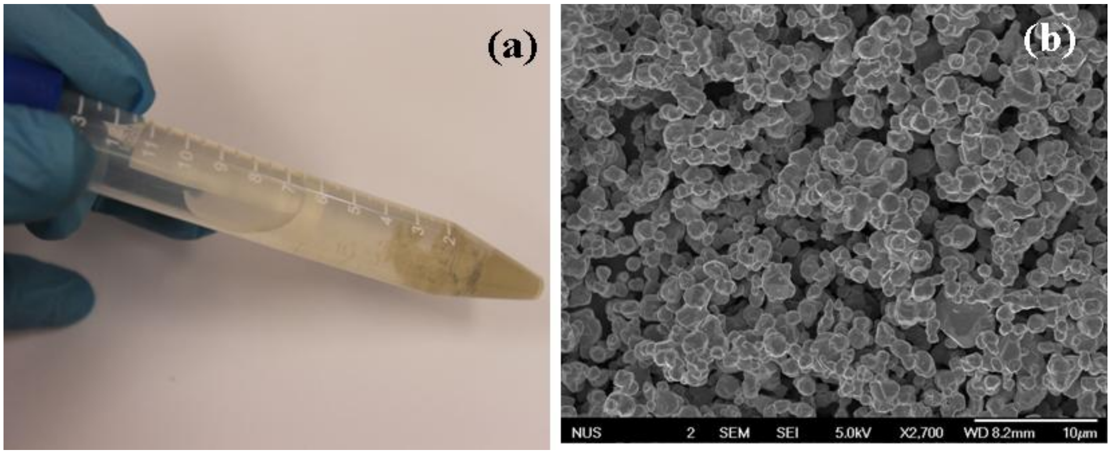

Fig. 8.1 (a) The photograph of the product obtained after reducing $AgNO_3$ with $NaBH_4$ in the absence of PVP, which was not soluble in water and settle down at the bottom of the test tube. (b) The SEM image of the obtained particles. The particles had size of ~ 1μm and were aggregated.

1. Synthesis of silver nanoparticle ink is shown in photographs

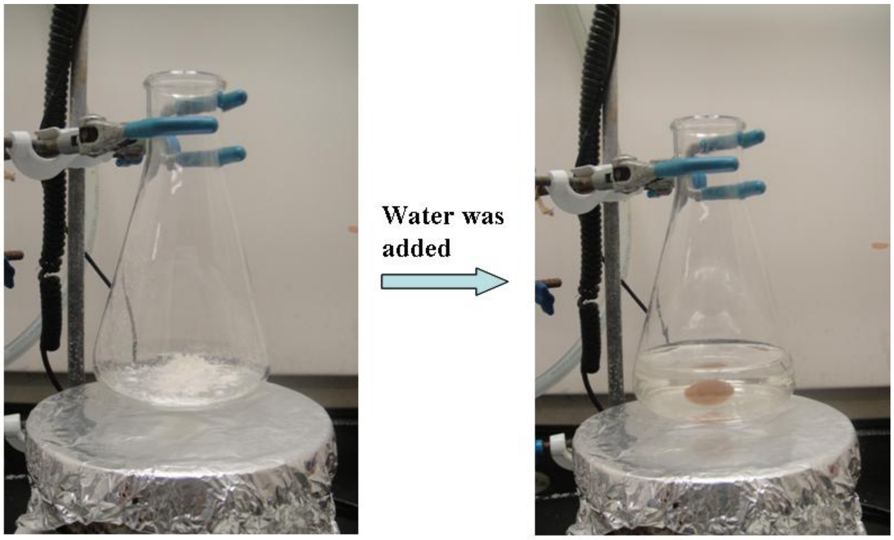

0.5 g of $AgNO_3$ + 0.5 g of PVP

$AgNO_3$ + PVP mixture was dissolved in 100 ml of water

$NaBH_4$ was added

Ag Ink obtained after the addition of $NaBH_4$

The solution was filtered

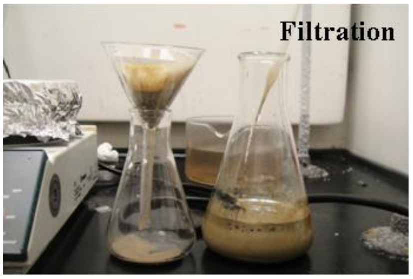

Ag Ink obtained after filtration

The Ag Ink was concentrated By ultracentrifugation

The Ag ink was centrifuged to concentrate the Ink

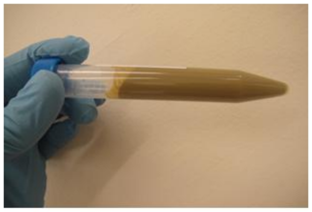

The Concentrated Ag Ink was dissolved in ethanol

8.2.2 Solar cell device fabrication and measurements

P3HT (30mg/ml) and PCBM (30mg/ml) were dissolved (1:1 ratio) in dichlorobenzene (DCB) solvent and spin coated on a ITO/PEDOT electrode using 800rpm at 70 s and annealed at 120°C for 10 min under N_2 atmosphere. Subsequently LiF (1nm) and Al (100 nm) evaporated at $1x10^{-6}$ bar vacuum to complete the device fabrication. The silver nanoparticle ink was deposited onto the P3HT-PCBM polymer film on the other end of device and the device structure is shown in fig.8.5a. The active layer film thickness was measured to be 120 nm by using surface profiler. The device structure is ITO/PEDOT:PSS (40nm)/P3HT:PCBM (120nm)/LiF (1nm)/Al (100nm). The I-V characteristics were measured by using solar simulator AMG 1.5 light source of $100mW/cm^2$ intensity. The light source employed was a Newport 300W xenon light source, controlled by a Newport digital exposure controller, which simulates the solar light through an AM 1.5G sunlight filter. The incident light intensity was focused and calibrated to 1 Sun (100 mW/cm^2) with a standard Si solar cell (PV measurements, USA).

8.3 Results and discussion

Preparation of Ag film on glass substrate

Figure 8.2A shows the appearance of Ag nanoparticle ink in ethanol solution with a concentration of 30 mg/ml. The TEM image of the Ag nanoparticles is shown in the inset of Fig. 1a. The Ag nanoparticle ink contains spherical nanoparticles with diameters in the range of 15-30 nm. The extinction spectrum of the Ag nanoparticles in solution (Fig. 8.2D) shows a sharp plasmon peak at 400 nm, which is typical for spherical Ag nanoparticles. Figures 8.2B&C shows SEM images of the Ag nanoparticle film formed by depositing the Ag nanoparticles dispersion onto the glass substrate at room temperature. The film is uniform and has metallic shiny brightness similar to the silver mirror (Fig. 8.2B inset). The formation of shiny silver mirror after solvent evaporation indicates that the nanoparticles are closely packed in the film.

The SEM images clearly show that the nanoparticles are self-aggregated and form an interconnected structure within the film. The extinction spectrum of a partially transparent film (Fig 8.2D) shows a broad spectrum spanning from visible to infrared, consistent with the SEM image of heavily aggregated structure.

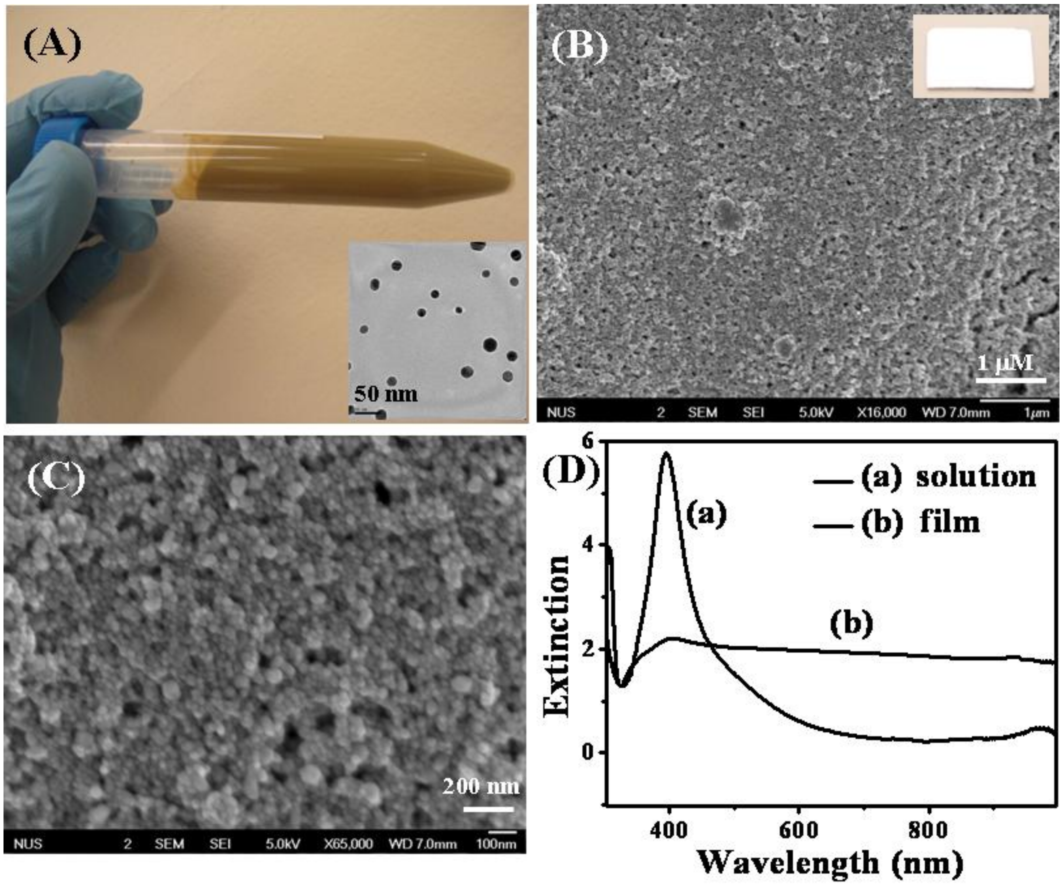

Fig. 8.2 (A) Ag nanoparticle ink in ethanol solution with a concentration of 30m/ml, The inset shows the TEM image of the Ag nanoparticles. (B)&(C) SEM image of the Ag nanoparticle film prepared by solvent evaporation, the inset of fig. B shows the shiny silver film on glass substrate. (D). The UV-visible extinction spectrum of the Ag nanoparticles in ethanol and Ag film

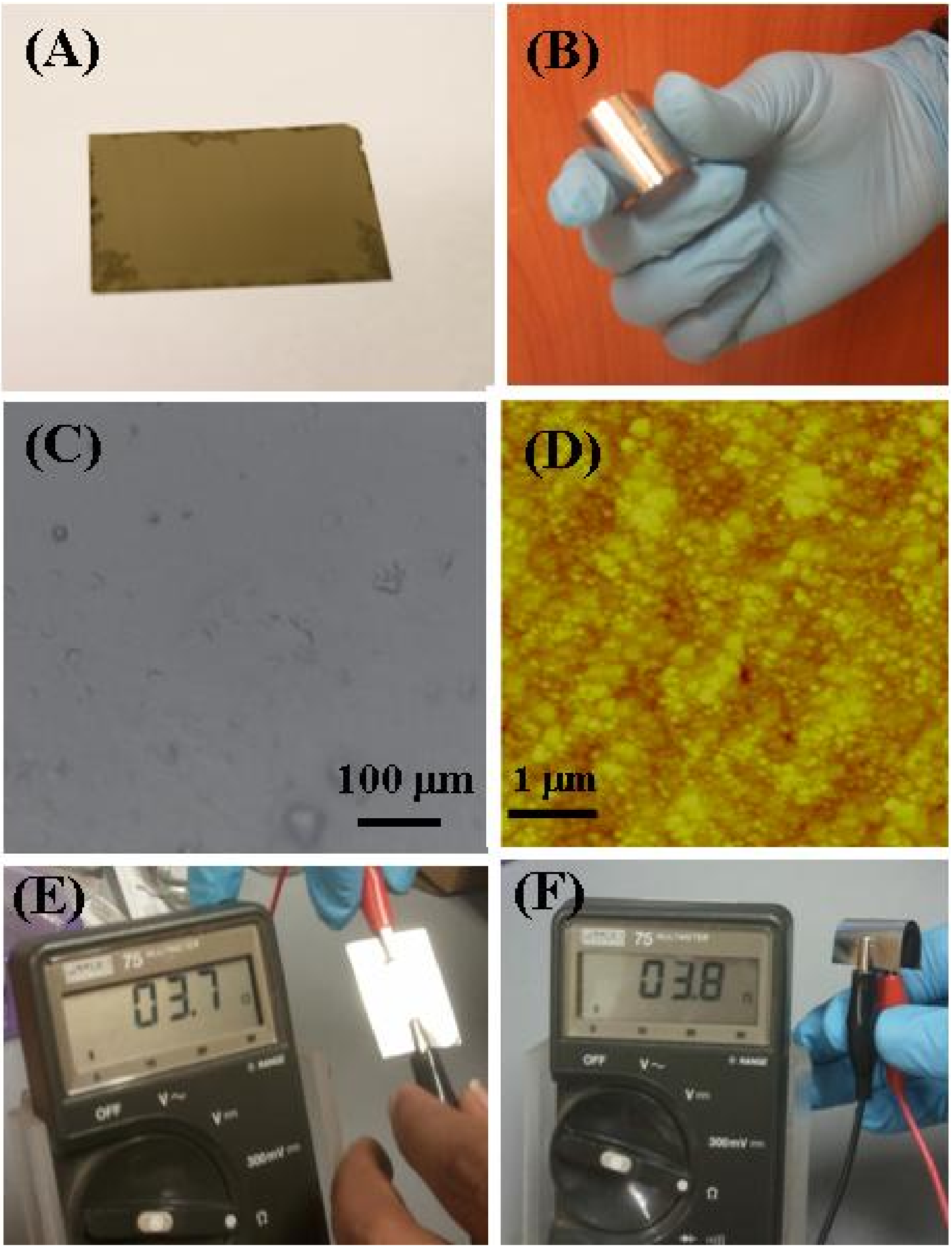

Fig. 8.3 (A) The Ag nanoparticle dispersion on plastic substrate. (B) Shiny silver film prepared on plastic substrate by solvent evaporation. (C) Optical microscope of the silver film on plastic substrate. (D) AFM image of the silver film on plastic substrate. (E&F) The resistance of the Ag nanoparticle film on plastic substrate before and after deformation.

Preparation of Ag film on glass substrate

The interesting phenomenon of self aggregation of Ag nanoparticles on glass substrate was utilized to fabricate conductive plastic substrates, which have potential applications in flexible plastic electronics. To fabricate conductive plastic substrates, the Ag nanoparticle dispersion was deposited onto the polyethylene terephthalate (PET) plastic substrate (Fig. 8.3A) and then the solvent was evaporated at room temperature under table light illumination. The Fig. 8.3B shows the resultant shiny silver film on a plastic substrate after solvent evaporation under light illumination at room temperature. It should be mentioned that the solvent evaporation can be speeded up by heating the substrate at a slightly raised temperature, e.g. 50^0C, or by using air dryer. These processes are still plastic compatible. Figure 8.3C shows an optical microscopic image of the Ag film on a plastic substrate. It can be seen that the film is smooth without any cracks. The AFM image of the Ag film on the plastic substrate (Fig 8.3D) shows that the nanoparticles were interconnected with each other

Previously Bibin et al.[54] have reported that the thiol capped silver nanoparticle films behaved like an insulator after solvent evaporation and the film had to anneal to 150-200^0C to make it conductive. Here in the current work, silver nanoparticles are capped with PVP through the coordination of nitrogen atom (N) in PVP.[62] However, due to the steric effect, PVP binds weakly to the silver nanoparticle surface compared to thiols and primary amines.[62] The weakly adsorbed PVP desorbs from the nanoparticles surface after the solvent evaporation and the Ag nanoparticles tend to self aggregate and make the film conductive. The Ag nanoparticle films on the plastic substrates exhibits a low resistance of 3.7 Ω (Fig. 8.3E). Furthermore, the silver is a ductile material, so the conductive silver film can tolerate elastic deformation of the plastic substrate. No significant change in the film resistance was observed when the film was bent by nearly 180 degrees (Fig.8.3E). The resistance remained nearly unchanged after many deformations.

Previously Magdassi et al.[52, 55] have observed formation of conductive metallic rings spontaneously at room temperature by solvent evaporation owing to “ring stain effect”. The formation of a coffee ring is a pattern left by a puddle of particle-laden liquid after it evaporates. The phenomenon is named for the characteristic ring-like deposit along the perimeter of a spill of coffee. The “ring stain effect” causes the particle aggregation due to the pressure exerted among the particles. To observe “ring stain effect”, special conditions such as very small drop size and fast evaporation rate were required to achieve high conductivity. Furthermore, the high conductivity was only observed along the perimeter of the ring, not the entire film. They also noticed that the Ag film prepared by solvent evaporation behaved like an insulator if there was no ring formation. In our present study, I have demonstrated fabrication of large area, uniform, highly conductive Ag films on the glass and plastic substrates by solvent evaporation, although no “ring stain effect” was observed.

The conductivity of the prepared Ag nanoparticle film was measured by using a four-point probe. The two-point probe substrate was prepared by thermal evaporation of four aluminium (Al) electrodes on glass substrate with a spacing of 4 mm. The Ag nanoparticle ink was droped onto these four probes. The conductivity was obtained by measuring the resistance of the Ag films using a GS 610 source measurement unit (Yokogawa). The conductivity was measured to be 0.7×10^5 S·cm^{-1}, which is only a few times lower than that of the bulk conductivity of Ag (~6.3×10^5 S·cm^{-1}). The lower conductivity of solution processed Ag film compared to bulk Ag is due to the void space present in the Ag film (Fig. 8.2C) formed by self aggregation of Ag nanoparticles after solvent evaporation. The conductivity of film prepared by this method is comparable to those of Ag films obtained by previously reported conventional sintering methods such as high temperature annealing, microwave and laser irradiation.[40, 51, 54, 58, 59, 61]

Solar cell fabrication using Ag Ink as cathode

In order to demonstrate the application of the Ag nanoparticle ink for organic electronics, I have fabricated a thin film solar cell by using P3HT-PCBM as the active layer and depositing the Ag nanoparticle ink onto the P3HT-PCBM film as the cathode. The device structure is shown in Figure 8.4A. (experimental procedures). The current density- voltage curves for P3HT-PCBM solar cell using solution processed Ag electrodes in the dark and under 100 mW/cm^2 light illumination are depicted in Figure 8.4B. For direct comparison, the P3HT-PCBM solar cell using vacuum evaporated Al as the cathode are measured under the same conditions. The device characteristics with Ag electrode are comparable to those of conventional vacuum evaporated Al electrodes. The open circuit voltage (Voc), current density (J_{sc}), fill factor and power conversion efficiency η is 0.56 V, 10.4 mA/cm^2, 38.6% and 2.25 % respectively for solar cell using the solution processed Ag electrode. In comparison, the open circuit voltage (Voc), current density (J_{sc}), fill factor and power conversion efficiency η for solar cell using vacuum evaporated Al electrode are 0.57 V, 11.5 mA/cm^2, 47.0% and 3.07 %, respectively. Interestingly no significant change in Voc was observed with solution processed Ag ink electrodes compared to vacuum evaporated Al electrode, which indicates no chemical or structural modification of active layer at the interface. The decrease in efficiency and fill factor could be due to slightly larger contact resistance between organic active layer and Ag electrodes compared to the evaporated Al electrodes. Although the overall characteristics of the solar cell using solution processed Ag electrode are slightly lower than those using vacuum evaporated Al electrode. Considering the unique advantages of solution processable Ag inks and mild temperature annealing, they are expected to have potential applications for printable low cost organic solar cells and other plastic electronics.

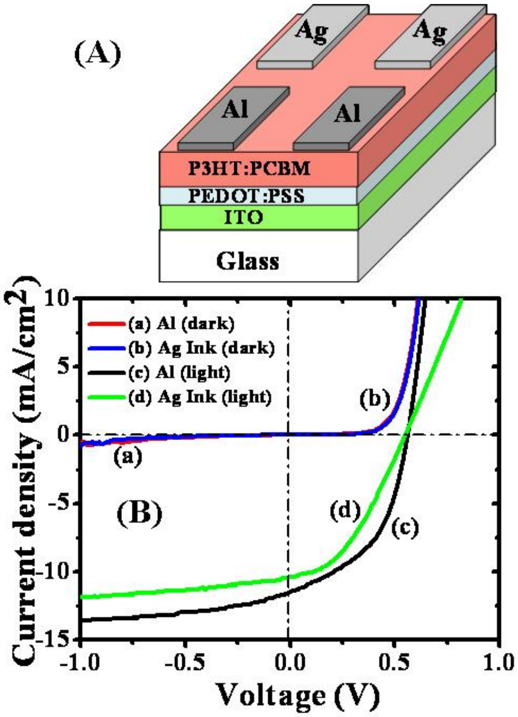

Fig. 8.4 Device structure of the solar cell. The Aluminium electrode was deposited by vacuum evaporation and the Ag electrode was deposited by solution process using aqueous Ag nanoparticle ink. The current density-voltage (J-V) curves for P3HT-PCBM organic solar cell fabricated using Al and Ag as cathodes in the dark and under 100mW/cm^2 light illumination

The conventional metal nanoparticle inks require additional post annealing at high temperatures or chemical treatments to make the metal films conductive. To use these metal films as electrodes in organic electronics using organic active layer, these high temperature annealing or chemical treatments could destroy the organic active layer. Those conventional metal nanoparticle inks thus cannot be used to fabricate electrical contacts directly onto the organic active layer via solution processing. Recently Gaynor et al.[43] have developed a laminated silver nanowire film electrode for organic solar cells to overcome the above mentioned problems. Instead of depositing the Ag nanowire directly onto the organic active layer, they first fabricated a Ag nanowire mesh on a glass substrate by drop-casting the suspension of Ag nanowires followed by annealing at 180^0C for 1hr to make the mesh conductive. Finally they laminated the Ag nanowire mesh onto the organic active layer as top electrode. This lengthy process limits the large scale fabrication of organic solar cells. Here, I have successfully demonstrated fabrication of conductive Ag films at very mild temperatures by using Ag nanoparticle inks. The prepared Ag nanoparticles ink can be directly deposited onto organic active layer to make electrical contacts. This method allows fast and large scale fabrication of conductive Ag films for organic electronics. The device characteristics obtained using the prepared Ag nanoparticle ink as cathode is comparable to those obtained by using conventional vacuum evaporated Al cathode electrodes.

8.4 Conclusion

I have reported silver nanoparticle ink that can be used to fabricate highly conductive films on glass and plastic substrates by depositing the nanoparticle dispersion onto the substrate and drying the solvent. The high conductivity was achieved by annealing the substrate at very mild temperatures due to the self aggregation of nanoparticles after drying the solvent. The conductive films fabricated on plastic substrates are highly flexible and nearly no change in the conductivity was observed by deforming the plastic substrate. The fabrication of conductive films by annealing at mild temperature will enable the fabrication of conductive patterns on various heat-sensitive substrates. Further, polymer solar cell was fabricated by depositing the cathode onto the polymer film using the Ag nanoparticle ink and 2.25% efficiency was observed. I expect that the fabrication of conductive films by self aggregation of nanoparticles at very mild temperature would have potential applications for all low cost printable solar cells and flexible plastic electronics.

8.5 References

1. B. D. Gates, *Science*, 2009, **323**, 1566-1567.
2. B. Y. Ahn, E. B. Duoss, M. J. Motala, X. Y. Guo, S. I. Park, Y. J. Xiong, J. Yoon, R. G. Nuzzo, J. A. Rogers and J. A. Lewis, *Science*, 2009, **323**, 1590-1593.
3. I. Osborne, M. Lavine and R. Coontz, *Science*, 2010, **327**, 1595-1595.
4. M. Caironi, E. Gili, T. Sakanoue, X. Y. Cheng and H. Sirringhaus, *Acs Nano*, 2010, **4**, 1451-1456.
5. W. Gaynor, J. Y. Lee and P. Peumans, *Acs Nano*, **4**, 30-34.
6. S. B. Fuller, E. J. Wilhelm and J. M. Jacobson, *J. Microelectromech.* **Syst.**, 2002, **11**, 54-60.
7. P. Andersson, R. Forchheimer, P. Tehrani and M. Berggren, *Adv. Funct. Mater.*, 2007, **17**, 3074-3082.
8. Y. Z. Guo and A. R. Guadalupe, *Sens. Actuators B.*, 1998, **46**, 213-219.

9. G. Kalita, M. Matsushima, H. Uchida, K. Wakita and M. Umeno, *J. Mater. Chem.*, 2010, **20**, 9713-9717.

10. K. H. An, W. S. Kim, Y. S. Park, Y. C. Choi, S. M. Lee, D. C. Chung, D. J. Bae, S. C. Lim and Y. H. Lee, *Adv. Mater.*, 2001, **13**, 497-500.

11. X. Crispin, F. L. E. Jakobsson, A. Crispin, P. C. M. Grim, P. Andersson, A. Volodin, C. van Haesendonck, M. Van der Auweraer, W. R. Salaneck and M. Berggren, *Chem. Mater.*, 2006, **18**, 4354-4360.

12. P. T. Bishop, L. J. Ashfield, A. Berzins, A. Boardman, V. Buche, J. Cookson, R. J. Gordon, C. Salcianu and P. A. Sutton, *Gold Bulletin*, 2010, **43**, 181-188.

13. J. Perelaer, P. J. Smith, D. Mager, D. Soltman, S. K. Volkman, V. Subramanian, J. G. Korvink and U. S. Schubert, *J. Mater. Chem.,* 2010, **20**, 8446-8453.

14. M. Layani, M. Gruchko, O. Milo, I. Balberg, D. Azulay and S. Magdassi, *Acs Nano*, 2009, **3**, 3537-3542.

15. S. Magdassi, M. Grouchko, O. Berezin and A. Kamyshny, *Acs Nano*, 2010, **4**, 1943-1948.

16. B. T. Anto, S. Sivaramakrishnan, L. L. Chua and P. K. H. Ho, *Adv. Funct. Mater.*, 2010, **20**, 296-303.

17. S. Magdassi, M. Grouchko, D. Toker, A. Kamyshny, I. Balberg and O. Millo, *Langmuir*, 2005, **21**, 10264-10267.

18. J. J. P. Valeton, K. Hermans, C. W. M. Bastiaansen, D. J. Broer, J. Perelaer, U. S. Schubert, G. P. Crawford and P. J. Smith, *J. Mater. Chem.*, 2010, **20**, 543-546.

19. R. W. Zhang, W. Lin, K. S. Moon and C. P. Wong, *Acs Appl. Mater. Interfaces,* 2010, **2**, 2637-2645.

20. J. W. Chung, S. W. Ko, N. R. Bieri, C. P. Grigoropoulos and D. Poulikakos, *Appl. Phy. Lett.*, 2004, **84**, 801-803.

21. J. Perelaer, B. J. de Gans and U. S. Schubert, *Adv. Mater.*, 2006, **18**, 2101-2104.

22. H. H. Lee, K. S. Chou and K. C. Huang, *Nanotechnology*, 2005, **16**, 2436-2441.

23. J. Perelaer, C. E. Hendriks, A. W. M. de Laat and U. S. Schubert, *Nanotechnology*, 2009, **20,** 165303.

24. H. S. Wang, X. L. Qiao, J. G. Chen, X. J. Wang and S. Y. Ding, *Mater. Chem. Phys.*, 2005, **94**, 449-453.

CHAPTER 9

CONCLUSIONS AND OUTLOOK

My doctoral dissertation has been focused on the investigation of nonlinear optical properties of gold and silver nanoparticles of various sizes and shapes and the development of metal (Au&Ag) nanoparticle inks for printable electronics. In Chapter 2, we explored the nonlinear optical limiting properties of silver nanoprisms. It was found that the silver nanoprisms exhibit strong optical limiting properties and even slightly better than that of carbon nanotube suspension, which was known as a benchmark optical limiter. Nonlinear scattering experiments suggest that nonlinear scattering should play an important role in the observed optical limiting effects.

In Chapter 3 and 4, we explored the synthesis and broadband optical limiting properties of oleylamine capped gold nanoparticles for both nanosecond and femto second laser pulses. The thresholds for the optical limiting properties of the oleylamine capped gold nanoparticles with 532 nm and 1064 nm laser pulses are lower than the CNT suspension that are known as a benchmark optical limiter. Scattering measurements show that the nonlinear scattering plays a very important role in the exceptional broad band optical limiting activity of oleylamine capped gold nanoparticles.

The investigation of linear and nonlinear optical properties of glutathione capped gold clusters is presented in chapter 5. The two-photon absorption crossection of these glutathione capped gold clusters was measured using femtosecond Z-scan technique to be ~189740 GM in water, which is much larger compared to those of organic fluorescent dyes and quantum dots. In addition, these gold clusters show exceptional photo-stability. The gold clusters also displayed very low toxicity to cells even at high concentrations of gold clusters. These biocompatible gold clusters can be used as fluorescent labels for bio-imaging. The exceptional properties of these gold clusters make them good alternative for bio-imaging and other nonlinear optical applications.

In Chapter 6, we have developed two simple methods assemble the gold nanoparticles into gold nanochains for nonlinear optical and surface enhanced Raman scattering applications. In the first method, gold nanochains were synthesized in a single step by reducing the gold slat with $NaBH_4$ in the presence of amino acid. Those gold nanochains display saturable absorption at lower intensities and reverse saturable absorption at higher intensities of 800nm femtosecond laser pulses. In the second method, we self assembled the spherical gold nanoparticles into gold nanochains using water soluble conjugated polymers. A longitudinal plasmon resonance band was formed as a result of the plasmon coupling of gold nanoparticles and it can be tuned from visible to near infrared by adjusting the polymer/Au molar ratio. The glass substrates modified with gold nanochains were used as a SERS substrate and a ~400 time's larger enhancement than that on the glass substrate modified with isolated spherical gold nanoparticles.

A simple, low cost and facile method has been developed for the preparation of alkylamine capped gold and silver nanoparticle inks dispersed in organic solvents. a facile solution processed method for the fabrication of highly efficient SERS substrates, which can detect analytes down to a few nM and flexible plastic substrates has been demonstrated for the first time using these metal(Au&Ag) nanoparticle "inks". The metal nanoparticle films were found to undergo insulator-to-metal transformations under annealing, with transition temperature mainly dependent on the capping agent. We have demonstrated the application of alkylamine capped metal nanoparticle inks as printable electrodes for graphene based field-effect transistor (FET). The metal nanoparticle films prepared by using these nanoparticle “inks” also displayed broadband (400-1100 nm) photo-response.

Organic solvents are compatible for printing the nanoparticles on thin plastic substrates, as most of the organic substrates can dissolve in organic solvents, so the nanoparticle inks dissolved in aqueous solvents are required for plastic electronics. Here in this project, we have reported a simple method for the preparation of the silver nanoparticle ink that can be printable at room temperature without post sintering. We have also demonstrated the fabrication of highly conductive silver films on glass as well as flexible plastic substrates using the silver nanoparticle ink prepared in our laboratory. Further more, we have demonstrated the application of this silver nanoparticle ink as cathode material for P3HT-PCBM bulk heterojunction solar cells been demonstrated and the efficiency obtained was 2.25%**.**

It is expected that the noble metal nanoparticles reported in this thesis would have potential applications for nonlinear optical devices. So it would be interesting to study the nonlinear optical properties of optical lenses doped with the nanoparticles reported in this thesis for device applications. Further more, the nanoparticle inks reported in this thesis can be produced in large scale in low preparation cost, so these nanoparticle inks can be printed in various electronic devices using ink-jet printing. The silver nanoparticle ink that is dispersed in aqueous solvent would have many potential applications for plastic electronics. More importantly, this silver nanoparticle ink can be printed on polymer films, that would avoid the usage of expensive equipments to fabricate the electrodes on polymeric films, for example in polymer solar cells. So these nanoparticles ink can be tested for many plastic electronic devises by printing the using ink-jet printer.